Departament d'Enginyeria Mecànica

UNIVERSITAT POLITÈCNICA DE CATALUNYA

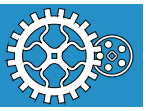

Contributions to meshless methodologies for the simulation of acoustic radiation and scattering problems

by

Javad Fakhraei

Supervised by

Robert Arcos Villamarín

Teresa Pàmies Gómez

Thesis submitted to obtain the title of
Doctor in Mechanical, Fluids and Aerospace Engineering

by the

Universitat Politècnica de Catalunya (UPC)

January 29, 2024

Abstract

Meshless methodologies have emerged as a valuable tool in the field of computational acoustics, offering an efficient approach to model complex acoustic phenomena. These innovative numerical techniques offer a promising alternative to traditional mesh-based methods to deal with scattering and radiation acoustic wave propagation problems. Unlike conventional mesh-based approaches, meshless methods do not rely on structured grids of the domain or its boundary, enabling more flexible and adaptive discretisation. The absence of a mesh eliminates the need for time-consuming grid generation and refinement, simplifying the simulation process and reducing the computational effort. This efficiency is especially valuable in addressing large-scale acoustic simulations, such as those encountered in environmental noise assessments and underwater acoustics.

This dissertation is particularly centred on the study and development of a novel group of numerical meshless methods related to boundary collocation approaches. These methods are employed to address problems involving the propagation of acoustic waves in unbounded domains. The novel approaches presented in this research offer several benefits with respect to existing methodologies, in terms of robustness, accuracy and computational efficiency. Furthermore, in contrast to a fully three-dimensional analysis, the approaches presented in this dissertation are formulated in the two-and-a-half-dimensional domain. This domain is particularly suited for scenarios where the system is subjected to longitudinally moving loads or sources and where the geometry of the system remains longitudinally invariant.

The meshless methodologies developed in this thesis mainly rely on two of the most well-established meshless methods in the field: the singular boundary method and the method of fundamental solutions. In the first instance, an approach based on a two-and-a-half-dimensional version of the singular boundary method is proposed and studied to address acoustic radiation and scattering problems. Subsequently, its applicability for real case acoustic scenarios is evaluated through simulations involving point source diffraction in the presence of thin noise barriers. As probably representing the most significant novelty of this dissertation, a hybrid method that combines the singular boundary method and the method of fundamental solutions is introduced. It is specifically devised to tackle acoustic

wave propagation problems featuring complex boundary geometries with corners and sharp edges. Finally, two modification techniques are proposed to enhance the previously mentioned approach based on the two-and-a-half-dimensional singular boundary method. The Burton–Miller formulation in a first instance, and a dual surface scheme in the second. These modifications aim to overcome the issue of spurious eigensolutions, which arises from the non-uniqueness solution problem associated with boundary collocation methods. To comprehensively assess the capabilities and performance of the proposed meshless methods, the available analytical solutions and alternative numerical strategies such as the well-known boundary element method are also utilised in various designed benchmark problems.

Acknowledgements

First of all, I would like to express my deepest appreciation to my supervisors, Prof. Robert Arcos and Prof. Teresa Pàmies, for their invaluable guidance and steadfast support throughout the entire process of completing this work. I am profoundly thankful for their expertise and the enduring friendship they have provided during my academic journey at the Universitat Politècnica de Catalunya (UPC).

I wish to express my sincere gratitude to Prof. Jordi Romeu, the director of my thesis project, for his consistent support during my doctoral studies.

I am also pleased to extend my grateful acknowledgement to Prof. Luís Godinho and Prof. Paulo Amado-Mendes for granting me the privilege of joining their research team as a visiting researcher at the University of Coimbra. Their invaluable guidance and the opportunity to collaborate with their team significantly enriched my research and expanded my academic horizons. I would also like to convey my appreciation to the members of their research group, whose warm hospitality made me feel welcome in Coimbra.

I would like to thank the financial support provided by the FPI-UPC 2017 grant (reference 07), funded by the Universitat Politècnica de Catalunya (UPC) and Banco Santander, Spain.

I am thankful to all the members of the LEAM who have directly and indirectly made this journey possible with their constant support, opinions, and recommendations.

Finally, I am delighted to extend my special thanks to my parents and sisters, who have consistently believed in me, supported me, and encouraged me to pursue my dreams. Without their unwavering support, none of my accomplishments would have been possible.

Dedication

To my family.

Contents

List of Figures

Chapter 1

Introduction

This chapter serves as the introductory section of the present thesis. It commences by providing an overview of the importance of numerical meshless methodologies in the field of computational acoustics. Afterwards, a justification for the emphasis on introducing practical numerical meshless methodologies to deal with acoustic wave propagation problems is presented. Finally, the chapter ends with a brief outline of the contents addressed in each subsequent chapter of the thesis.

1.1 Overview

The work presented in this thesis concerns the study and development of a particular class of numerical meshless methods belonging to the boundary collocation strategies. The research is specifically oriented towards the field of computational acoustics, addressing the simulation of acoustic wave propagation problems such as radiation and scattering in unbounded domains, relevant to several science and engineering applications.

In a general perspective, approaches to simulate acoustic wave propagation problems can be classified into two categories: analytical solutions and numerical approaches. Analytical solutions are mostly restricted to a few basic and simple geometries, which limits their applicability to real engineering problems. However, due to their outstanding accuracy, they are highly regarded to be considered as a reference for validating numerical approaches. On the other hand, numerical methods are mainly utilised to simulate problems involving boundaries featuring intricate geometries, despite they are typically less accurate and incur higher computational costs in comparison to analytical methods.

Alongside the extensive adoption of conventional numerical mesh-based techniques for simulating acoustic wave propagation problems in large-scale domains, meshless methods have also been introduced in order to overcome the inherent numerical challenges posed by the former class of methods in this sort of problems. These challenges include diverse aspects in mesh generation, the significant influence of mesh quality on numerical results, the complexity of their formulations and corresponding implementations and the considerable computational resources required when employing mesh-based methods.

Most numerical mesh-based methods rely on the discretisation of either the domain or its boundary. Speaking specifically about two of the most widely used methods in computational acoustics, the finite element method (FEM) [1] is built upon the principle of domain discretisation, while the boundary element method (BEM) [2] is based on the discretisation of the boundary. With respect to the FEM, the BEM has been typically considered to be more effective when solving problems with unbounded domains, because of two outstanding advantages: the

order of dimensionality of its associated domain is reduced by one and its ability of naturally fulfil the Sommerfeld's radiation condition at infinity. Despite this significant superiority, it is worth mentioning that the BEM still suffers the already mentioned numerical issues associated with the meshing process.

In this context, emerging boundary-type meshless methods such as the method of fundamental solutions (MFS) [3, 4] and the singular boundary method (SBM) [5, 6] have demonstrated their merits as excellent alternatives to the standard BEM. These methods rely on a completely distinct discretisation strategy, which need only a collocation point distribution along the boundary, together with a set of source points offering significant advantages over the standard BEM. They circumvent challenges associated with the meshing process and eliminate the need for connectivity information existing in the mesh-based methods resulting in optimal, fast and computationally efficient strategies. Furthermore, these methods are mathematically simpler and generally easier to implement compared to mesh-based methods due to the simplicity of their formulation, since the boundary conditions are discretised only at discrete collocation points and there is no need for an estimation of the continuous distribution of the field variables along the boundary, as is required by the BEM.

As an alternative to fully three-dimensional (3D) analysis of acoustic wave propagation problems within large-scale domains, this dissertation specifically examines an efficient approach formulated in the two-and-a-half-dimensional (2.5D) domain for modelling acoustic wave propagation problems. This approach can be adopted to exploit the invariability of the system under study along its longitudinal direction to simplify the simulation process. Particularly, this scheme only requires cross-section discretisation of the system, as the spatial coordinate along the invariant direction is subjected to a domain transformation using the Fourier transform. This modelling strategy has been widely employed in engineering applications, particularly in acoustical and structural dynamics analyses [7–13].

1.2 Justification of the research

Due to the presented benefits over mesh-based methods, meshless methods are receiving growing attention in the field of computational acoustics. In this context, the present thesis particularly focuses on studying and developing one of the most well-known and novel meshless methods in the field: the SBM approach. In the computational acoustics field, this method has been proposed in the last decade to model bounded and unbounded acoustic domains. The developments presented in this thesis concentrate on exterior acoustic problems, while it is worth mentioning that they could be easily adapted to deal with bounded acoustic domains, as well.

The SBM stands as a highly promising alternative to the BEM because of its outstanding benefits regarding computational implementation and efficiency. Apart from the known merits associated with its boundary-based nature, the SBM demonstrates the following advantages in computational acoustics with respect to the BEM:

1. The SBM eliminates the need for a boundary mesh and the numerical integrations required to deal with the singularities arising in the application of the BEM, mitigating the numerical challenges encountered in the simulation of acoustic problems using the BEM.

2. The SBM typically demands less computer memory to achieve a similar accuracy levels since it reduces the number of fundamental solution evaluations.

3. The SBM offers mathematical simplicity, ease of programming, and high suitability to result in fast algorithms.

4. Recent investigations shown that the SBM provides higher numerical accuracy and convergence rates than the BEM.

The MFS is another well-known numerical meshless method that has been further investigated in the context of the present thesis. The MFS offers notable advantages in computational efficiency and formulation simplicity. A key distinction between the MFS and SBM is the superior accuracy of the MFS, particularly for non-complex smooth boundary geometries. However, strong numerical challenges

when implementing the MFS for problems involving intricate boundary geometries have been reported in the literature as well as in this PhD thesis. In general, this thesis concludes that the SBM demonstrates higher stability and broader applicability for practical engineering problems compared to the MFS.

The main goal of this dissertation is the development of fast, computationally efficient and practical numerical meshless methodologies to deal with acoustic wave propagation problems in unbounded domains. This objective has been achieved by taking the distinct advantages offered by the SBM and MFS methodologies to a more advanced development stage, resulting in methods with significantly enhanced capabilities in comparison with state-of-the-art approaches. To accomplish this, the following tasks have been pursued:

1. To develop a 2.5D SBM approach for acoustic radiation and scattering problems in the framework of longitudinally invariant and infinite structures.
2. To assess the effectiveness of the proposed 2.5D SBM for practical scenarios, specifically focusing on the application to acoustic thin barriers utilised in road and railway traffic contexts.
3. To devise a novel hybrid SBM-MFS methodology for acoustic wave propagation problems involving complex or intricate boundary geometries that may inherently possess the benefits of both SBM and MFS methods.
4. To study the influence on the performance of the 2.5D SBM, induced by fictitious eigenfrequencies resulting from the non-uniqueness solution problem in the 2.5D context.
5. To develop modification techniques to effectively address the issue of fictitious eigensolutions that arise in the 2.5D SBM.

1.3 Thesis Outline

This dissertation is organised in six chapters. Except for Chapters 1 and 6, which present the introduction and conclusions of this work, respectively, each chapter incorporates its own literature review within its introduction.

As evidenced, Chapter 1 provides an overview of the issues under consideration, the justification for conducting this research, and a breakdown of the content of each chapter.

In Chapter 2, a 2.5D SBM approach for acoustic radiation and scattering problems in the framework of longitudinally infinite and invariant structures is presented and studied. The chapter begins with an introduction to the proposed method along with a review of other existing numerical methodologies in the field. Afterwards, the mathematical formulation of the proposed 2.5D SBM approach is presented. Subsequently, the performance of the method is demonstrated in the framework of different acoustic benchmark examples. In this context, the feasibility, validity and numerical accuracy of the proposed 2.5D SBM are assessed in a detailed comparison with the available analytical solutions and alternative numerical strategies including the 2.5D MFS and the 2.5D BEM strategies.

Chapter 3 focuses on the applicability of the proposed 2.5D SBM methodology for practical engineering problems. To do so, the 2.5D SBM approach is employed to simulate a typical point source diffraction problem in the presence of acoustic thin barriers. The chapter commences with an introduction consisting of a literature review of the numerical approaches to analyse this kind of problems. In the following, the 2.5D SBM is particularly examined as a tool for the simulation of the acoustic response in both spatial and temporal domains with non-moving and moving source scenarios, respectively. The calculations are done by considering the barrier to be subjected to both rigid and absorbing boundary conditions.

Chapter 4 is concerned with proposing a novel hybrid SBM-MFS methodology for acoustic wave propagation problems. The proposed methodology is particularly devised to solve problems with complex boundary geometries containing geometric singularities such as corners and sharp edges. The chapter starts reviewing modification strategies to overcome the geometric singularity problem in the context of the MFS and the SBM approaches. Afterwards, the numerical formulation of the proposed hybrid methodology is described. Subsequently, designed benchmark examples to demonstrate the validity and accuracy of the proposed hybrid scheme are presented. In the final step, the applicability of the proposed hybrid SBM-MFS methodology to predict the acoustic performance of a T-shaped thin barrier is also investigated.

Chapter 5 investigates the problem of spurious eigensolutions in the context of the 2.5D SBM adopted for exterior acoustic wave propagation problems. It proposes two numerical modification techniques based on the Burton–Miller's formulation in one case and the dual surface method in the other, aiming to mitigate this numerical difficulty in the 2.5D SBM. After a brief literature review on the fictitious eigenfrequency problem in the SBM and BEM approaches, the chapter proceeds to outline the mathematical formulations governing the enhanced versions of the 2.5D SBM within proposed modification strategies. In the next step, the acoustic radiation problems of an infinitely circular cylinder and star-like object are considered to study the validity, feasibility and effectiveness of the proposed modified schemes to deal with the spurious eigensolutions problem in the 2.5D SBM.

Finally, the conclusions from this research are summarised in Chapter 6, together with some guidelines for future work.

Chapter 2

2.5D singular boundary method for exterior acoustic radiation and scattering problems

In this chapter, a numerical methodology based on a 2.5D SBM to deal with acoustic radiation and scattering problems in the context of longitudinally invariant structures is proposed and studied. In the proposed 2.5D SBM, the desingularisation provided by the subtracting and adding-back technique is used to determine the origin intensity factors. These origin intensity factors are derived by means of the origin intensity factors of the Laplace equation. The feasibility, validity and accuracy of the proposed method are demonstrated for two acoustic benchmark problems: the acoustic radiation and wave scattering problems for an infinite cylinder. In order to comprehensively assess the proposed 2.5D SBM schemes in terms of numerical accuracy and computational efficiency, the analyses are conducted by employing the available analytical solutions and other numerical methodologies, including the 2.5D MFS and the 2.5D BEM.

The chapter is organised as follows: In Section 2.1, a brief literature overview of numerical methodologies addressing acoustic radiation and scattering problems is presented. Section 2.2 outlines the mathematical modelling of the proposed 2.5D SBM approach. In Section 2.3, the numerical results and the corresponding discussions are presented, including the verification study of the proposed 2.5D

SBM method, evaluated within the context of two acoustic benchmark examples. Finally, the chapter concludes in Section 2.4 with important remarks derived from the discussions presented.

2.1 Introduction

Problems related to acoustic waves propagation in unbounded domains are frequently encountered in many engineering applications. The domain-type discretisation methods, such as the FEM, are not efficient when dealing with this kind of problems, since they require a massive domain meshing, especially at high frequencies, which is often computationally costly [1]. As an alternative approach, the BEM is found to be more efficient for unbounded domain problems, since its boundary-oriented modelling inherently allows for an efficient treatment of such domains [2]. However, despite the fact that the BEM only requires a mesh of the boundary instead of the full domain, it involves an intricate mathematical formulation together with some numerical issues, such as regularisation procedures to deal with the singularities arisen from the fundamental solutions, fully populated system matrices and troublesome surface meshing in 3D complex domains. Leaving the complex formulae aside, these circumstances result in an increase on computational time and memory requirements, which is probably the main drawback of the BEM.

Due to these disadvantages, a new generation of boundary-type meshless numerical methods that require neither domain nor boundary meshing have been developed in the last two decades. Among meshless methods, the MFS has been extensively used to solve a variety of acoustic problems thanks to its merits on being mathematically simple, easy-to-program, and automatically satisfying the Sommerfeld's radiation condition at infinity. Two of the earliest works regarding the application of the MFS to acoustic problems were presented by Shippy and Kondapalli [14, 15]. Later, Karageorghis [16] used the MFS with fixed sources for the solution of Helmholtz eigenvalue problems. Fairweather et al. [3] reviewed the previous developments of the MFS for scattering and radiation problems in fluids and solids, establishing a general benchmark for its application. Karageorghis et al. [17] employed the MFS for detecting a sound-soft scatterer surrounding a host acoustic homogeneous medium due to a given point source inside it. Qu et al. [18] applied the localised MFS (LMFS) to solve the 2D interior Helmholtz equation at high frequencies. The presented numerical examples showed that the LMFS has a lower computational complexity than the traditional MFS and it can be used for

simulating large-scale acoustic problems with complicated geometries. Although a significant amount of research has been carried out to enhance the applicability of the MFS, the method still has a serious disadvantage: it is strongly sensible to the location of the virtual boundary, particularity for geometrically complex problems, and there is a lack of systematic and efficient approaches to determine its optimal position which restrains the application of MFS to real engineering problems. Several modification schemes have been devised to solve this drawback by investigating approaches where the virtual sources are placed directly on the physical boundary. Some of these methods include the boundary collocation method (BCM) [19], the boundary knot method (BKM) [20], the localised boundary knot method (LBKM) [21, 22], the singular meshless method (SMM) [23] and the singular boundary method (SBM) [24], to name just a few.

The SBM was firstly presented by Chen and Wang [24]. Research conducted last years on the topic have shown that this method is an effective alternative to overcome some drawbacks of the other techniques, like the limited applicability, low accuracy and ill-conditioning problems. In the following, some studies regarding the method applicability for acoustics analysis are listed. Fu et al. [25] proposed the improved singular boundary method (ISBM) for acoustic radiation and scattering problems, which is a combination of the classical SBM with the Burton-Miller's formulation. Numerical results demonstrate that this modification scheme enhances the accuracy of the solution in the vicinity of the corresponding interior eigenfrequencies. Fu et al. [26] applied the SBM for solving water wave-structure interaction and SH wave scattering problems. Qu et al. [27] applied a fast multipole accelerated SBM for the 3D Helmholtz equation in low-frequency regimes. In another study, Qu et al. [28] introduced a diagonal form of the fast multipole SBM to overcome the high computational requirements of the SBM interpolation matrix for high-frequency acoustic radiation and scattering problems. To reduce the high computational requirements of the SBM in 3D problems, Li [29] presented a fast SBM to solve 3D Helmholtz equations that employs the pre-corrected fast Fourier transform (PFFT) to accelerate the SBM numerical process. The results showed that the PFFT-SBM has an advantage over the standard SBM in terms of memory and CPU time. Fu et al. [30] developed the SBM in conjunction with the fast Toeplitz-type matrix solvers (FTMS) for acoustic wave propagation

analysis at low and moderate frequencies in periodic structures. The numerical results demonstrated that by employing this method, the computational time and storage requirements are significantly reduced with respect to traditional SBM routines. Recently, Wang et al. [31] proposed the localised singular boundary method (LSBM) to solve the Laplace and Helmholtz equations in 2D arbitrary domains. Compared with the traditional SBM, the proposed LSBM can effectively avoid the boundary layer effect (appearing for field points located close to the boundary) and requires less memory storage and computational effort because the produced interpolation system matrices are sparse and banded.

Typically, the SBM utilises the single-layer fundamental solutions as kernel functions and introduces the so-called origin intensity factors (OIFs) to circumvent the singularities of the fundamental solutions where the collocation and source points coincide. It approximates the solution of the problem with a linear combination of fundamental solutions of the governing equation of interest. The vital issue in the SBM is the determination of the OIFs, which can be calculated through empirical, analytical or numerical techniques. In the original SBM, the inverse interpolation technique (IIT) [24] was proposed to evaluate the OIFs by using sample solutions of the governing equation of the problem. Gu and Chen [32] adopted the subtracting and adding-back (SAB) technique to efficiently calculate the OIFs in the case of Neumann boundary condition, avoiding the need for sample solutions used in earlier SBM developments. Fu et al. [33] compared three methodologies for the OIFs determination on Neumann and Dirichlet boundaries in exterior wave propagation problems: the IIT; a semi-analytical technique that combines the SAB technique and the IIT; and a semi-analytical technique based on the integral mean value of the Laplace fundamental solution. Results show that semi-analytical solutions provided a higher numerical stability, being the second methodology the one showing the best accuracy. Li et al. [34] presented new explicit empirical formulas to determine the OIFs on Neumann and Dirichlet boundary conditions for 2D and 3D Laplace and Helmholtz equations. With these empirical formulas, the OIFs can be obtained without the need of using the SAB or numerical integration. A strictly mathematical regularised approach for the evaluation of the OIFs for the 3D Helmholtz equation at high frequencies was provided in [35]. The novelty of the work is to propose two artificially constructed general solutions that can be

used to directly evaluate the OIFs by using the SAB technique, which yields on a fully integration- and mesh-free technique. The numerical demonstrations show that the proposed OIF formulas can be successfully used to avoid the singularity and hyper singularity problems encountered in the application of the SBM or the BEM. Nevertheless, accurately determining the OIFs for problems with Dirichlet boundary condition still remains an open issue. Recent studies have introduced some numerical and empirical formulas to evaluate the OIFs for Dirichlet boundary condition case [36–38].

In some acoustic wave propagation analyses required in engineering applications, such as environmental noise assessments for road and railway transportation systems, the computational domain can be assumed to be longitudinally invariant, meaning that the geometry of the system is considered to have a constant cross-section along its longitudinal direction. The methodologies to solve these problems can be constructed in the framework of the two-and-a-half-dimensional (2.5D) domain. The 2.5D domain is reached by the application of the Fourier transform to the governing equations along the coordinate associated with the invariant direction. Then, the system can be solved in a 2D framework and the 3D solutions can be obtained by using the corresponding Fourier inverse transform. Thus, the advantage of this approach is the reduction of the discretisation domain dimensionality by one, which results in strong reduction of the computational costs and memory requirements in the context of mesh-based approaches [39]. Regarding this benefit, the computational efficiency can be further enhanced if meshless methods are employed when dealing with unbounded domain problems.

Methodologies based on the 2.5D formulation are being used nowadays to model engineering acoustic problems. Sheng and Zhong [40] proposed a 2.5D acoustic BEM to simulate the sound radiation of high-speed railway slab tracks subjected to a moving harmonic load. A similar model has been used recently by Li et al. [10] to simulate the noise transmission from the wheels, rails and sleepers to the external surfaces of a train, and by Deng et al. [11] to study the noise insulation capabilities of poro-elastic panels. Ghangale et al. [8] presented a combined methodology based on a 2.5D structural FEM-BEM and a 2.5D acoustic BEM for the prediction of re-radiated noise in underground simple tunnels. Also, some studies have employed 2.5D meshless methodologies to analyse engineering

acoustic problems. In this regard, the potential applications of the 2.5D MFS for the prediction of re-radiated noise in railway traffic systems were discussed in [7, 8]. Recently, the 2.5D SBM [41] has been preliminary proposed and tested for acoustic problems excited by harmonic point sources. The numerical results verified the effectiveness and accuracy of the proposed approach and reported a significant reduction of memory storage in comparison with the 3D acoustic SBM.

The objective of this chapter is to propose and study, in a computational context, a 2.5D SBM approach to deal with acoustic wave propagation problems in where the geometry and mechanical properties of the system are longitudinally constant. In the proposed 2.5D SBM, the desingularisation provided by the SAB technique is used to determine the OIFs. These OIFs are derived by means of the OIFs of the Laplace equation due to the same order of the singularities in the fundamental solutions of Laplace and Helmholtz equations. The feasibility, validity and accuracy of the proposed 2.5D SBM are investigated in the framework of two benchmark examples: the acoustic radiation and wave scattering problems of an infinite cylinder. In order to make a detailed assessment of the proposed approach, other methodologies are applied and then compared in terms of numerical accuracy and computational efficiency. These alternative approaches are the 2.5D MFS and the 2.5D BEM considering linear and quadratic boundary elements (referred to as the 2.5D LE-BEM and the 2.5D QE-BEM, respectively, from now on). In all examples, the available analytical solutions are used as a reference method for the accuracy comparisons. Furthermore, the effect on the 2.5D SBM accuracy induced by considering the exact geometry of the boundary instead of the node-based approximation is also investigated in this study.

2.2 Mathematical formulation

In this section, the formulation of the proposed 2.5D SBM is presented. In a first instance, the acoustic problem is formulated in the 2.5D domain. Secondly, the proposed SBM approach is described in detail in the 2.5D context.

2.2.1 2.5D formulation for acoustic problems

The problem under consideration is the propagation of acoustic waves in a 3D homogeneous isotropic medium Ω. In this problem the pressure field can be modelled in the frequency domain by the well-known Helmholtz equation

$$\nabla^2 p\left(\mathbf{x}\right) + k^2\, p\left(\mathbf{x}\right) = 0 \quad \text{for} \quad \mathbf{x} \in \Omega, \tag{2.1}$$

where $\nabla^2 = \dfrac{\partial^2}{\partial x^2} + \dfrac{\partial^2}{\partial y^2} + \dfrac{\partial^2}{\partial z^2}$ denotes the Laplacian operator, $p(\mathbf{x})$ represents the acoustic pressure at a generic point $\mathbf{x} = \{x, y, z\}^{\mathrm{T}}$ inside the domain, k is the acoustic wavenumber, in a 3D context, equal to ω/c, ω is the angular frequency and c is the sound wave speed in the medium. Two kinds of boundary conditions are usually considered: the Dirichlet boundary condition

$$p(\mathbf{x}) = p_b(\mathbf{x}) \quad \text{for} \quad \mathbf{x} \in \Gamma, \tag{2.2}$$

or the Neumann boundary condition

$$v(\mathbf{x}) = \frac{1}{\mathrm{i}\rho\omega}\frac{\partial p(\mathbf{x})}{\partial \mathbf{n}_b} = v_b(\mathbf{x}) \quad \text{for} \quad \mathbf{x} \in \Gamma, \tag{2.3}$$

where $\mathbf{n}_b$ is the unit outward normal vector to the physical boundary at the point $\mathbf{x}$, p_b and v_b are the prescribed pressure and normal velocity fields at the boundary, respectively, ρ is the medium density and $\mathrm{i} = \sqrt{-1}$. If the geometry of the problem can be considered invariant in the x direction, Eq. (2.1) can be transformed to the wavenumber domain using a Fourier transform of the form

$$\bar{f}\left(k_x, y, z, \omega\right) = \int_{-\infty}^{+\infty} f\left(x, y, z, \omega\right) \mathrm{e}^{\mathrm{i}k_x x}\mathrm{d}x, \tag{2.4}$$

where k_x is the wavenumber associated with the longitudinal direction x and f can be the pressure p or the velocity v fields. The bar notation is used to denote that the variable is expressed in the wavenumber domain. This transformation results in the 2.5D version of the system equations, represented by the 2D modified Helmholtz equation

$$\nabla^2 \bar{p}(\mathbf{x}) - k_a^2\, \bar{p}(\mathbf{x}) = 0 \quad \text{for} \quad \mathbf{x} \in \Omega, \tag{2.5}$$

where $\nabla^2 = \dfrac{\partial^2}{\partial y^2} + \dfrac{\partial^2}{\partial z^2}$, $k_a = \sqrt{k_x^2 - k^2}$ can be seen as the acoustic wavenumber for the 2.5D domain and the generic point $\mathbf{x}$ has become $\mathbf{x} = (y, z)$. The Dirichlet and Neumann boundary conditions can be also transformed to the 2.5D domain, resulting in

$$\bar{p}(\mathbf{x}) = \bar{p}_b(\mathbf{x}) \quad \text{for} \quad \mathbf{x} \in \Gamma, \tag{2.6a}$$

$$\bar{v}(\mathbf{x}) = \frac{1}{\mathrm{i}\rho\omega} \frac{\partial \bar{p}(\mathbf{x})}{\partial \mathbf{n}_b} = \bar{v}_b(\mathbf{x}) \quad \text{for} \quad \mathbf{x} \in \Gamma. \tag{2.6b}$$

2.2.2 SBM for 2.5D acoustic problems

The SBM approximates the solution of the problem in a given domain with a linear combination of fundamental solutions of the governing differential equation. To achieve this, the SBM firstly determines a set of virtual sources that complies with the prescribed boundary conditions evaluated in a set of collocation points placed along the boundary Γ. In contrast to the MFS, the collocation and source points of the SBM are placed on the physical boundary, avoiding the need of an auxiliary one. For the proposed 2.5D SBM approach described in this chapter, it is also assumed that the set of collocation points is geometrically coincident with the set of virtual sources. This scheme is illustrated in Figure 2.1. Virtual sources can be then subsequently used to evaluate the response in the domain. The method employs the OIFs to evaluate the interpolation matrix terms associated with the coincident source–collocation points.

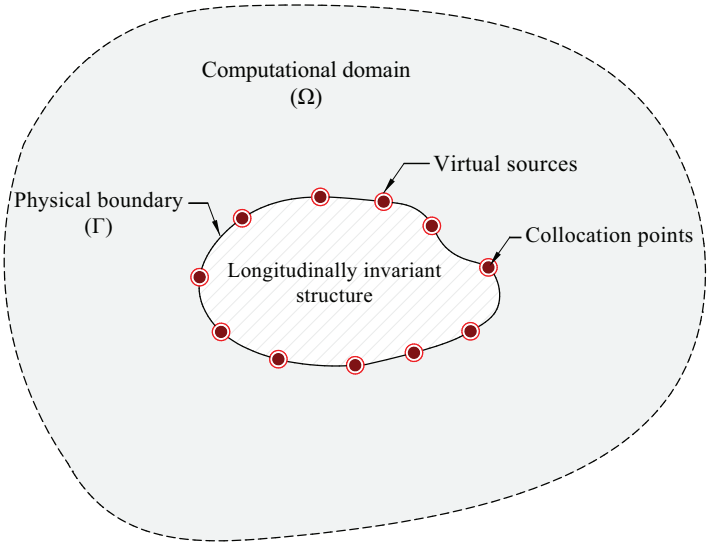

FIGURE 2.1: Schematic sketch of the SBM approach with the adopted sources and collocation points distributions. Red circles denote virtual sources and brown dots represent collocation points.

Thus, the SBM approximates the acoustic pressure $\bar{p}$ and particle velocity $\bar{v}$ at a generic point $\mathbf{x}$ considering the effect of N sources located at positions $\mathbf{s}_j$, being $(j = 1, 2, ..., N)$, resulting in the expressions

$$\bar{p}(\mathbf{x}) = \sum_{j=1}^{N} \alpha_j \, \bar{G}(\mathbf{x}, \mathbf{s}_j, k_a) \quad \text{for} \quad \mathbf{x} \in \Omega, \tag{2.7a}$$

$$\mathrm{i}\rho\omega\bar{v}(\mathbf{x}) = \sum_{j=1}^{N} \alpha_j \, \bar{H}(\mathbf{x}, \mathbf{s}_j, k_a, \mathbf{n}_x) \quad \text{for} \quad \mathbf{x} \in \Omega, \tag{2.7b}$$

where α_j $(j = 1, 2, ..., N)$ are the unknown source strengths and

$$\bar{G}(\mathbf{x}, \mathbf{s}, k_a) = \begin{cases} \dfrac{1}{2\pi} K_0(k_a r) & \text{for} \quad k_a \neq 0, \\ G^{\mathrm{L}}(\mathbf{x}, \mathbf{s}) & \text{for} \quad k_a = 0, \end{cases} \tag{2.8a}$$

$$\bar{H}(\mathbf{x}, \mathbf{s}, k_a, \mathbf{n}_x) = \frac{\partial \bar{G}(\mathbf{x}, \mathbf{s}, k_a)}{\partial \mathbf{n}_x} = \begin{cases} -\dfrac{k_a}{2\pi} K_1(k_a r) \dfrac{\partial r}{\partial \mathbf{n}_x} & \text{for} \quad k_a \neq 0, \\ H^{\mathrm{L}}(\mathbf{x}, \mathbf{s}, \mathbf{n}_x) & \text{for} \quad k_a = 0, \end{cases} \tag{2.8b}$$

are the 2.5D fundamental solutions of the sound pressure and particle velocity, respectively, for the modified Helmholtz equation. K_0 and K_1 are the modified Bessel functions of the second kind of order zero and one, respectively, r is the distance between the source point $\mathbf{s}$ and the arbitrary field point $\mathbf{x}$, $\mathbf{n}_x$ arbitrary unit vector that represents the direction along which the particle velocity is calculated, while $G^{\mathrm{L}}(\mathbf{x},\mathbf{s})$ and $H^{\mathrm{L}}(\mathbf{x},\mathbf{s},\mathbf{n}_x)$ are the fundamental solutions of potential and flux of the 2D Laplace equation, respectively, which take the form

$$G^{\mathrm{L}}(\mathbf{x},\mathbf{s}) = -\frac{1}{2\pi}\ln(r), \tag{2.9a}$$

$$H^{\mathrm{L}}(\mathbf{x},\mathbf{s},\mathbf{n}_x) = \frac{\partial G^{\mathrm{L}}(\mathbf{x},\mathbf{s})}{\partial \mathbf{n}_x} = -\frac{1}{2\pi r}\frac{\partial r}{\partial \mathbf{n}_x}. \tag{2.9b}$$

Eqs. (2.7a) and (2.7b) can be transformed to evaluate the response at the mth collocation point $\mathbf{s}_m$ as

$$\bar{p}(\mathbf{s}_m) = \alpha_m \bar{G}_{mm} + \sum_{j=1, j\neq m}^{N} \alpha_j \, \bar{G}(\mathbf{s}_m, \mathbf{s}_j, k_a) \quad \text{for} \quad \mathbf{s}_m \in \Gamma, \tag{2.10a}$$

$$\mathrm{i}\rho\omega\bar{v}(\mathbf{s}_m) = \alpha_m \bar{H}_{mm} + \sum_{j=1, j\neq m}^{N} \alpha_j \, \bar{H}(\mathbf{s}_m, \mathbf{s}_j, k_a, \mathbf{n}_b) \quad \text{for} \quad \mathbf{s}_m \in \Gamma, \tag{2.10b}$$

where $\bar{G}_{mm}$ and $\bar{H}_{mm}$ are defined as the OIFs of the 2.5D fundamental solutions of Helmholtz equation. Thus, the source strengths for the Dirichlet boundary condition can be obtained by

$$\boldsymbol{\alpha} = \bar{\mathbf{G}}^{-1}\bar{\mathbf{p}}_b, \tag{2.11}$$

while for the Neumann boundary condition they can be computed as

$$\boldsymbol{\alpha} = \bar{\mathbf{H}}^{-1}\bar{\mathbf{v}}_b, \tag{2.12}$$

where $\bar{\mathbf{G}}$ and $\bar{\mathbf{H}}$, the latter one contains $\frac{1}{\mathrm{i}\rho\omega}$, are the SBM interpolation matrices, being their diagonal terms the previously mentioned OIFs, and where $\boldsymbol{\alpha}$ is a vector that collects all source strengths while $\bar{\mathbf{p}}_b$ and $\bar{\mathbf{v}}_b$ are vectors that collect the imposed boundary conditions evaluated at all collocation points.

Due to the same order of the singularities arising for small source-receiver distances

in both fundamental solutions of Laplace and Helmholtz equations, $\bar{G}_{mm}$ and $\bar{H}_{mm}$ can be derived via the asymptotic form of the fundamental solutions of the 2D Laplace equation when the source-receiver distance is small, as [42]

$$\bar{G}_{mm} = \begin{cases} G^{\mathrm{L}}_{mm} - \dfrac{1}{2\pi}\left(\ln\left(\dfrac{k_a}{2}\right) + \gamma\right) & \text{for} \quad k_a \neq 0, \\ G^{\mathrm{L}}_{mm} \quad \text{for} \quad k_a = 0, \end{cases} \tag{2.13a}$$

$$\bar{H}_{mm} = H^{\mathrm{L}}_{mm}, \tag{2.13b}$$

where G^{L}_{mm} and H^{L}_{mm} are respectively the OIFs of the fundamental solutions of 2D Laplace equation and γ is the Euler constant. The detailed derivations of Eqs. (2.13a) and (2.13b) are given in Appendix B. By using the desingularisation provided by the SAB technique, the OIFs for the fundamental solutions of 2D Laplace equation can be derived as [30, 32, 33]

$$G^{\mathrm{L}}_{mm} = \frac{1}{L_m}\int_{\Gamma_s} G^{\mathrm{L}}(\mathbf{x}_m, \mathbf{s}_j)\,\mathrm{d}\Gamma_s(\mathbf{s}) = -\frac{1}{2\pi}\ln\left(\frac{L_m}{2\pi}\right), \tag{2.14a}$$

$$H^{\mathrm{L}}_{mm} = \frac{1}{L_m}\left(1 - \sum_{j=1, j\neq m}^{N} L_j H^{\mathrm{L}}(\mathbf{x}_m, \mathbf{s}_j, \mathbf{n}_b)\right), \tag{2.14b}$$

where L_j is the half length of the curve between the $(j-1)$th collocation or source point and the $(j+1)$th ones, as shown in Figure 2.2. Note that, for the special case when $k_a = 0$, the modified Helmholtz equation reduces to the Laplace equation. Accordingly, the chosen fundamental solutions and OIFs for this particular case should be the ones associated to the Laplace equation.

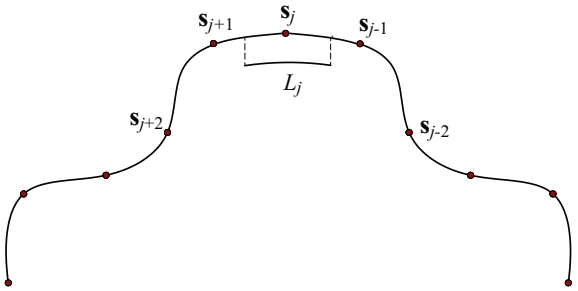

FIGURE 2.2: Schematic configuration of the source points and the corresponding L_j to the jth source. The same configuration applies for the collocation points and the distance L_m.

2.3 Numerical results and discussions

In this section, a study of the validity and accuracy of the proposed 2.5D SBM is presented. Two benchmark examples are used in this regard: the acoustic radiation and wave scattering problems of an infinite cylinder. For these problems, the proposed method is compared with the available analytical solutions as well as three other numerical methods: the 2.5D LE-BEM, the 2.5D QE-BEM and the 2.5D MFS approaches. Both 2.5D LE-BEM and 2.5D QE-BEM approaches have been constructed based on OpenBEM software presented in [43]. In all calculations, the sound wave speed has been considered to be as $c = 340$ m/s, while the density of the medium adopted is $\rho = 1.225$ kg/m^3.

Along this study, the pressure and velocity at $x = 0$ due to unitary harmonic boundary conditions of the general form $\delta(x)\,\mathrm{e}^{\mathrm{i}\omega t}$ are used for comparison purposes and they can be computed from the inverse Fourier transform, corresponding to the Fourier transform defined in Eq. (2.4), as

$$f_0 = f\left(0, y, z, \omega\right) = \frac{1}{2\pi}\int_{-\infty}^{+\infty} \bar{f}\left(k_x, y, z, \omega\right) \mathrm{d}k_x, \tag{2.15}$$

where f could represent either pressure p or velocity v fields, as before. Moreover, the numerical accuracy is proposed to be evaluated in a set of N_t test points by

the root mean square error (RMSE) defined as

$$\mathrm{RMSE} = \frac{\sqrt{\dfrac{1}{N_t}\displaystyle\sum_{k=1}^{N_t} |p_{0n}(\mathbf{x}_k) - p_{0a}(\mathbf{x}_k)|^2}}{\sqrt{\dfrac{1}{N_t}\displaystyle\sum_{k=1}^{N_t} |p_{0a}(\mathbf{x}_k)|^2}}, \tag{2.16}$$

where $p_{0n}(\mathbf{x}_k)$ and $p_{0a}(\mathbf{x}_k)$ are the acoustic pressures computed at the kth test point by the numerical methods and analytical solutions, respectively.

For the implementation of the 2.5D MFS, it is also assumed the same number of virtual sources than collocation points. Regarding both boundary element approaches, the amount of Gaussian points adopted for the integration is 8. To implement the 2.5D SBM, two scenarios are considered. In the first one, it is supposed that the 2.5D SBM uses the exact geometrical data from the curve equation of the boundary to determine the influence lengths L_i, used to calculate the OIFs, and to obtain the normal vectors, required for the computation of the 2.5D fundamental solutions. To facilitate the comparisons, this method is called 2.5D SBM-EGD in this study. In the second scenario, the 2.5D SBM utilises only the nodal geometry data, and it is referred to as 2.5D SBM-NGD approach. Hereby, it is assumed that the 2.5D SBM discretises the boundary to the collocation points by considering a linear shape of the boundary between them. For the 2.5D SBM-NGD approach, the OIFs are calculated numerically considering this approximated boundary.

2.3.1 Example 2.1. Radiation problem of an infinite pulsating cylinder

The problem under consideration in this example is the sound field generated by an infinitely long pulsating cylinder. For this case, the analytical solution of the induced pressure field in the wavenumber-frequency domain is [40]

$$p(r, k_a) = \frac{i\rho\omega v_n K_0(k_a r)}{k_a K_1(k_a a)} \quad \text{for} \quad r \geq a, \tag{2.17}$$

where a is the radius of the cylinder, r is the distance between the evaluation point and the cylinder axis, v_n is the amplitude of the vibration velocity of the cylinder boundary in the radial direction.

In this simulation, a cylinder of unit radius is considered and a radial pulsating displacement of the form $u_n(t) = \delta(x)\mathrm{e}^{\mathrm{i}\omega t}$ is adopted as a Neumann boundary condition. In this boundary condition, the radial displacement is applied uniformly in all points of the boundary. A $\delta(x)$ distribution of the boundary condition in the longitudinal direction is selected since it is an adequate choice to verify the method for any potential longitudinal distribution of the boundary condition. This comes from the fact that a delta distribution $\delta(x)$ transforms into a constant spectrum in the wavenumber domain, allowing for a verification of the method all along the wavenumber spectrum at once. Regarding the 2.5D MFS, the auxiliary boundary where the virtual sources are uniformly distributed is a concentric circle of radius $a - d$, being d the distance between the physical and auxiliary boundaries.

To obtain the RMSE, a set of $N_t = 100$ test points, uniformly distributed along the y-z plane over a circumference of radius $r = 1.1$ m, centred at the cylinder axis, is adopted. Two frequencies are considered for the present RMSE analysis: 100 Hz and 2000 Hz. The pressures p_0 delivered by the different methods at each test point are computed via (2.15), in which the numerical integration is carried out by the trapezoidal rule using a logarithmic sampling for the wavenumber with a total amount of 2^8 sampling points ranging between 10^{-3} rad/m and a higher limit, the latter being specifically determined for each frequency. The number of collocation points or nodes per wavelength (referred to also as N/λ or nodes/wavelength from now on) is varying in the range of $2 - 20$, where $\lambda = 2\pi c/\omega$.

The results of the described error analysis comparing the different numerical approaches are illustrated in Figure 2.3. Overall, it can be observed that with an increasing number of collocation points or boundary nodes at the two selected frequencies, the error associated with each numerical method decreases. Consequently, it can be stated that all methods are verified against the analytical solution for this calculation example. Going into detail in Figure 2.3, it can be observed that the 2.5D MFS shows the most accurate solutions among all methods, with one exception occurring at the frequency of 100 Hz when the MFS is employed with an auxiliary boundary with $d = 0.1$ m. As depicted, the 2.5D MFS

solutions are sensitive to the placement of the fictitious boundary and only using the optimal fictitious boundary leads to much higher accuracy for all N/λ values considered. Comparing the results obtained from the 2.5D SBM and the 2.5D BEM, it is found that the 2.5D SBM-NGD presents a higher numerical accuracy than the 2.5D LE-BEM. On the other hand, the 2.5D SBM-EGD converges rapidly, in this particular case, to the analytical solution. Thus, it can be observed that the 2.5D SBM-EGD shows more accuracy than the 2.5D QE-BEM at the frequency of 2000 Hz for $N/\lambda > 6$. However, this situation is reversed when considering the 2.5D SBM-NGD, which delivers solutions with less accuracy than the 2.5D QE-BEM. The results obtained indicate how strongly the accuracy of the SBM solutions is affected by the exact or the approximated definitions of the boundary shape. This conclusion is specially relevant to denote the strong effect that the uncertainty of the geometrical definition of the boundary has over the accuracy of the proposed method. This is of special importance in the application of the proposed scheme to real engineering problems, which retain an inherent uncertainty on the parametric definition of boundary geometries.

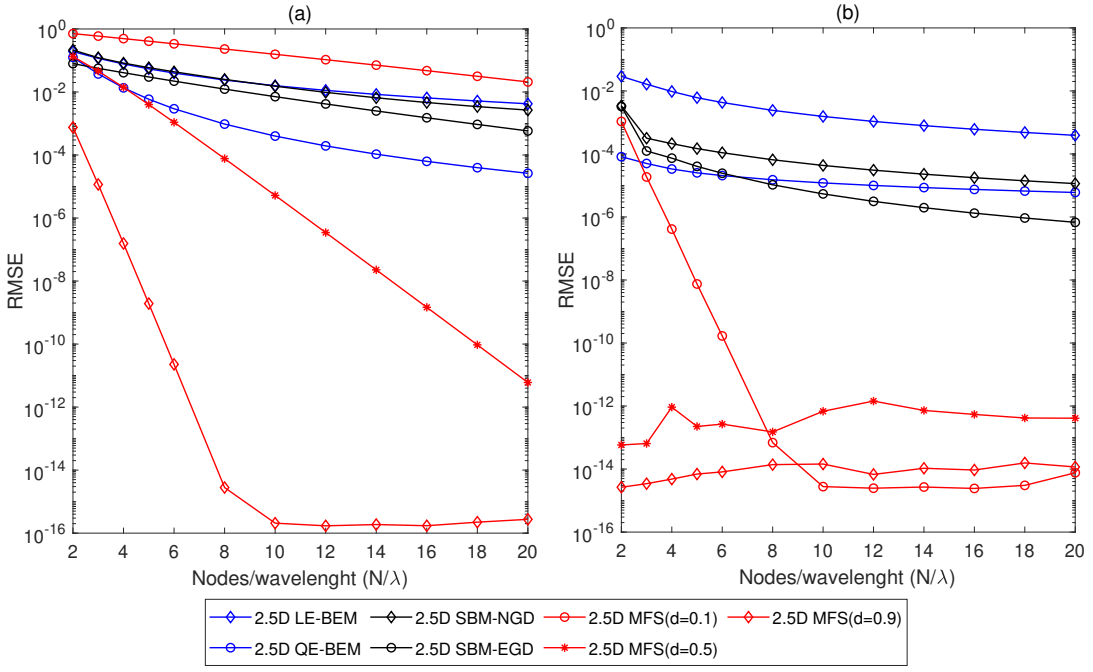

FIGURE 2.3: RMSE analysis of the different methods considered for the radiation problem of an infinite pulsating cylinder obtained at the frequencies of (a) 100 Hz and (b) 2000 Hz. The corresponding upper limit of the wavenumber sampling considered for integration at the frequency of 100 Hz is 10 rad/m. At the frequency of 2000 Hz, the corresponding higher limit is 60 rad/m.

2.3.2 Example 2.2. Wave scattering problem of an infinite cylinder

In this case, the scattering problem of an infinite cylinder subjected to an incident plane wave of the form $\delta(x)\mathrm{e}^{\mathrm{i}ky}\mathrm{e}^{\mathrm{i}\omega t}$ propagating along the horizontal direction y is considered. The analytical solution of the scattering field is [44]

$$p(r,\theta) = -\frac{J_0'(k_a a)}{H_0'(k_a a)} H_0^{(1)}(k_a r) - 2\sum_{n=1}^{\infty} \mathrm{i}^n \frac{J_n'(k_a a)}{H_n'(k_a a)} H_n^{(1)}(k_a r)\cos n\theta \qquad \text{for} \quad r \geq a, \quad 0 \leq \theta \leq 2\pi, \tag{2.18}$$

where (r,θ) represents the location of the evaluation point in the polar coordinate system, J_n is the Bessel function of the order n, $H_n^{(1)}$ is the Hankel function of the first kind of order n and the prime denotes their differentiation with respect to its argument. As before, a cylinder of unit radius has been considered. As in the previous example, the analysis is done for the frequencies of 100 Hz and 2000 Hz. The analytical solution is calculated by using 150 terms for the series appearing in (2.18), which ensures double precision accuracy.

Figure 2.4 displays the results of the RMSE analysis for the wave scattering problem under consideration and for the different numerical methods studied. The same set of test points presented in the previous example is also adopted here. The results illustrate that, at both frequencies selected, the 2.5D MFS approach consistently shows the most accurate performance, expect when its auxiliary boundary is positioned at a distance of $d = 0.1$ m. However, the method strongly relies on an optimal placement of the fictitious boundary, specially at low N/λ. All the other methods stably converge to the analytical solution by increasing N/λ. Comparing the 2.5D SBM and 2.5D BEM approaches, it can be observed that, at the frequency of 100 Hz, similar to Example 1, the 2.5D SBM-NGD competes with the accuracy levels of the 2.5D LE-BEM under the same N/λ. For this frequency, these two methods are delivering errors one or two orders of magnitude higher than the 2.5D QE-BEM at large N/λ. For this problem, as seen in the previous example, the 2.5D QE-BEM shows higher accuracy than the 2.5D SBM-EGD as N/λ increase. On the other hand, at the frequency of 2000 Hz different trends are observed. As N/λ increase, the 2.5D SBM-NGD shows a numerical accuracy

one or two orders of magnitude better than the 2.5D LE-BEM. The 2.5D SBM-NGD also delivers more accurate solutions than the 2.5D QE-BEM at $N/\lambda \leq 6$, a behaviour not observed in Example 1. In contrast to the behaviour observed in Example 1, the 2.5D SBM-EGD exhibits lower accuracy than the 2.5D QE-BEM when $N/\lambda > 6$.

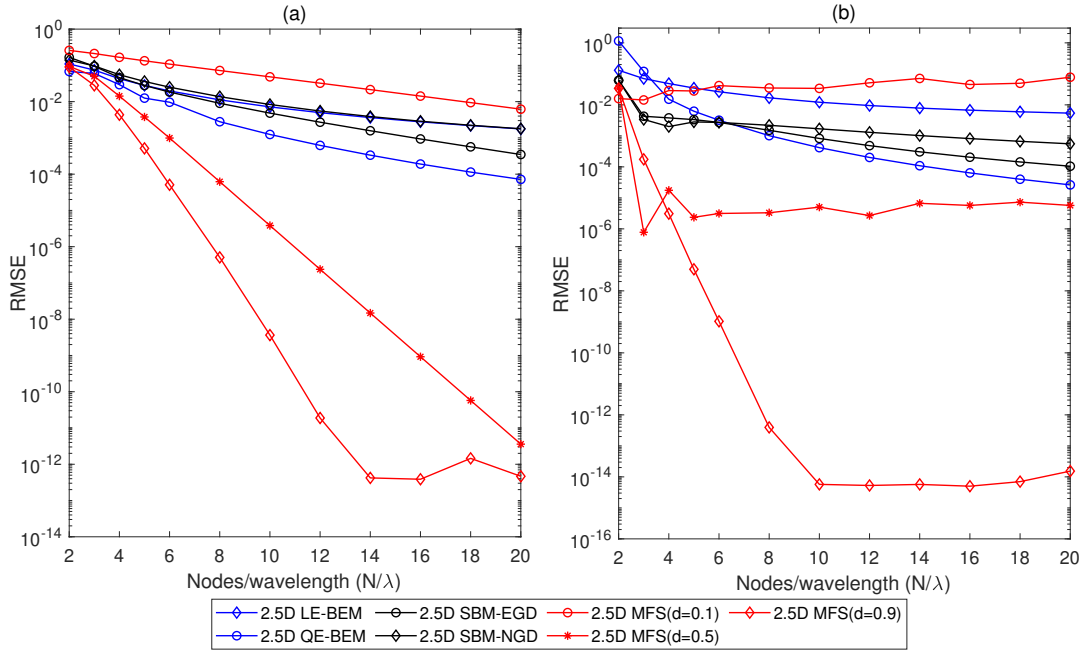

FIGURE 2.4: RMSE analysis of the different methods considered for the scattering problem of an infinite cylinder obtained at the frequencies of (a) 100 Hz and (b) 2000 Hz. The corresponding upper limit of the wavenumber sampling considered for integration at the frequency of 100 Hz is 1.8 rad/m. At the frequency of 2000 Hz, the corresponding higher limit is 36.9 rad/m.

2.4 Conclusions

This chapter presents a 2.5D SBM approach for the simulation of acoustic radiation and scattering problems in the framework of longitudinally infinite and invariant structures. The method determines the OIFs associated with the 2.5D fundamental solutions of the Helmholtz equation by means of the OIFs of the fundamental solutions of the Laplace equation, taking advantage of the same singularity order in both fundamental solutions. These OIFs are derived by applying a desingularisation procedure based on the SAB technique. The proposed 2.5D

SBM has been implemented considering two different calculation scenarios of the influence lengths and unit normals. The first scenario is considering the exact shape equation of the boundary while the second one performs a nodal-based approximation, being these methods referred to as the 2.5D SBM-EGD and the 2.5D SBM-NGD, respectively. The feasibility and accuracy of the present schemes are studied through two benchmark examples: the acoustic radiation and wave scattering problems of an infinitely long cylinder. In order to make a detailed assessment of the proposed 2.5D SBM schemes, the available analytical solutions and other numerical methodologies including the 2.5D MFS and the 2.5D BEM with linear and quadratic elements are employed and compared in terms of numerical accuracy and computational efficiency.

The detailed comparison performed demonstrates the validity and accuracy of the present 2.5D SBM schemes. As a newfound conclusion, it is indicated that the 2.5D SBM-NGD provides higher numerical accuracy compared to the 2.5D LE-BEM but lower than the 2.5D QE-BEM. On the other hand, the 2.5D SBM-EGD consistently delivers higher accuracy levels compared to the 2.5D LE-BEM across all scenarios. It also competes with the accuracy levels of the 2.5D QE-BEM at high frequencies being the scattering problem a case where the 2.5D SBM-EGD is not reaching the quadratic BEM performance at $N/\lambda>6$. It is worth noting that, although the 2.5D MFS performs the most accurate results in the circular domain examples, its solutions are highly sensitive to the optimal placement of the fictitious boundary, demonstrating the robustness issues of that method with respect to the other ones studied. It should be highlighted that the numerical accuracy of the 2.5D SBM solutions is intensely affected by the exact or approximated definitions of the boundary shape. The results indicate that choosing the approximate nodal data of the boundary over its exact one significantly reduces the accuracy and convergence trend of the 2.5D SBM. This is particularly crucial when applying the proposed scheme to real engineering problems, where accurately defining the boundary geometry poses a significant challenge, prompting a preference for the approximated boundary definition.

In terms of computational efficiency, the present 2.5D SBM schemes inherits various advantages with respect to the former methods. Due to its meshless nature, the proposed 2.5D SBM scheme performs more efficiently than equivalent 2.5D

BEM approaches thanks to avoiding two procedures: the construction of a boundary mesh and the sophisticated numerical integration over the singularities that BEM approaches normally carry out. Furthermore, the method is found to be more robust than the 2.5D MFS, since it does not need to deal with the troublesome placement of the fictitious boundary which is revealed to be a complex and time-consuming procedure especially in the case of irregular boundary geometries.

Overall, the 2.5D SBM is an accurate and computationally fast numerical method and it is suggested as a potential alternative to other available 2.5D numerical methods for acoustic analysis.

Chapter 3

Application of the 2.5D singular boundary method for assessing the acoustic performance of thin barriers

This chapter is mainly dedicated to investigate the applicability and feasibility of the proposed 2.5D SBM approach, outlined in Chapter 2, to address practical engineering problems regarding to the propagation of acoustic waves in unbounded domains. Specifically, this chapter focuses on studying the problem of point source diffraction in the presence of thin noise barriers. To tackle this particular problem, the proposed 2.5D SBM is implemented considering a half-space medium instead of a fully unbounded one. The investigation is conducted for two distinct scenarios: the first involves a non-moving source, while the second scenario deals with a moving source problem. Furthermore, the chapter presents a study on the potential use of noise-absorbing materials combined with the barrier, which are introduced by imposing acoustic absorption boundary conditions within the framework of the developed 2.5D SBM approach.

The chapter is organised as follows. In Section 3.1, a brief literature overview of the importance of the barrier utilisation in reduction of noise pollution, along with the numerical strategies to simulate this sort of problems are presented. Section 3.2

outlines the mathematical formulation of the proposed 2.5D SBM approach when dealing with half-space problems. Based on this formulation, the acoustic response due to non-moving and moving sources is derived. Section 3.3 discusses the numerical results of the simulations conducted, including non-moving and moving source scenarios, subsequently. Finally, the chapter ends in Section 3.4, providing key insights drawn from the earlier discussions.

3.1 Introduction

Nowadays, due to the extensive construction of roadways, railways, and mass rapid transit systems worldwide, many developed cities and metropolitan areas are encountering problems related to inevitable proximity of roads and rail tracks to residential areas. A prominent issue arising from this proximity is the noise generated by the passage of vehicles and trains, whereby airborne noise travels through the air and impacts nearby buildings. Consequently, traffic noise pollution is being emerged as a critical urban sustainability concern that significantly influences human health and, overall, quality of life. Within this context, there is a growing emphasis on devising effective strategies to mitigate noise resulting from traffic. Scientific community and technical research are increasingly focusing on this matter, leading to the proposal of various practical solutions. One such approach involves the installation of barriers placed between the noise source and the nearby buildings, which is one of the most common protection solutions used against traffic noise pollution.

In recent years, many empirical and numerical methods have been employed to evaluate the effectiveness of sound barriers in reducing noise levels. Among these methods, the BEM has gained widespread utilisation for achieving this objective. This preference for the BEM stands up from its capability to efficiently analyse acoustic barriers characterised by intricate shapes and complex boundary conditions. Duhamel [45] employed the BEM to calculate the sound pressure distribution around a longitudinally invariant noise barrier with arbitrary cross-section and, through this approach, a comparison was presented to assess the effectiveness of barriers with different cross-sectional shapes. Ishizuka and Fujiwara [46] conducted experiments to assess the effectiveness of road traffic noise barriers with different shapes and surface characteristics, employing the BEM in a 2D framework. Their findings demonstrated that incorporating absorbing and soft edges significantly enhances the barrier efficiency. However, it is found that barrier shape modifications result in a slight improvement in efficiency. The BEM, formulated in the a 2.5D framework, has also been employed for simulating problems related to 3D acoustic wave diffraction by barriers [47, 48]. The concept of the dual BEM, a formulation that combines both standard and hyper-singular integral equations to

deal with radiation and scattering problems involving thin bodies, has been proposed to evaluate the acoustic effectiveness of thin noise barriers [49, 50]. More recently, some investigations have employed isogeometric analysis (IGA) in the context of the BEM, introducing the IGA-BEM strategy. This approach has been utilised to study the shape optimisation of acoustic barriers, offering notable advantages by overcoming the challenges associated with time-consuming meshing and re-meshing strategies during the optimisation process [51, 52].

In the last years, meshless methods have been employed alongside the BEM to tackle problems related to acoustic barriers. Various investigations have discussed the potential of the MFS to address problems involving barriers. Costa et al. [53] applied the MFS to assess the acoustic behaviour of thin T-shaped barriers. The model was developed by employing appropriate Green's functions, derived from the image-source technique, which enable limiting the number of discretised surfaces and reducing the computational cost associated with the model. Veloso et al. [54] employed the MFS to evaluate the effectiveness of noise barriers based on the concept of periodic metamaterials, in this case implemented with cylinders covered by porous and granular materials. The periodic fundamental solutions were introduced in the context of the proposed MFS model to impose the periodicity characteristics of the resulting acoustic field. Martins et al. [55] proposed the application of the MFS to evaluate the insertion loss provided by sonic crystal barriers when mitigating traffic noise in a 2D simulation context. The results obtained show that the MFS is particularly well suited to the requirements of the problem, largely due to the geometric characteristics of the circular shaped barriers employed, showing clear advantages regarding discretisation procedures and computational efficiency, when compared to BEM- and FEM-based approaches. Godinho et al. [56] proposed to combine the MFS with an adaptive-cross approximation (ACA) strategy introducing an effective ACA–MFS technique in order to efficiently analyse very large sonic crystal barriers, which can incorporate several hundreds of scatterers. Although previous studies have demonstrated the efficiency of MFS when dealing with noise barrier-related problems, it is also known that the method requires modification strategies to manage the complexity of barrier geometries.

Aside the MFS, the SBM has also been found as a promising meshless alternative strategy for the numerical simulation of problems related to sound barriers. However, due to its recent development, there are relatively few studies in the literature that explore its applicability to noise barrier-related problems. Wei et al. [41] employed the 2.5D SBM to solve the problem of point source diffraction in the presence of a T-shaped thin barrier. Their numerical results show the distinct advantages of the 2.5D SBM, including its formulation simplicity and the reduction of computer memory needs, in comparison to the 3D FEM and 3D SBM. In another study, Wei et al. [57] applied the 2.5D SBM in conjunction with the direct differentiation method (DDM) as a method to develop acoustic sensitivity analysis for the scattering problem of a rigid T-shaped barrier. The numerical experiments demonstrate that the proposed 2.5D SBM-DDM is able to obtain the accurate pressure sensitivities with less CPU time and memory compared with numerical methods formulated in a 3D framework, including the 3D FEM and 3D SBM. Recently, Liu and Wang [58] has proposed a novel SBM-based technique, in a 2D framework, for the thickness optimisation of porous materials distributed on sound barriers. In the proposed scheme, the Burton–Miller-type SBM is utilised to simulate the external sound field problem, while the method of moving asymptotes is employed to solve the corresponding optimisation problem. Numerical simulations were conducted for two case studies, involving T-shaped and Y-shaped sound barriers. The results show a good agreement between the proposed algorithm and a 2D FEM, indicating the reliability and effectiveness of this novel approach.

Nevertheless, the SBM encounters fully populated coefficient matrix in mid-high frequency 3D acoustic problems, demanding at least six discretisation points per wavelength to deliver accurate solution [5, 59] and resulting in huge computational costs when dealing with complex/large systems arising in engineering applications. Despite the advantage of discretisation simplicity and that no integration along the boundary is required, the SBM is still computationally expensive when simulating problems of this type. When the problem in hands can be approximated to a longitudinally invariant system, 2.5D schemes are the ideal choice to save computational effort. This is the case of the acoustic performance of noise barriers, a problem that can be naturally handled with 2.5D strategy. In this context, this chapter specifically investigates the applicability of the 2.5D SBM approach,

presented in the previous chapter, for modelling the problem of acoustic point source diffraction in the presence of noise thin barriers. To tackle this problem, the proposed 2.5D SBM approach has been adapted to account for a half-space acoustic medium instead of an entirely unbounded one by using the corresponding fundamental solutions based on the image-source technique. Two specific point source are investigated in the analyses: the first one considers a stationary sound source, while the second deals with a moving one. Moreover, this study further investigates the feasibility of using noise-absorbing materials distributed on barriers which involves imposing acoustic absorption boundary conditions in the context of the developed 2.5D SBM approach.

3.2 Mathematical formulation

3.2.1 Problem specification

Let's consider the problem of acoustic wave propagation in a 3D homogeneous isotropic medium Ω, extended infinitely along the x direction, in the presence of a thin barrier situated above an infinite plane ground, as illustrated in Figure 3.1. For this problem, when the system equations are transformed into the 2.5D domain, as described in Section 2.2.1, the representation of the pressure field in the wavenumber-frequency domain is obtained through the 2D modified Helmholtz equation as

$$\nabla^2 \bar{p}(\mathbf{x}) - k_a^2 \, \bar{p}(\mathbf{x}) = 0 \quad \text{for} \quad \mathbf{x} \in \Omega. \tag{3.1}$$

Due to the nature of the problem described, employing half-space fundamental solutions to model the unbounded domain is more adequate than using full-space ones since they naturally handle the ground surface. Using these fundamental solutions, the ground is treated as an infinite plane on which the sound waves are reflected. Half-space fundamental solutions can be derived using the image-source technique. When the ground is assumed to be perfectly reflecting, an hypothesis adopted here, the mirrored source is equal to the original one. Thus, by introducing an image source mirrored relative to the horizontal axis y, as depicted in Figure 3.2,

the associated 2.5D fundamental solutions for addressing such scenarios can be represented as

$$\bar{G}(\mathbf{x},\mathbf{s},k_a) = \begin{cases} \dfrac{1}{2\pi}\left(K_0(k_a r) + K_0(k_a r')\right) & \text{for} \quad k_a \neq 0, \\ -\dfrac{1}{2\pi}\left(\ln(r) + \ln(r')\right) & \text{for} \quad k_a = 0, \end{cases} \tag{3.2a}$$

$$\bar{H}(\mathbf{x},\mathbf{s},k_a,\mathbf{n}_x) = \begin{cases} -\dfrac{k_a}{2\pi}\left(K_1(k_a r) + K_1(k_a r')\right)\dfrac{\partial r}{\partial \mathbf{n}_x} & \text{for} \quad k_a \neq 0, \\ -\dfrac{1}{2\pi}\left(\dfrac{1}{r} + \dfrac{1}{r'}\right)\dfrac{\partial r}{\partial \mathbf{n}_x} & \text{for} \quad k_a = 0, \end{cases} \tag{3.2b}$$

where $r = \sqrt{(x-x_0)^2 + (y-y_0)^2}$ and $r' = \sqrt{(x-x_0)^2 + (y+y_0)^2}$.

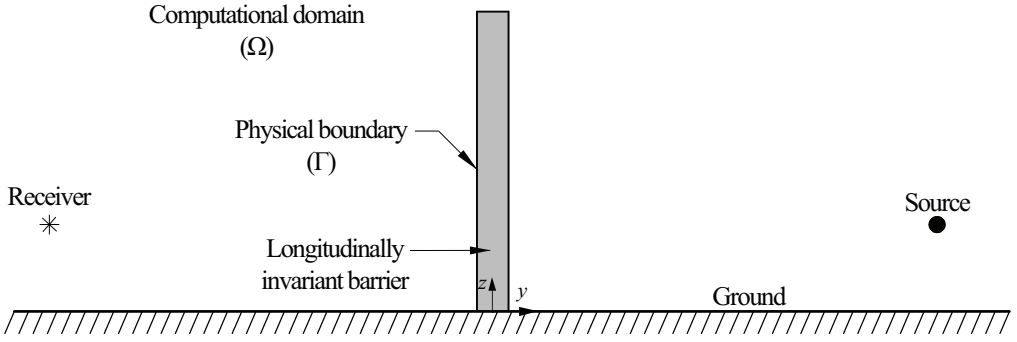

FIGURE 3.1: Geometry of the problem under consideration.

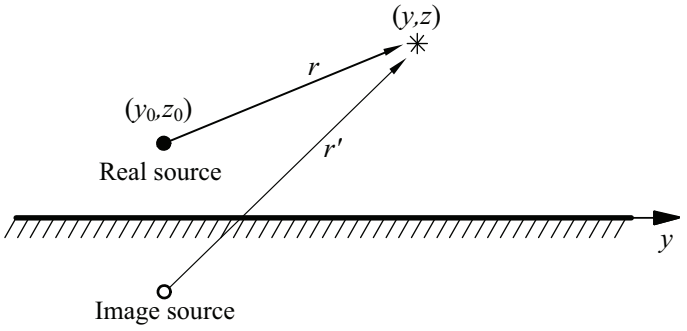

FIGURE 3.2: Illustrative representation of the image-source technique employed in half-space domain problems.

The incident wave field at the barrier due to the external harmonic pressure source positioned at $\mathbf{x}_0$ should also be determined using the half-space fundamental solutions. Thus, accounting for a perfectly reflecting ground, the incident pressure field in wavenumber-frequency domain at any arbitrary point $\mathbf{x}$ can be given by

$$\bar{p}_{\text{inc}}\left(\mathbf{x}, \mathbf{x}_0\right) = \frac{\mathrm{i}}{4}\left(H_0^{(1)}\left(k_a r\right) + H_0^{(1)}\left(k_a r'\right)\right). \tag{3.3}$$

For the above-stated problem, three different boundary conditions for the barrier free surfaces are usually considered:

1. A soft barrier. This is the Dirichlet boundary condition where the total pressure is zero at the boundary. It should be pointed out that the soft surface represents ideal conditions and no practical materials are presenting these conditions over the whole frequency range.

2. A hard barrier. This is the Neumann boundary condition where the normal component of the particle velocity is zero at the boundary.

3. An absorbing barrier. This is the Robin boundary condition that can be used to model barriers that included absorbing materials at their surfaces.

The Dirichlet, Neumann and Robin boundary conditions can be represented in the wavenumber-frequency domain as

$$\begin{aligned} &\bar{p}_{\text{tot}}(\mathbf{x}) = \bar{p}_{\text{inc}}(\mathbf{x}) + \bar{p}_{\text{dif}}(\mathbf{x}) = 0 \quad \text{for} \quad \mathbf{x} \in \Gamma, \\ &\bar{p}_{\text{dif}}(\mathbf{x}) = -\bar{p}_{\text{inc}}(\mathbf{x}) = \bar{p}_b(\mathbf{x}) \quad \text{for} \quad \mathbf{x} \in \Gamma, \end{aligned} \tag{3.4}$$

$$\begin{aligned} &\frac{\partial \bar{p}_{\text{tot}}(\mathbf{x})}{\partial \mathbf{n}_b} = \frac{\partial \bar{p}_{\text{inc}}(\mathbf{x})}{\partial \mathbf{n}_b} + \frac{\partial \bar{p}_{\text{dif}}(\mathbf{x})}{\partial \mathbf{n}_b} = 0 \quad \text{for} \quad \mathbf{x} \in \Gamma, \\ &\frac{\partial \bar{p}_{\text{dif}}(\mathbf{x})}{\partial \mathbf{n}_b} = -\frac{\partial \bar{p}_{\text{inc}}(\mathbf{x})}{\partial \mathbf{n}_b} = \mathrm{i}\rho\omega\bar{v}_b(\mathbf{x}) \quad \text{for} \quad \mathbf{x} \in \Gamma, \end{aligned} \tag{3.5}$$

$$\begin{aligned}
&\frac{\partial \bar{p}_{\mathrm{tot}}(\mathbf{x})}{\partial \mathbf{n}_b} + \mathrm{i}Z\bar{p}_{\mathrm{tot}}(\mathbf{x}) = 0 \quad \text{for} \quad \mathbf{x} \in \Gamma, \\
&\left(\frac{\partial \bar{p}_{\mathrm{inc}}(\mathbf{x})}{\partial \mathbf{n}_b} + \frac{\partial \bar{p}_{\mathrm{dif}}(\mathbf{x})}{\partial \mathbf{n}_b}\right) + \mathrm{i}Z\left(\bar{p}_{\mathrm{inc}}(\mathbf{x}) + \bar{p}_{\mathrm{dif}}(\mathbf{x})\right) = 0 \quad \text{for} \quad \mathbf{x} \in \Gamma, \\
&\frac{\partial \bar{p}_{\mathrm{dif}}(\mathbf{x})}{\partial \mathbf{n}_b} + \mathrm{i}Z\bar{p}_{\mathrm{dif}}(\mathbf{x}) = -\frac{\partial \bar{p}_{\mathrm{inc}}(\mathbf{x})}{\partial \mathbf{n}_b} - \mathrm{i}Z\bar{p}_{\mathrm{inc}}(\mathbf{x}) = \mathrm{i}\rho\omega\bar{v}_b(\mathbf{x}) + \mathrm{i}Z\bar{p}_b(\mathbf{x}) \quad \text{for} \quad \mathbf{x} \in \Gamma,
\end{aligned} \tag{3.6}$$

respectively, where $\bar{p}_{\mathrm{tot}}$ and $\bar{p}_{\mathrm{dif}}$ denote the total pressure field and the diffracted pressure field, respectively, and Z represents the surface impedance parameter which relates the boundary conditions as

$$Z = \frac{\bar{p}_b(\mathbf{x})}{\bar{v}_b(\mathbf{x})} \quad \text{for} \quad \mathbf{x} \in \Gamma. \tag{3.7}$$

3.2.2 2.5D SBM for half-space medium

The previously proposed 2.5D SBM, detailed in Chapter 2, is now applied to solve the above-specified problem. A general representation of the 2.5D SBM approach utilised for this problem is schematically illustrated in Figure 3.3.

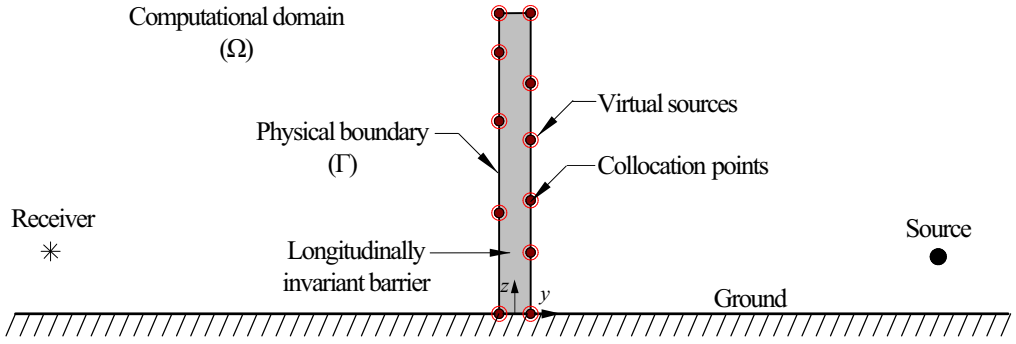

FIGURE 3.3: Schematic representation of the 2.5D SBM approach adopted with an example of collocation and source points distributions. Collocation points are denoted by brown solid dots while virtual sources are indicated by red circles.

Thus, the system responses including acoustic pressure and particle velocity can be obtained using Eqs. (2.7a) and (2.7b), respectively, taking into account that

the half-space 2.5D fundamental solutions specified in Eqs. (3.2a) and (3.2b) are replacing with the full-space ones. Note that the calculation of unknown source strengths and associated OIFs for the cases with the Dirichlet and Neumann boundary conditions in the current half-space problem follows the same procedures outlined in the previous chapter. However, for scenarios involving the Robin boundary condition, a combination of the Dirichlet and Neumann boundary conditions must be established for the relevant collocation points, resulting in

$$\begin{aligned} &\mathrm{i}\rho\omega\bar{v}(\mathbf{s}_m) + \mathrm{i}Z\bar{p}(\mathbf{s}_m) = \alpha_m \left(\mathrm{i}Z\bar{G}_{mm} + \bar{H}_{mm}\right) + \\ &\sum_{j=1, j\neq m}^{N} \alpha_j \left[\mathrm{i}Z\bar{G}(\mathbf{s}_m, \mathbf{s}_j, k_a) + \bar{H}(\mathbf{s}_m, \mathbf{s}_j, k_a, \mathbf{n}_b)\right] \quad \text{for} \quad \mathbf{s}_m \in \Gamma. \end{aligned} \tag{3.8}$$

Consequently, the source strengths when the Robin boundary condition is imposed can be obtained as

$$\boldsymbol{\alpha} = \left(\frac{Z}{\rho\omega}\bar{\mathbf{G}} + \bar{\mathbf{H}}\right)^{-1} \left(\frac{Z}{\rho\omega}\bar{\mathbf{p}}_b + \bar{\mathbf{v}}_b\right), \tag{3.9}$$

note that within the matrix $\bar{\mathbf{H}}$, $(\mathrm{i}\rho\omega)^{-1}$ is incorporated.

3.2.3 Moving sources

In the previous sections, the mathematical expressions describing the acoustic responses of the system in the wavenumber-frequency domain were presented. This formulation allows for obtaining the response of the system due to sources with any time and longitudinal space distributions. Specifically, moving sources can be naturally handled in this domain. In this section, the formulation of the pressure field response around the barrier due to the action of a moving source in the longitudinal direction is presented in the basis of the wavenumber-frequency domain responses obtained with the proposed 2.5D SBM.

The wave equation for the sound pressure field in the time domain produced by a source moving along the longitudinal direction can be mathematically expressed as

$$\nabla^2 p\left(\mathbf{x}, t\right) - \frac{1}{c^2}\frac{\partial^2 p\left(\mathbf{x}, t\right)}{\partial t^2} = s(t)\,\delta\left(\mathbf{x} - \mathbf{x}_0(t)\right) \quad \text{for} \quad \mathbf{x} \in \Omega, \tag{3.10}$$

where $p\left(\mathbf{x},t\right)$ is the acoustic pressure evaluated at a generic point $\mathbf{x}$ in space and time t and where $\mathbf{x}_0 = \{x_0(t), y_0, z_0\}^{\mathrm{T}}$ denotes the position of the source, which has an amplitude of $s(t)$. Taking into account the longitudinal invariance of the system, a double Fourier transform can be applied on Eq. (3.10), leading to

$$\begin{aligned}
&\nabla^2 \bar{p}\left(k_x,y,z,\omega\right) - k_a\,\bar{p}\left(k_x,y,z,\omega\right) = \\
&= \int_{-\infty}^{\infty}\int_{-\infty}^{\infty} s(t)\delta\left(\mathbf{x}-\mathbf{x}_0(t)\right)\mathrm{e}^{-\mathrm{i}\omega t}\mathrm{e}^{\mathrm{i}k_x x}\mathrm{d}x\mathrm{d}t \\
&= \left(\int_{-\infty}^{\infty}\int_{-\infty}^{\infty} s(t)\delta\left(x-x_0(t)\right)\mathrm{e}^{\mathrm{i}k_x x}\mathrm{e}^{-\mathrm{i}\omega t}\mathrm{d}x\mathrm{d}t\right)\delta\left(y-y_0\right)\delta\left(z-z_0\right) \\
&= S\left(k_x,\omega\right)\,\delta\left(y-y_0\right)\delta\left(z-z_0\right),
\end{aligned} \tag{3.11}$$

where

$$S\left(k_x,\omega\right) = \int_{-\infty}^{\infty} s(t)\,\mathrm{e}^{\mathrm{i}k_x x_0(t)}\,\mathrm{e}^{-\mathrm{i}\omega t}\,\mathrm{d}t. \tag{3.12}$$

By applying a double inverse Fourier transform over ω, the time domain signal of the pressure recorded at the receiver can be obtained as

$$p\left(\mathbf{x},t\right) = \frac{1}{(2\pi)^2}\int_{-\infty}^{\infty}\int_{-\infty}^{\infty} S\left(k_x,\omega\right)q\left(k_x,y,z,\omega\right)\mathrm{e}^{-\mathrm{i}k_x x}\,\mathrm{e}^{\mathrm{i}\omega t}\mathrm{d}k_x\mathrm{d}\omega, \tag{3.13}$$

where $q\left(k_x,y,z,\omega\right) = q\left(y,z,k_a\right)$ is the pressure response in the wavenumber-frequency domain due to a source of the form $\delta\left(y-y_0\right)\delta\left(z-z_0\right)\mathrm{e}^{\mathrm{i}\omega t}\mathrm{e}^{-\mathrm{i}k_x x}$ that can be obtained as described in previous sections.

Let's consider a scenario of uniform motion with a constant speed U, described by the expression $x_0(t) = x_0 + Ut$. Thus, Eq. (3.12) can be rewritten as

$$S\left(k_x,\omega\right) = \int_{-\infty}^{\infty} s(t)\,\mathrm{e}^{\mathrm{i}k_x(x_0+Ut)}\,\mathrm{e}^{-\mathrm{i}\omega t}\,\mathrm{d}t = \mathrm{e}^{\mathrm{i}k_x x_0}\,\hat{s}\left(\omega-k_x U\right). \tag{3.14}$$

where $\hat{s}$ denotes the Fourier transform of s from time to frequency domain. The speed of the source induces a frequency shift, known as the Doppler effect. Consequently, the pressure can be expressed as

$$p\left(\mathbf{x},t\right) = \frac{1}{(2\pi)^2}\int_{-\infty}^{\infty}\int_{-\infty}^{\infty}\mathrm{e}^{-k_x x_0}\,\hat{s}\left(\omega-k_x U\right)q\left(y,z,k_a\right)\mathrm{e}^{-\mathrm{i}k_x x}\,\mathrm{e}^{\mathrm{i}\omega t}\,\mathrm{d}k_x\mathrm{d}\omega. \tag{3.15}$$

For a harmonic source with a unit amplitude pulsating at the angular frequency ω_0, the source signal is expressed as $s(t) = \cos(\omega_0 t) = \mathrm{Re}(\mathrm{e}^{\mathrm{i}\omega_0 t})$. It can be demonstrated that the response to this source can be obtained by adopting $s(t) = \mathrm{e}^{\mathrm{i}\omega_0 t}$ and taking the real part of the resulting response. Consequently, the response to the considered harmonic source can be written from Eq. (3.15) as

$$\begin{aligned} p\left(\mathbf{x},t\right) &= \mathrm{Re}\left[\frac{1}{2\pi}\int_{-\infty}^{\infty}\int_{-\infty}^{\infty}\mathrm{e}^{-k_x x_0}\,\delta\left(\omega-\omega_0-k_x U\right)q\left(y,z,k_a\right)\mathrm{e}^{-\mathrm{i}k_x x}\,\mathrm{e}^{\mathrm{i}\omega t}\,\mathrm{d}k_x\mathrm{d}\omega\right] \\ &= \mathrm{Re}\left[\frac{\mathrm{e}^{\mathrm{i}\omega_0 t}}{2\pi}\int_{-\infty}^{\infty}\mathrm{e}^{\mathrm{i}k_x(x_0+U-x)}\,q\left(y,z,\sqrt{\left(\frac{\omega_0+k_x U}{c}\right)^2-{k_x}^2}\right)\mathrm{d}k_x\right], \end{aligned} \tag{3.16}$$

where the time evolution of response amplitude can be simply written as

$$A(t) = \frac{1}{2\pi}\mathrm{Re}\left[\int_{-\infty}^{\infty}\mathrm{e}^{\mathrm{i}k_x(x_0+U-x)}\,q\left(y,z,\sqrt{\left(\frac{\omega_0+k_x U}{c}\right)^2-{k_x}^2}\right)\mathrm{d}k_x\right]. \tag{3.17}$$

3.3 Numerical results and discussion

In this section, a study on the feasibility of the proposed 2.5D SBM to solve practical acoustic scenarios involving noise barriers in the context of road and rail transport applications is presented. In this respect, the proposed method is employed to analyse the problem of a point source diffraction in the presence of a noise thin barrier. Figure 3.4 illustrates a schematic configuration of the problem currently under investigation. In this analysis, a straight-wall barrier of 2 m height having a uniform thickness of 0.1 m located over a rigid ground is considered. The base of the barrier is located at the origin of coordinates and its geometry is assumed to be constant along the x direction. To study the problem of non-moving source diffraction on the barrier, a point source is located at the position $(0, 2, 0.5)$ m and the pressure is calculated at a receiver positioned at $(0, -2, 0.5)$ m.

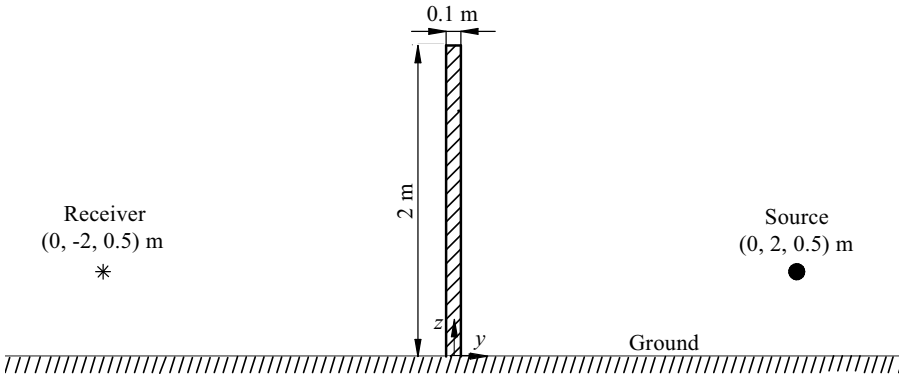

FIGURE 3.4: Schematic sketch depicting the straight-wall noise barrier, the acoustic point source under consideration, and the selected receiver point.

Considering the potential utilisation of the barrier composed of various materials, this analysis also studies the influence of different material impedances on the acoustic response of the barrier. To preserve the generality of the developments, the material impedance can be characterised using the absorption coefficient (α), taking into account $p_r = R\,p_{\text{inc}}$ and $v_r = R\,v_{\text{inc}}$, where R is determined by $R = \sqrt{1-\alpha}$. Here, R represents the reflection coefficient, p_r and p_{inc} denote the reflected pressure and incident pressure, respectively, and v_r and v_{inc} correspond to the reflected velocity and incident velocity, respectively. In other words, the material impedance (Z) can be expressed as [55, 60]

$$Z = \frac{p_{\text{inc}} + R\,p_{\text{inc}}}{v_{\text{inc}} + R\,v_{\text{inc}}} = \frac{p_{\text{inc}}}{v_{\text{inc}}}\left(\frac{1+\sqrt{1-\alpha}}{1-\sqrt{1-\alpha}}\right) = \rho c\left(\frac{1+\sqrt{1-\alpha}}{1-\sqrt{1-\alpha}}\right). \tag{3.18}$$

The analysis is conducted for various values of α, including $\alpha = 0$ which corresponds to the scenario of a totally rigid barrier, as well as $\alpha = 0.1$, 0.3 and 0.5. For cases where $\alpha \neq 0$, the calculations are carried out considering the Robin boundary condition at the barrier boundary.

In order to implement the 2.5D SBM method for this problem, a total of 168 collocation points, uniformly distributed along the barrier boundary, are considered. Moreover, a set of source points is positioned to coincide entirely with the collocation points. Furthermore, the 2.5D QE-BEM is used as the reference model. In this evaluation, the 2.5D QE-BEM is employed with a very dense mesh considering $N/\lambda = 100$. This quite large density selection was made to guarantee a reference

solution capable of providing highly accurate results. The calculations have been conducted at two selected frequencies considering that the source pulsates at 200 Hz in the first case and 500 Hz in the second one.

Figure 3.5 displays the results obtained for the pressure amplitude at different longitudinal positions for the scenario where $\alpha = 0$, representing a totally rigid barrier under investigation. It can be observed, in a general point of view, that the proposed 2.5D SBM exhibits a good agreement with the reference solution, the 2.5D QE-BEM, across the two selected frequencies. Considering a scenario without presence of the barrier, it is also interesting to note that the addition of the barrier results in a significant decrease in pressure level at receiver.

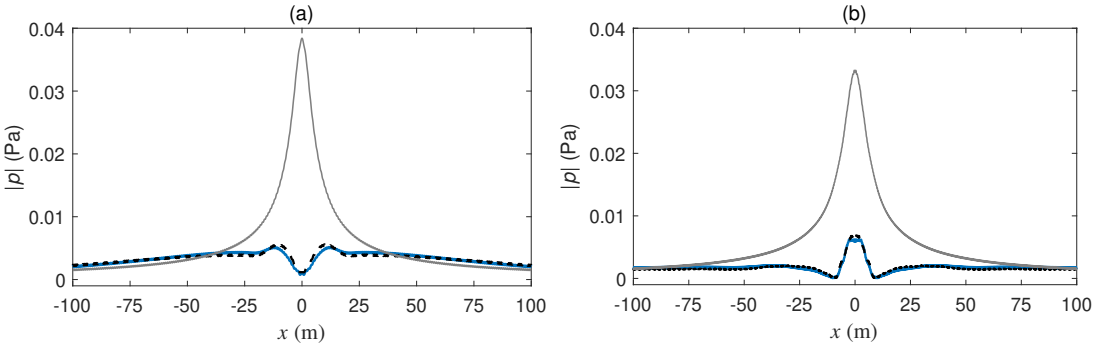

FIGURE 3.5: Sound pressure at the receiver point calculated by the 2.5D QE-BEM (solid blue line) and the proposed 2.5D SBM (dashed black line) at the frequencies of (a) 200 Hz and (b) 500 Hz, for the case when $\alpha = 0$. Solid gray lines depict results obtained when the barrier is not taken into account.

In Figure 3.6, which presents the results delivered by the 2.5D SBM for various sound absorption coefficients at the selected frequencies, a noticeable trend is found. As the sound absorption coefficient increases, the pressure levels at the receiver decrease steadily. Indeed, considering the results for the higher absorption coefficient i.e. $\alpha = 0.5$, it can be seen that lowest sound pressure levels are computed, which demonstrates a remarkable improvement when compared with the results computed for $\alpha = 0$. Similar trends have been documented in prior studies addressing barriers made of diverse materials [53, 55].

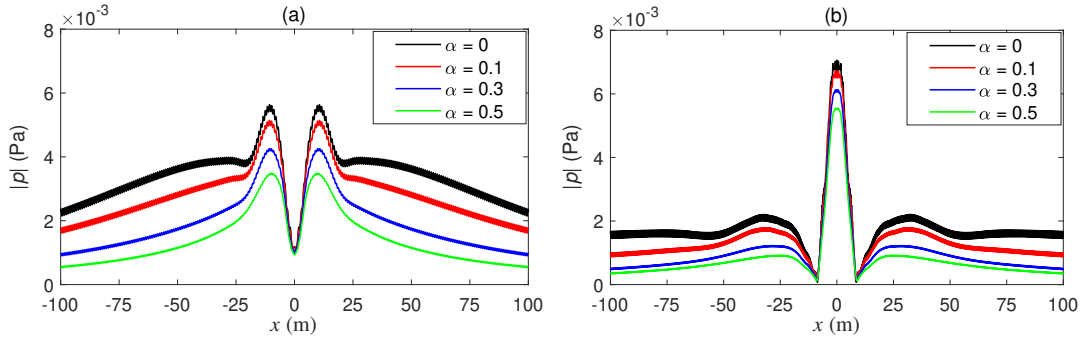

FIGURE 3.6: Pressure at the receiver calculated by the proposed 2.5D SBM for various values of the sound absorption coefficient at the frequencies of (a) 200 Hz and (b) 500 Hz.

In the following, the previous study is extended to the case of a moving source, wherein the source point moves longitudinally, in parallel with the barrier. In this context, it becomes particularly interesting to present and discuss the results in the temporal domain. Hereby, it is supposed that the source speed is constant, having a position that is a function of the time as $(x_0 + Ut, 2, 0.5)$ m, while the pressure is being calculated at the receiver point. The calculations have been done considering two selected speeds of the source: 50 m/s and 100 m/s, and, again, taking into account a monopole source pulsating at 200 Hz in one case and and 500 Hz in the second one, at each speed. In all considered scenarios, it is presumed that the source is at $x = 0$ at $t = 0$. Thus, the source is at the same longitudinal position as the receiver at this moment. The source strength can be written as $s(t) = cos(\omega_0 t)$. At the receiver point, the acoustic pressure response induced by this source is characterised by Eq. (3.16). To avoid excessive complexity in the figures that subsequently present the results, the amplitude $A(t)$ of the pressure time histories defined in Eq. (3.17) is chosen to illustrate the response.

Results for a rigid barrier, i.e. $\alpha = 0$, computed by the proposed 2.5D SBM is presented in Figure 3.7. From a general perspective, one can observe different behaviours for negative and positive times, induced by the Doppler effect. Note that the Doppler effect becomes stronger when the source travels at a speed of 100 m/s, compared to the case when the source moves at a speed of 50 m/s. Conversely, when the source moves at 100 m/s, the transient signal gets compressed compared to the one associated with 50 m/s, resulting in a correspondingly higher perceived frequency. When comparing the results obtained at the two selected frequencies, it

is seen that the barrier attenuation effect is more stronger for the source pulsating at 500 Hz compared to that at 200 Hz.

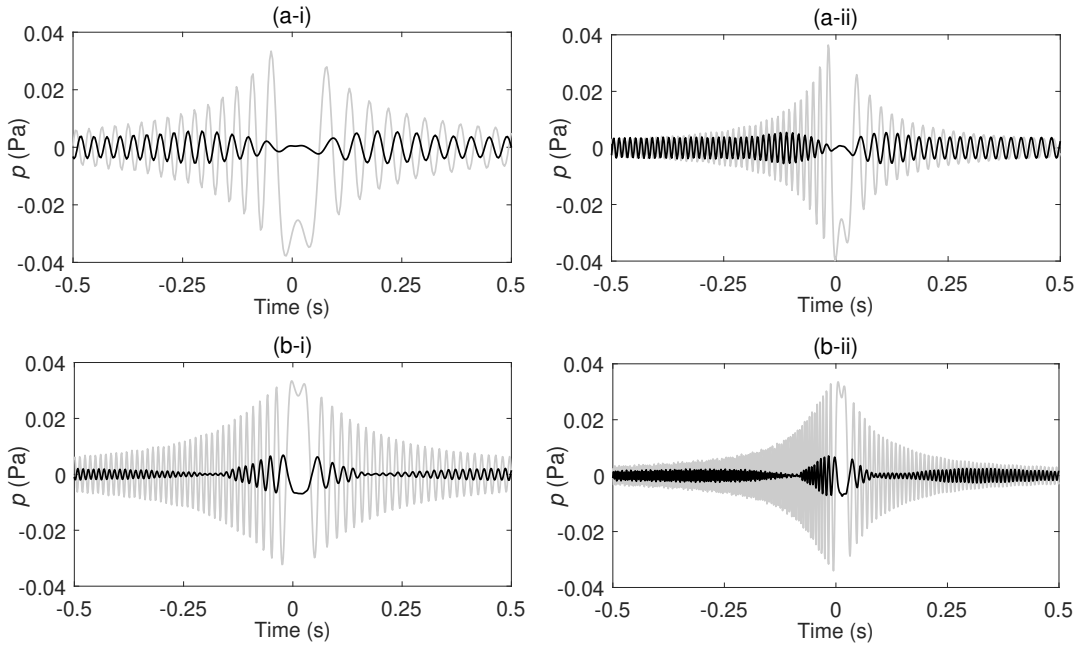

FIGURE 3.7: Amplitude of the pressure time history at the receiver point calculated by the proposed 2.5D SBM at the frequencies of (a) 200 Hz and (b) 500 Hz and at the speeds of (i) 50 m/s and (ii) 100 m/s, for the case of a totally rigid barrier. Solid gray lines depict pressures obtained when the barrier is not taken into account.

In Figure 3.8, a comparison is depicted, illustrating the pressure time histories recorded at the receiver in two scenarios: one with a totally rigid barrier and the other with a barrier featuring a sound absorption coefficient of $\alpha = 0.3$. The results have been computed using the 2.5D SBM, adopted with an imposed Neumann boundary condition when $\alpha = 0$ and with a Robin boundary condition when $\alpha = 0.3$. It is seen from Figure 3.8 that a greater reduction in sound pressure level is achieved when the barrier is enhanced with sound absorption materials.

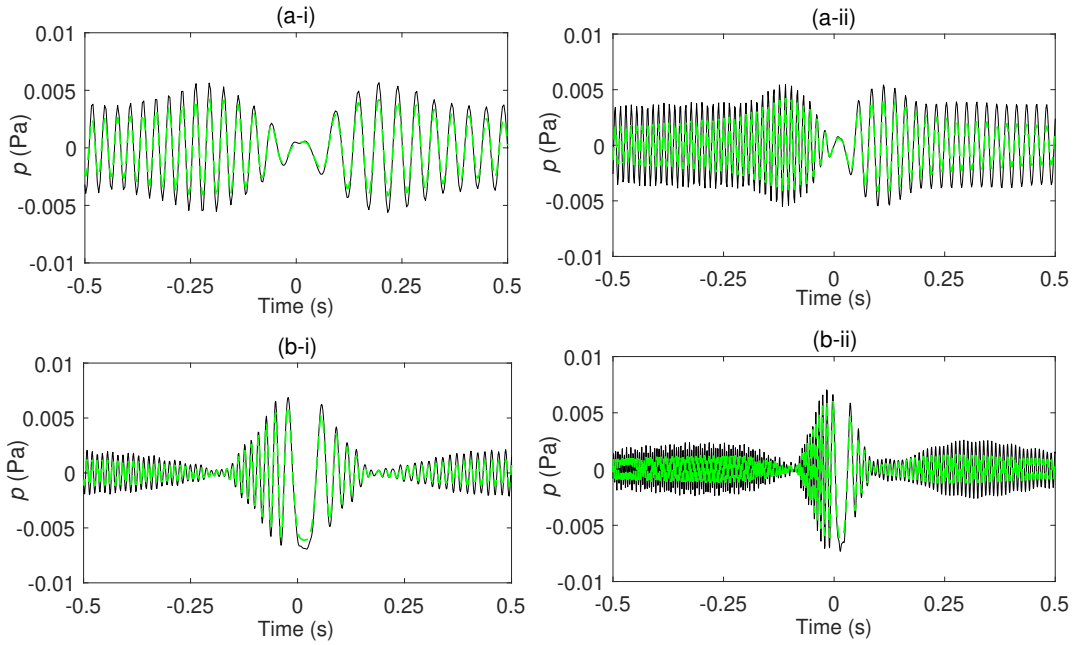

FIGURE 3.8: Amplitude of the pressure time history at the receiver point calculated by the proposed 2.5D SBM at the frequencies of (a) 200 Hz and (b) 500 Hz and at the speeds of (i) 50 m/s and (ii) 100 m/s, in the presence of a totally rigid barrier (solid black lines) and when a barrier with absorption coefficient of $\alpha = 0.3$ is considered (dashed green lines).

3.4 Conclusions

This chapter has particularly focused on investigating the applicability and effectiveness of the proposed 2.5D SBM approach for addressing real and practical engineering noise wave propagation problems. In this regard, the method has been specifically utilised to analyse the problem of point source diffraction in the presence of a thin barrier. This problem is of considerable importance in the context of mitigating noise pollution, particularly concerning road and rail transportation systems.

In order to analyse this particular problem, the proposed 2.5D SBM was implemented considering the medium to be a half-space instead of a fully unbounded medium. To do so, the image-source technique is employed to account for a totally reflecting plane surface representing the ground surface. The 2.5D SBM allows for converting the original 3D problem into a combination of 2D problems in which the

barrier boundary is defined by just a line. This, combined with the computational benefits of the SBM offers an efficient evaluation of the noise mitigation induced by barriers with constant cross-sections, compared to the former state-of-the-art strategies. In this context, two distinct scenarios have been studied: the case where the source is harmonic but remains at the same position and the case where the harmonic source is moving, at a constant speed, in the longitudinal direction. Obtained results showed that the method is giving similar responses to a densely meshed implementation of the 2.5D QE-BEM, demonstrating a satisfactory agreement between these methods. Particularly, the results show the expected strong Doppler effect observed when the source travels at higher velocities. Additionally, it is observed that the barrier attenuation effect is more stronger at higher frequencies and when absorbing boundaries are included, being these results in line, again, with previous numerical and experimental studies on the topic.

Chapter 4

A novel hybrid SBM-MFS methodology for acoustic wave propagation problems

In this chapter, a novel hybrid meshless approach that combines the SBM and the MFS to deal with 2D exterior acoustic wave propagation problems is proposed and studied. The methodology is particularly devised to solve problems with complex boundary geometries containing geometric singularities such as corners and sharp edges. It employs the SBM to model intricate segments of these geometries and the MFS for the smooth ones. The proposed hybrid SBM-MFS method is studied in a 2D context in the framework of three benchmark examples involving acoustic radiation problems of circular-, square- and L-shaped objects in a full-space acoustic medium. In addition, the applicability of the proposed hybrid SBM-MFS methodology to predict the acoustic performance of a T-shaped thin barrier is also investigated. These examples are specifically designed to assess the feasibility, validity and accuracy of the hybrid SBM-MFS approach in comparison with the available analytical solutions and alternative numerical strategies such as the MFS, the SBM and the BEM.

This chapter is organised as follows: In Section 4.1, a brief overview of modification techniques employed in the context of the SBM, MFS and BEM approaches to tackle problems involving geometric singularities along the boundary is provided.

Section 4.2 presents the proposed formulation of the novel hybrid SBM-MFS method. Section 4.3 lays on an assessment of the validity and accuracy of the proposed methods in the context of the three benchmark examples involving the acoustic radiation problems. In Section 4.4, the applicability of the proposed method addressing the problem of acoustic line source diffraction through a T-shaped thin barrier is investigated. Finally, Section 4.5 concludes this chapter with the most important findings extracted from the conducted numerical analyses.

4.1 Introduction

Problems related to acoustic wave propagation radiated or scattered by structures with complex geometries need to be solved in many practical engineering applications. One of the major difficulties in these problems is how to accurately deal with geometrical singularities when sharp edges and/or corners are present on the boundary of the structure involved. Analytical methods are mostly restricted for simple geometries, such as circular cylinders and spheres and, therefore, they are generally not suitable for problems involving complex geometries, since exact solutions are not typically available for many of these cases. As an alternative approach, the BEM has been extensively employed for studying the radiation and scattering of sound when dealing with complex geometries of the boundary. However, it is widely acknowledged that the classical BEM exhibits a significant loss of accuracy when dealing with boundary geometrical singularities. This is primarily attributed to the discontinuity of normal vectors at these singularities [61].

In order to overcome this BEM drawback, some modification techniques or complementary procedures have been suggested by various authors. In this regard, Chen et al. [62] employed the dual BEM in order to obtain an efficient solution of the Helmholtz equation in the presence of geometric singularities when solving time-harmonic wave problems in a membrane containing one or more fixed edge stringers or cracks. An effective treatment for the singularities in both isotropic and anisotropic 2D Helmholtz-type equations has been proposed by Marin et al. [63], in where the standard BEM is modified by a change of variables to account for the presence of singularities. To tackle the issues of indefinite normal vector and discontinuity of the normal velocity at sharp edges or corners, Yan [61] defined the normal vectors at the nodes rather than the elements. Then, instead of using the normal velocity, the module of the velocity was proposed since it is unique even at sharp edges and corners, ensuring that all variables in the acoustic boundary element method are always well-defined. Gilvey et al. [64] used an enriched approximation for the BEM based on the asymptotic singular behaviour of scattered fields at sharp corners that enables efficient and accurate solutions of the Helmholtz equation in the context of wave scattering problems involving polygonal obstacles. Numerical examples demonstrate that this approach is a suitable

choice for convex scatterers and also for multiple scattering objects that give rise to multiple reflections.

Instead of the BEM, the MFS has been found as a very popular alternative numerical strategy to solve acoustic wave propagation problems featuring intricate boundary geometries. Nevertheless, it's worth noting that the classical MFS encounters significant difficulties when handling boundary domains containing corners or cracks, clearly stronger than the complications arising when analysing this kind of geometrically complex domains with BEM. Thus, a modification of the MFS formulation is required in order to make it applicable to such singular problems. In this context, Marin [65] proposed a combination of the MFS and the singularity subtraction technique (SST) to overcome this difficulty by subtracting the corresponding singular functions from the original MFS solution, as given by the asymptotic expansion of the solution near the singularity point. The proposed MFS-SST was successfully examined for problems associated with the Helmholtz and the modified Helmholtz equations in 2D complex domains containing edge cracks and V-notches. Antunes et al. [66] proposed an enrichment technique for the standard MFS to address Helmholtz problems occurring in domains with corners and cracks. This technique involved incorporating an additional set of corner-adapted non-smooth shape functions. Koochak Dezfouli et al. [67] proposed a modification of the MFS to deal with geometrically complex boundaries for which particular sources are split in several sub-sources with equal intensities. Results obtained by using the proposed method showed a significant reduction of the computational time and the condition number of the MFS coefficient matrix.

Although the SBM demonstrates to be more suitable to deal with geometrically complex boundaries than MFS, it is worth noting that this method still encounters significant challenges in delivering accurate solutions when it is applied to solve problems involving geometrical singularities of the boundary such as corners, sharp edges and cracks. In order to remedy this numerical issue, some studies proposed to modify the SBM using specific techniques. In this regard, Lin et al. [68] employed the SBM in conjunction with the SST for acoustic problems to remove the severely adverse effect of the boundary singularities on the SBM solution accuracy and stability. Ma et al. [69] introduced an enriched SBM formulation, referred to as the DDE-SBM, which incorporates the domain decomposition technique to

deal with the singular behaviour of the acoustic response near cracks. The results obtained show that the proposed DDE-SBM can accurately characterise the singular behaviour of the solution in the neighbourhood of the crack tip, providing a simpler modelling process while ensuring both high solution accuracy and a well-conditioned coefficient matrix. Lin et al. [70] made the first attempt to employ the LSBM in conjunction with the Chebyshev collocation scheme (CCS), named as the CCS-LSBM, for the numerical simulation of inhomogeneous elliptic boundary value problems when dealing with complex geometries. The proposed CCS-LSBM method demonstrates high accuracy and efficiency in solving problems with mixed boundary conditions and complex computational domains.

Thus, the previous review demonstrates the availability of various techniques that offer effective methodologies based on the MFS or the SBM to tackle problems involving complex boundary geometries. However, the use of these techniques may compromise some of the most important advantages of the MFS and the SBM, such as their simplicity of formulation and superior computational efficiency, particularly in the case of the MFS. The present chapter proposes a novel hybrid SBM-MFS approach for exterior acoustic problems that may preserve the advantages of the conventional MFS while also providing the ability to accurately handle problems with complex boundary geometries, overcoming one of the most important drawbacks of the traditional MFS. The proposed novel method adopts a SBM-based approach by placing virtual sources on the physical boundary, specifically targeting the intricate segments such as those containing sharp edges. Meanwhile, the remaining sources are positioned on an auxiliary boundary, following the approach suggested by the MFS. The feasibility, validity and accuracy of the proposed method are studied in detail for three acoustic benchmark examples in the context of an error analysis framework. The first example considers the acoustic radiation problem of a circular object, representing a case with a smooth boundary geometry. The second and third examples, which are specifically devised to assess the applicability of the proposed method to deal with problems including geometrical singularities, deal with the acoustic radiation problems of square- and L-shaped objects, respectively. Furthermore, the applicability of the proposed hybrid SBM-MFS methodology to predict the acoustic performance of thin barriers

is also investigated in this study. Numerical simulations are performed for evaluating the insertion loss in a typical line source diffraction problem in the presence of a T-shaped acoustic barrier.

4.2 Mathematical formulation

The problem under consideration is the propagation of acoustic waves in an infinite 2D homogeneous isotropic medium induced by a boundary condition on a closed surface Γ to its corresponding exterior domain Ω. In this context, the pressure field in the domain can be mathematically expressed in the frequency domain by the well-known Helmholtz equation

$$\nabla^2 p\left(\mathbf{x}\right) + k^2\, p\left(\mathbf{x}\right) = 0 \quad \text{for} \quad \mathbf{x} \in \Omega, \tag{4.1}$$

where $\nabla^2 = \dfrac{\partial^2}{\partial y^2} + \dfrac{\partial^2}{\partial z^2}$, $p\left(\mathbf{x}\right)$ represents the acoustic pressure at a generic point $\mathbf{x} = \{x, y\}^{\mathrm{T}}$ inside the domain, k is the acoustic wavenumber, which is equal to ω/c, ω is the angular frequency and c is the sound wave speed in the medium. For this boundary value problem, the Dirichlet or Neumann boundary conditions are typically prescribed as

$$p\left(\mathbf{x}\right) = p_b\left(\mathbf{x}\right) \quad \text{for} \quad \mathbf{x} \in \Gamma, \tag{4.2a}$$

$$v\left(\mathbf{x}\right) = \frac{1}{\mathrm{i}\rho\omega}\frac{\partial p\left(\mathbf{x}\right)}{\partial \mathbf{n}_b} = v_b\left(\mathbf{x}\right) \quad \text{for} \quad \mathbf{x} \in \Gamma, \tag{4.2b}$$

respectively, where $\mathbf{n}_b$ is the unit outward normal vector to the physical boundary, p_b and v_b are the prescribed pressure and normal velocity at the boundary, respectively, ρ is the medium density and $\mathrm{i} = \sqrt{-1}$.

4.2.1 Hybrid SBM-MFS approach for exterior acoustic problems

In this section, a novel hybrid SBM-MFS methodology to deal with the above-stated problem is developed and formulated. The method is particularly devised

to be applied for arbitrary boundaries with complex geometries involving geometric singularities such as corners or sharp edges. The proposed method employs a combination of MFS and SBM sources for which the latter ones are placed at the intricate segments of the geometry, especially those consisting of sharp edges. A general overview of the proposed hybrid methodology is schematically illustrated in Figure 4.1, where a framework example of sources and collocation points distributions is presented. As depicted, this methodology considers a set of N_C collocation points and distributes them along the physical boundary. As mentioned, the method adopts two different sets of virtual sources: the first set consists of N_S virtual sources positioned along the boundary, referred to as source points of the SBM nature, while the second set contains N_M virtual sources distributed outside the computational domain on an auxiliary boundary, referred to as source points associated to the MFS. In the present work, this virtual boundary is considered to be a reduced scale version of the physical boundary, a common practice when employing the MFS. As shown in Figure 4.1, j and h indices are used to iterate over the sets of SBM and MFS sources, respectively. Thus, it is considered that the jth virtual source is located at a position $\mathbf{s}_j^S$ and the hth virtual source at $\mathbf{s}_h^M$. In the following, the mathematical formulation of the described hybrid scheme is outlined in detail.

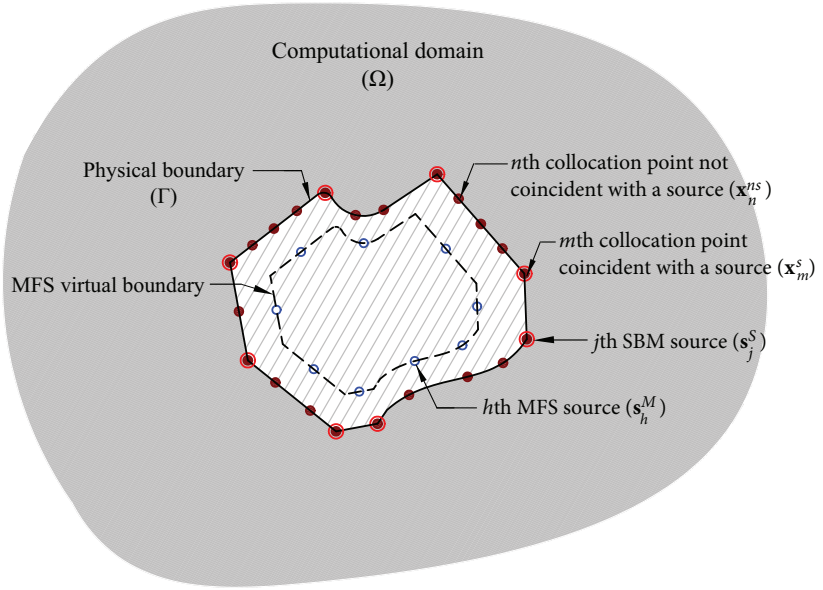

FIGURE 4.1: Schematic sketch of the hybrid SBM-MFS approach. The collocation points are denoted by brown solid dots and the virtual sources associated with the SBM and MFS are denoted by red and blue circles, respectively.

Similarly to the MFS and SBM approaches, the proposed hybrid SBM-MFS methodology is also a collocation approach that uses the single-layer fundamental solutions as its kernel functions. Thus, the method estimates the acoustic responses in the given medium through a linear combination of those single-layer fundamental solutions of the governing differential equation, in this example represented by Eq. (4.1). To achieve this, the method discretises the boundary conditions on the set of collocation points and places the virtual sources within the physical boundary and also the virtual boundary located outside the computational domain, following the previously described scheme. The virtual sources strengths are determined by forcing them to generate the prescribed boundary conditions at the stipulated set of collocation points. These virtual sources can be then used to evaluate the response in the domain. Accordingly, the proposed hybrid SBM-MFS approximates the acoustic pressure p and particle velocity v at a generic point $\mathbf{x}$ in the domain Ω by the combined response induced by the $N_S + N_M$ virtual sources as

$$p\left(\mathbf{x}\right) = \sum_{j=1}^{N_S} \alpha_j^S \, G\left(\mathbf{x}, \mathbf{s}_j^S, k\right) + \sum_{h=1}^{N_M} \alpha_h^M \, G\left(\mathbf{x}, \mathbf{s}_h^M, k\right) \quad \text{for} \quad \mathbf{x} \in \Omega, \tag{4.3a}$$

$$\mathrm{i}\rho\omega v\left(\mathbf{x}\right) = \sum_{j=1}^{N_S} \alpha_j^S \, H\left(\mathbf{x}, \mathbf{s}_j^S, k, \mathbf{n}_x\right) + \sum_{h=1}^{N_M} \alpha_h^M \, H\left(\mathbf{x}, \mathbf{s}_h^M, k, \mathbf{n}_x\right) \quad \text{for} \quad \mathbf{x} \in \Omega, \tag{4.3b}$$

where α_j^S and α_h^M represent the strengths of the jth and hth virtual sources, associated with the SBM and MFS sources, respectively, and

$$G\left(\mathbf{x}, \mathbf{s}, k\right) = \frac{1}{2\pi} K_0\left(kr\right), \tag{4.4a}$$

$$H\left(\mathbf{x}, \mathbf{s}, k, \mathbf{n}_x\right) = \frac{\partial G\left(\mathbf{x}, \mathbf{s}, k\right)}{\partial \mathbf{n}_x} = -\frac{k}{2\pi} K_1\left(kr\right) \frac{\partial r}{\partial \mathbf{n}_x}, \tag{4.4b}$$

are the 2D fundamental solutions of the sound pressure and particle velocity, respectively, for the modified Helmholtz equation.

In the case that the problem in hands could be better modelled using a half-space instead of a fully unbounded medium, the presence of totally reflecting plane surface can be taken into account by utilising the image-source technique, as described in Section 3.2.1. Thus, the corresponding fundamental solutions to

be used in this type of problems can be written as

$$G\left(\mathbf{x},\mathbf{s},k\right)=\frac{1}{2\pi}K_0\left(kr\right)+\frac{1}{2\pi}K_0\left(kr'\right), \tag{4.5a}$$

$$H(\mathbf{x},\mathbf{s},k,\mathbf{n}_x)=\frac{\partial G\left(\mathbf{x},\mathbf{s},k\right)}{\partial \mathbf{n}_x}=\left(-\frac{k}{2\pi}K_1\left(kr\right)-\frac{k}{2\pi}K_1\left(kr'\right)\right)\frac{\partial r}{\partial \mathbf{n}_x}, \tag{4.5b}$$

where $r=\sqrt{(x-x_0)^2+(y-y_0)^2}$ and $r'=\sqrt{(x-x_0)^2+(y+y_0)^2}$.

In the MFS, there is typically a certain degree of flexibility regarding the placement of the collocation points. However, in the SBM, they are deliberately selected to coincide precisely with the virtual source locations. Therefore, two sets of collocation points are considered in the proposed hybrid SBM-MFS strategy: the set of collocation points that are coincident with SBM sources and another set for the remaining sources. The former set consists of N_C^s sources, while the latter set consists of N_C^{ns} sources. Moreover, it is considered that the mth collocation point coincident with a virtual source is located at $\mathbf{x}_m^s$, and that the nth collocation point not coincident with one is located at $\mathbf{x}_n^{ns}$, as illustrated in Figure 4.1. Specifically, the whole distribution of the collocation points can be formally defined as $\{\mathbf{x}_1,\ \ldots,\ \mathbf{x}_{N_C}\}=\{\mathbf{x}_1^s,\ \ldots,\ \mathbf{x}_m^s,\ \ldots,\ \mathbf{x}_{N_C^s}^s\}\cup\{\mathbf{x}_1^{ns},\ \ldots,\ \mathbf{x}_n^{ns},\ \ldots,\ \mathbf{x}_{N_C^{ns}}^{ns}\}$. Note that the set of collocation points coincident with virtual sources fully corresponds to the set of SBM sources positions as $\{\mathbf{x}_1^s,\ \ldots,\ \mathbf{x}_m^s,\ \ldots,\ \mathbf{x}_{N_C^s}^s\}=\{\mathbf{s}_1^S,\ \ldots,\ \mathbf{s}_j^S,\ \ldots,\ \mathbf{s}_{N_S}^S\}$, expressing that both sets are equal and equally sorted. Noting, too, that in the particular scenario where no SBM virtual sources are considered ($N_S=N_C^s=0$) the hybrid method appears to be a fully MFS. Conversely, when no MFS virtual sources are adopted ($N_M=N_C^{ns}=0$), it transitions into a fully SBM approach.

In order to determine the unknown source strengths, Eqs. (4.3a) and (4.3b) can be transformed to evaluate the response at the collocation points located on the boundary. In particular, to avoid the singularities of the fundamental solutions arising when those expressions are utilised to obtain the solution on the collocation points geometrically coincident with SBM sources, the OIFs should be included in the expressions. Taking this into account, Eqs. (4.3a) and (4.3b) are transformed

to different expressions depending on which is the targeted collocation point, as

$$p\left(\mathbf{x}_m^s\right) = \alpha_m^S\, G_{mm} + \sum_{j=1, j\neq m}^{N_S} \alpha_j^S\, G\left(\mathbf{x}_m^s, \mathbf{s}_j^S, k\right) + \sum_{h=1}^{N_M} \alpha_h^M\, G\left(\mathbf{x}_m^s, \mathbf{s}_h^M, k\right) \quad \text{for} \quad m = 1, 2, ..., N_C^s, \tag{4.6a}$$

$$\mathrm{i}\rho\omega v\left(\mathbf{x}_m^s\right) = \alpha_m^S\, H_{mm} + \sum_{j=1, j\neq m}^{N_S} \alpha_j^S\, H\left(\mathbf{x}_m^s, \mathbf{s}_j^S, k, \mathbf{n}_b\right) + \sum_{h=1}^{N_M} \alpha_h^M\, H\left(\mathbf{x}_m^s, \mathbf{s}_h^M, k, \mathbf{n}_b\right) \quad \text{for} \quad m = 1, 2, ..., N_C^s, \tag{4.6b}$$

$$p\left(\mathbf{x}_n^{ns}\right) = \sum_{j=1}^{N_S} \alpha_j^S\, G\left(\mathbf{x}_n^{ns}, \mathbf{s}_j^S, k\right) + \sum_{h=1}^{N_M} \alpha_h^M\, G\left(\mathbf{x}_n^{ns}, \mathbf{s}_h^M, k\right) \quad \text{for} \quad n = 1, 2, ..., N_C^{ns}, \tag{4.6c}$$

$$\mathrm{i}\rho\omega v\left(\mathbf{x}_n^{ns}\right) = \sum_{j=1}^{N_S} \alpha_j^S\, H\left(\mathbf{x}_n^{ns}, \mathbf{s}_j^S, k, \mathbf{n}_b\right) + \sum_{h=1}^{N_M} \alpha_h^M\, H\left(\mathbf{x}_n^{ns}, \mathbf{s}_h^M, k, \mathbf{n}_b\right) \quad \text{for} \quad n = 1, 2, ..., N_C^{ns}, \tag{4.6d}$$

where G_{mm} and H_{mm} are the OIFs of the fundamental solutions of the modified Helmholtz equation in the considered problem, which are described in Section 4.2.2. Therefore, the source strengths resulting from the prescribed Dirichlet and Neumann boundary conditions can be obtained, respectively, as

$$\boldsymbol{\alpha} = \mathbf{G}^{-1}\mathbf{p}_b, \tag{4.7a}$$

$$\boldsymbol{\alpha} = \mathbf{H}^{-1}\mathbf{v}_b, \tag{4.7b}$$

where $\mathbf{G}$ and $\mathbf{H}$, the latter one contains $(\mathrm{i}\rho\omega)^{-1}$, are the hybrid SBM-MFS interpolation matrices that consolidate the information in Eqs. (4.6a), (4.6b), (4.6c) and (4.6d) in a matrix form, $\boldsymbol{\alpha}$ is the vector that collects all source strengths, and $\mathbf{p}_b$ and $\mathbf{v}_b$ are vectors that collect the imposed boundary conditions evaluated at all collocation points. Once the source strengths have been computed, the acoustic responses are obtained by means of Eqs. (4.3a) and (4.3b).

4.2.2 Determining the OIFs in the context of the proposed approach

In this section, the required OIFs to be utilised in the context of the proposed hybrid SBM-MFS formulation are derived. To achieve this, the present study assumes that these OIFs can be determined through the ones that are extracted out by formulating the problem using a fully SBM approach. It is reached by adopting a particular case when no MFS sources are considered ($N_M = 0$) and, additionally, when the sets of collocation points and SBM virtual sources are fully coincident ($N_C^s = N_S$).

Thus, in order to derive the OIFs associated by the SBM approach, this method proposes adopting a desingularization process based on the subtracting and adding-back technique [26, 33]. Moreover, due to the fact that the order of the singularities arising in both fundamental solutions of Laplace and Helmholtz equations is equal, G_{mm} and H_{mm} can be derived via the asymptotic form of the fundamental solutions of the 2D Laplace equation when the source-receiver distance is small, as [42]

$$G_{mm} = {G^{\mathrm{L}}}_{mm} - \frac{1}{2\pi}\left(\ln\left(\frac{k}{2}\right) + \gamma\right), \tag{4.8a}$$

$$H_{mm} = H^{\mathrm{L}}_{mm}, \tag{4.8b}$$

where

$$G^{\mathrm{L}}_{mm} = \frac{1}{L_m}\int_{\Gamma_s} G^{\mathrm{L}}(\mathbf{x}^s_m, \mathbf{s}^S)\,\mathrm{d}\Gamma_s(\mathbf{s}) = -\frac{1}{2\pi}\ln\left(\frac{L_m}{2\pi}\right), \tag{4.9a}$$

$$H^{\mathrm{L}}_{mm} = \frac{1}{L_m}\left(1 - \sum_{j=1, j\neq m}^{N_S} L_j H^{\mathrm{L}}(\mathbf{x}^s_m, \mathbf{s}^S_j, \mathbf{n}_b)\right), \tag{4.9b}$$

are, respectively, the OIFs on Dirichlet and Neumann boundary conditions for 2D exterior Laplace problems, being

$$G^{\mathrm{L}}(\mathbf{x},\mathbf{s}) = -\frac{1}{2\pi}\ln(r), \tag{4.10a}$$

$$H^{\mathrm{L}}(\mathbf{x},\mathbf{s},\mathbf{n}_x) = \frac{\partial G^{\mathrm{L}}(\mathbf{x},\mathbf{s})}{\partial \mathbf{n}_x} = -\frac{1}{2\pi r}\frac{\partial r}{\partial \mathbf{n}_x}, \tag{4.10b}$$

the fundamental solutions of potential and flux associated with the 2D Laplace equation, respectively.

Finally, it should be noted that, even a fully SBM approach is employed, only the OIFs associated with coincident collocation and source points appearing when employing the hybrid SBM-MFS method should be finally computed. Therefore, one key advantage of the hybrid method to be highlighted is a reduction of the computational costs due to the fact that OIFs calculations are reduced with respect to a fully SBM approach.

4.3 Numerical verification of the proposed hybrid SBM-MFS method

In this section, a study on the feasibility, validity and accuracy of the proposed hybrid SBM-MFS is presented. This study is carried out through three benchmark 2D acoustic problems. The first one involves the radiation problem of a circular object representing a case where a totally smooth boundary geometry is adopted. The second and third examples deal with the radiation problems of square- and L-shaped objects, respectively, within the context of complex boundaries that include geometric singularities. Furthermore, the MFS, the SBM and the BEM approaches are also employed in the framework of these examples for comparative purposes, in order to conduct a detailed assessment between the proposed and classical numerical methods in terms of numerical accuracy and computational efficiency. It is worth emphasising that the inclusion of these BEM strategies in the comparison studies presented in this study serves the sole purpose of providing a benchmark from a well-established method. A discussion about the performance

of BEM, SBM and MFS approaches dealing with these types of problems can be found in [71].

The results of the study discussed in this section are generally presented within the framework of the RMSE analysis, initially outlined in Section 2.3, and have been reformulated here to account for 2D calculations as

$$\text{RMSE} = \frac{\sqrt{\dfrac{1}{N_t}\displaystyle\sum_{k=1}^{N_t} |p_n(\mathbf{x}_k) - p_a(\mathbf{x}_k)|^2}}{\sqrt{\dfrac{1}{N_t}\displaystyle\sum_{k=1}^{N_t} |p_a(\mathbf{x}_k)|^2}}, \tag{4.11}$$

where $p_n(\mathbf{x}_k)$ and $p_a(\mathbf{x}_k)$ represent the acoustic pressures computed at the kth test point by numerical methods and analytical solutions, respectively.

To obtain the described RMSE in all benchmark examples, a set of $N_t = 100$ test points uniformly distributed over a circumference that surrounds the studied physical object, centred at $(0, 0)$ and with a radius of $2a$, where a is a geometrical parameter being later specifically defined in each example, is considered. Two frequencies are selected to carry out the error analysis in the present study: 100 Hz and 2000 Hz. The analysis is carried out for a varying number of collocation points (or nodes, for the case of the BEM) per wavelength, referred compactly as N/λ or nodes/wavelength from now on, in a range of $2 \leq N/\lambda \leq 22$, where $\lambda = 2\pi c/\omega$. For all computations, the acoustic medium is considered to be air, with an assumed density of $\rho = 1.225$ kg/m^3 and a corresponding wave speed of $c = 340$ m/s.

4.3.1 Example 4.1. Radiation problem of a circular object

The problem under consideration in this example is the 2D acoustic radiation of a circular object. This problem is separately investigated for Dirichlet and Neumann boundary conditions. For the Dirichlet boundary condition case, the distribution of the pressure along the boundary is proposed to be

$$p_b = \cos(4\theta), \tag{4.12}$$

and, consequently, the analytical solution of the induced pressure field due to the proposed boundary condition in the frequency domain is given by [26]

$$p\left(r,\theta\right)=-\frac{H_4^{(1)}\left(kr\right)}{H_4^{(1)}\left(ka\right)}\cos\left(4\theta\right)\quad\text{for}\quad r\geq a\quad\text{and}\quad 0\leq\theta\leq 2\pi. \tag{4.13}$$

In the second case, the adopted acoustic normal velocity prescribed along the boundary (v_b) is

$$\mathrm{i}\rho\omega v_b=k\cos\left(4\theta\right), \tag{4.14}$$

and the analytical solution of the radiation field in the frequency domain is [25]

$$p(r,\theta)=-\frac{kaH_4^{(1)}\left(kr\right)}{kaH_3^{(1)}\left(ka\right)-4H_4^{(1)}\left(ka\right)}\cos\left(4\theta\right)\quad\text{for}\quad r\geq a\quad\text{and}\quad 0\leq\theta\leq 2\pi, \tag{4.15}$$

where a is the radius of the circular object, (r,θ) represents the location of the evaluation point in the polar coordinate system and $H_n^{(1)}$ is the Hankel function of the first kind of order n. These analytical solutions of the considered problems are adopted as the reference methods in all comparative studies for the assessment of the proposed numerical methods through the RMSE.

In this simulation, a circular object of radius $a=1$ m centred at $(0,0)$ is considered and, accordingly, the collocation points are uniformly distributed along a circumference of radius $a=1$. In order to implement the MFS method, it is supposed that the number of virtual sources are equal to the collocation points and the sources are uniformly arranged on a circumference, being this virtual boundary a reduced scale version of the physical one, with radius r_s, defined within the range of $0<r_s<a$. In the calculation, three trial values of r_s are adopted: 0.1 m, 0.5 m and 0.9 m. The schematic configuration of the MFS approach adopted for $r_s=0.5$ m is illustrated in Figure 4.2a. To deploy the hybrid SBM-MFS method, two different arrangements of virtual sources are assumed, being referred to as the one-in-between (OIB) and part-to-part (PP) configurations, as illustrated in Figure 4.2b and c, respectively. In the OIB configuration, the neighbouring points of each SBM source point serve as collocation points without coincident sources

at those locations. In the PP configuration, all SBM sources are grouped in four equal sectors distributed along the boundary. In both arrangements, 50 % of the virtual sources are SBM-type sources and the remaining source are of MFS type.

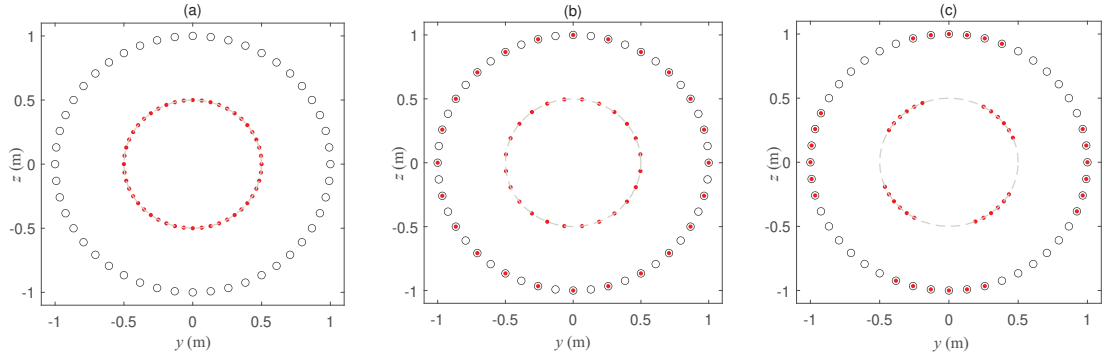

FIGURE 4.2: Distributions of the collocation points (black circles) and virtual sources (red dots) in Example 1 for the case of a fictitious boundary of radius $r_s = 0.5$ m, adopted for (a) the MFS method and the hybrid SBM-MFS method with (b) the OIB and (c) PP configurations.

The results in terms of RMSE analysis comparing the different numerical approaches when dealing with Example 1 are illustrated in Figures 4.3 and 4.4, for the case of the Dirichlet and Neumann boundary conditions, respectively. Overall, it can be observed that for the two frequencies selected, as the number of collocation points increase, the associated error delivered by each numerical method studied decrease and, consequently, all methods are converging to the analytical solutions. Therefore, it can be stated that all methods are verified for this calculation example when the Dirichlet and Neumann boundary conditions are imposed. A detailed examination of the results obtained using the different methods reveals that, at the frequency of 100 Hz, both the MFS and hybrid SBM-MFS methods demonstrate superior accuracy compared to the SBM or BEM approaches when considering fictitious boundaries of radii $r_s = 0.1$ m and $r_s = 0.5$ m. Conversely, both SBM and BEM deliver more accurate results than the MFS and SBM-MFS methods when adopting $r_s = 0.9$ m. At the frequency of 2000 Hz, the MFS and hybrid SBM-MFS with OIB configuration generally provide more accurate results than both SBM and BEM approaches for all fictitious boundaries considered. However, the hybrid SBM-MFS with PP configuration adopted with $r_s = 0.9$ m shows to be less accurate than the SBM and BEM. It can be also observed that for the two frequencies selected, the most accurate results are delivered when the

associated auxiliary boundary of the MFS and its hybrid version is located at $r_s = 0.1$ m. Focusing on the particular results obtained with the hybrid SBM-MFS, it can be noted that the method is generally delivering solutions with more accuracy when the OIB configuration is adopted instead of the PP one. It can be also seen that both the MFS and hybrid SBM-MFS solutions are strongly sensitive to the placement of the fictitious boundary and, in some situations when the fictitious boundary is close to the physical one, these methods could even shown to be less accurate than SBM and BEM approaches. Finally, a comparison between the MFS and the hybrid SBM-MFS approaches leads to the conclusion that the hybrid method is able to achieve accuracy levels as high as the MFS for such a geometrically smooth problem as the radiation of a circular object.

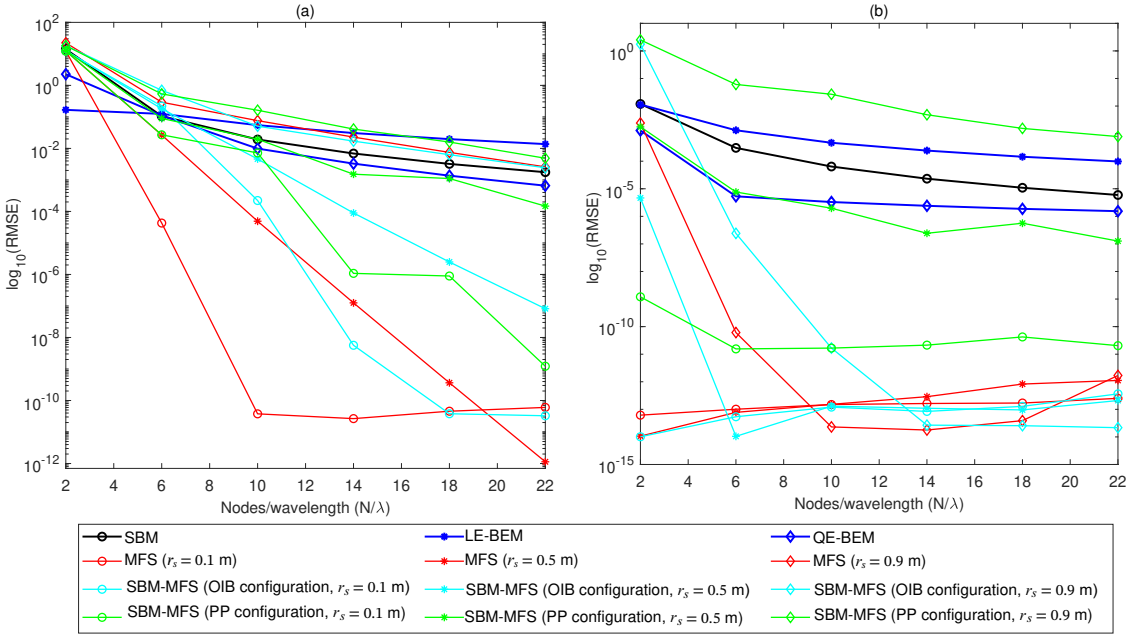

FIGURE 4.3: RMSE analysis of the different methods for the radiation problem of a circular boundary subjected to a Dirichlet boundary condition at the frequencies of (a) 100 Hz and (b) 2000 Hz.

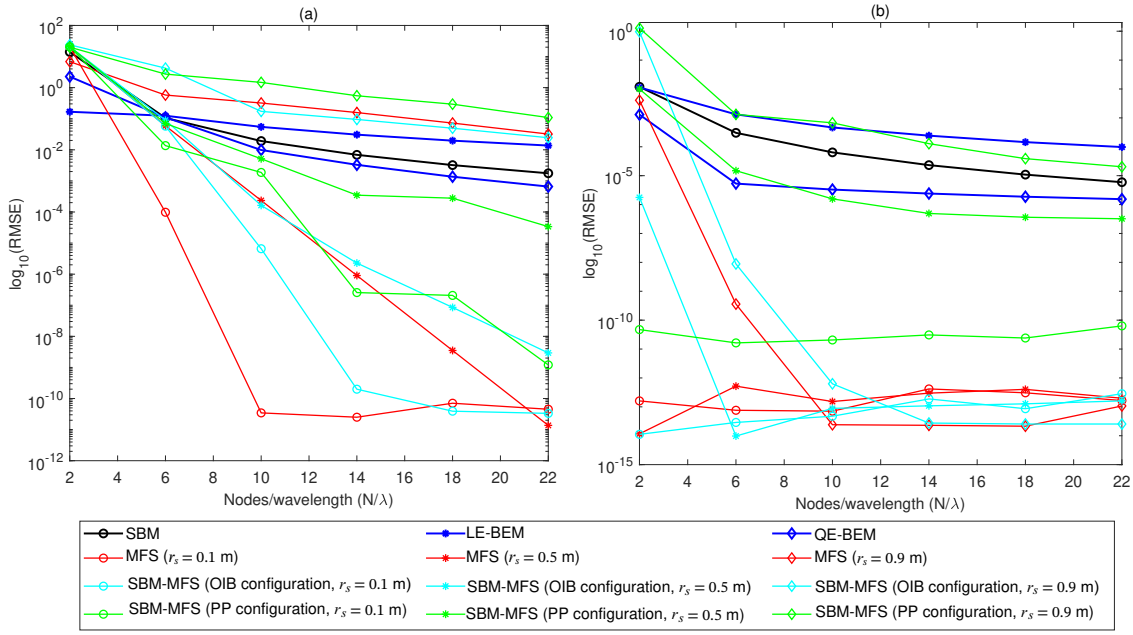

FIGURE 4.4: RMSE analysis of the different methods for the radiation problem of a circular boundary subjected to a Neumann boundary condition at the frequencies of (a) 100 Hz and (b) 2000 Hz.

After evaluating the accuracy and convergence trends of the proposed method with respect to other existing approaches in the case of a circular boundary, the frequency response functions for the acoustic radiation problems defined in Example 1 employing the studied methods are hereafter investigated. In this regard, the RMSE is computed for frequencies varying from 1 Hz to 2000 Hz using a discretisation scheme which adopts 6 N/λ at the maximum frequency of interest (referred compactly as $N/\lambda_{2\text{kHz}} = 6$), which results in a total of 222 uniformly distributed collocation points/nodes. Results are plotted in Figure 4.5. It can be observed that due to the non-uniqueness solution problem, the SBM and BEM approaches perform to deliver low levels of accuracy at the vicinity of the fictitious eigenfrequencies of the corresponding interior problems associated with both Dirichlet and Neumann boundary conditions scenarios. These fictitious eigenfrequencies arise at the zeros of $J_4(ka) = 0$, being J_n the Bessel function of the first kind of order n, as discussed and concluded in [72, 73]. Regarding the MFS and the hybrid SBM-MFS, it has been observed that, from a general perspective, these methods demonstrate high accuracy across the entire frequency spectrum for the adopted boundary conditions, with the incurred errors being consistently very

small. In particular, errors associated with these methods are approximately 10 orders of magnitude lower than those of the LE-BEM in these calculations. Thus, it is found that the devised hybrid SBM-MFS method can naturally overcome the non-uniqueness solution problem exhibited by purely boundary-type methods such as the SBM or the BEM. This feature of the proposed hybrid method comes from its particular formulation which considers some MFS-type virtual sources outside the domain of interest.

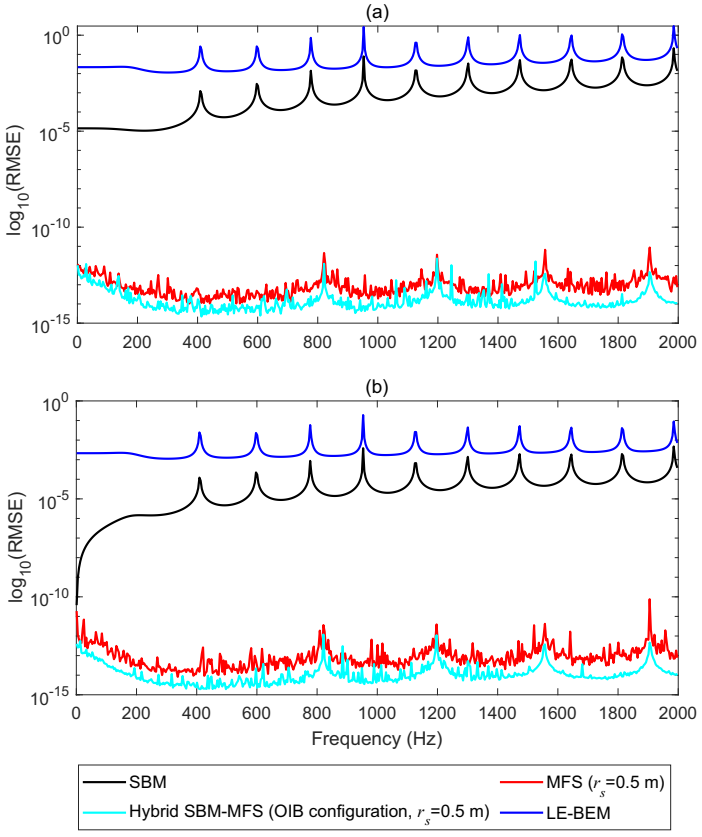

FIGURE 4.5: RMSE analysis of the different methods for the radiation problem of the infinite cylinder under (a) Dirichlet boundary condition and (b) Neumann boundary condition, obtained at frequencies varying from 1 Hz to 2000 Hz.

Once again, it is demonstrated that the MFS remains the superior method for handling circular boundary geometries. However, it is found that the novel hybrid SBM-MFS approach can reach similar performance levels to the MFS for this specific case. The real benefits of the proposed hybrid approach will be observed in the following cases, in where the boundary geometry is not smooth, containing sharp edges or corners.

4.3.2 Example 4.2. Radiation problem of a square-shaped object

In this example, the 2D radiation problems of a square-shaped object under a Dirichlet boundary condition as well as when subjected to a Neumann boundary condition are separately studied. In order to rely on an analytical solution when conducting the numerical studies for this complex boundary case, the prescribed boundary conditions are set to produce the exact response of the problem in Example 1 when considering a radius r_c for the circular object. To do so, Eq. (4.13) is employed to determine the prescribed boundary condition in the Dirichlet case as

$$p_b\left(r_b,\theta\right) = -\frac{H_4^{(1)}\left(kr_b\right)}{H_4^{(1)}\left(kr_c\right)}\cos\left(4\theta\right) \quad \text{for} \quad 0 \leq \theta \leq 2\pi, \tag{4.16}$$

being (r_b, θ) the pasteurisation of the squared boundary in polar coordinates. In the Neumann boundary condition case, the imposed acoustic velocity along the boundary should be defined by

$$\mathrm{i}\rho\omega v_b\left(r_b,\theta\right) = \nabla p_b \cdot \mathbf{n}_b \quad \text{for} \quad 0 \leq \theta \leq 2\pi. \tag{4.17}$$

As a consequence of imposing this specially designed boundary conditions, the radiation patterns on the acoustic medium are exactly defined by the analytical solutions of a circular object of radius r_c given by Eqs. (4.13) and (4.15) for the Dirichlet and Neumann boundary conditions, respectively. In this example, r_c is set to be 0.3 m.

The particular problem considered in this Example 2 is a square with side length of $a = 1$ m. Accordingly, the collocation points are distributed with a uniform arrangement along the square's boundary, ensuring that there is always a collocation point at each corner of the geometry. Regarding the MFS and hybrid SBM-MFS implementations, it is supposed that the fictitious boundaries adopted for these methods have also a square shape scaled with respect to the physical boundary. Thus, the parameter d, constrained to be $0 < d < 1$, is here defined as the scale factor for the fictitious boundary in these methods. In the current calculation, a uniform sampling of 100 values for the scale factor d ranging between 0.2 and

0.8 is considered. The underlying idea of this specific comparison is to examine the extent to which the methods are dependent on the location of the fictitious boundary. The described configurations of the MFS and hybrid SBM-MFS methodologies are schematically illustrated in Figure 4.6, for the case when $d = 0.5$. In these distributions, it is assumed that the number of sources is 20% less than the number of collocation points. This strategy is assumed for this Example to examine the feasibility of reducing the number of source points below the number of collocation points, which increases the computational efficiency of the method. In addition, for the hybrid SBM-MFS approach, 70% of the virtual sources are assumed to be of the MFS type and the remaining 30% are SBM-type sources. The latter ones are intentionally located at the corners of the square.

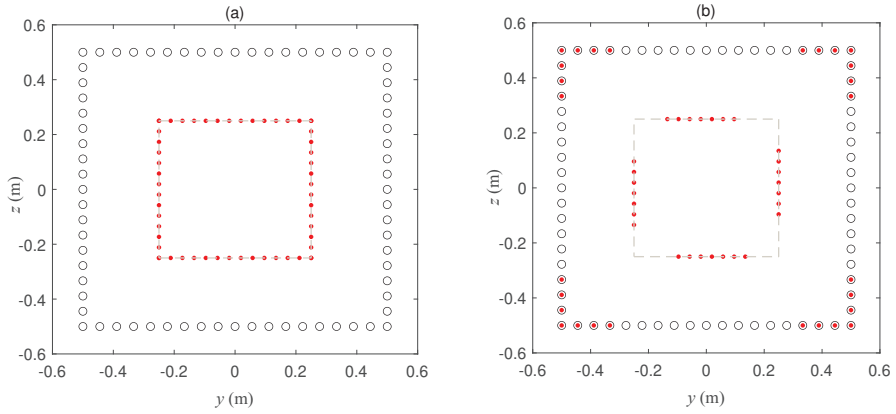

FIGURE 4.6: Distributions of the collocation points (black circles) and virtual sources (red dots) adopted for (a) the MFS and (b) the hybrid SBM-MFS approaches in the context of Example 2. Fictitious boundary case: $d = 0.5$.

Figures 4.7 and 4.8 display the RMSE analysis of the different numerical methods for benchmark Example 2 adopted for the Dirichlet and Neumann boundary conditions, respectively. The results obtained show that both MFS and hybrid SBM-MFS methods are consistently providing high accurate results for the two boundary condition scenarios studied. This holds true for all considered values of the scale factor of the fictitious boundary, for both selected frequencies and approximately for $N/\lambda > 4$. Although the performances of the methods are found to be sensitive to the placement of the virtual boundary, the delivered levels of accuracy are demonstrated to be significantly higher than the other methods studied. It is worth mentioning that a considerable enhancement in the performance

of the hybrid method, when compared to the SBM, is achieved just with 30% of the sources to be of the SBM type, being an important point to highlight the computational benefits of the proposed hybrid approach saving computational costs along the OIFs calculation. Benefits of using the MFS and hybrid SBM-MFS methods are especially remarkable in the Neumann boundary condition case, for which both the SBM and BEM strategies display very low levels of accuracy along with low convergence rates. This is due to the fact that these methods encounter difficulties when handling the discontinuities of the normal vectors at the corners of the square.

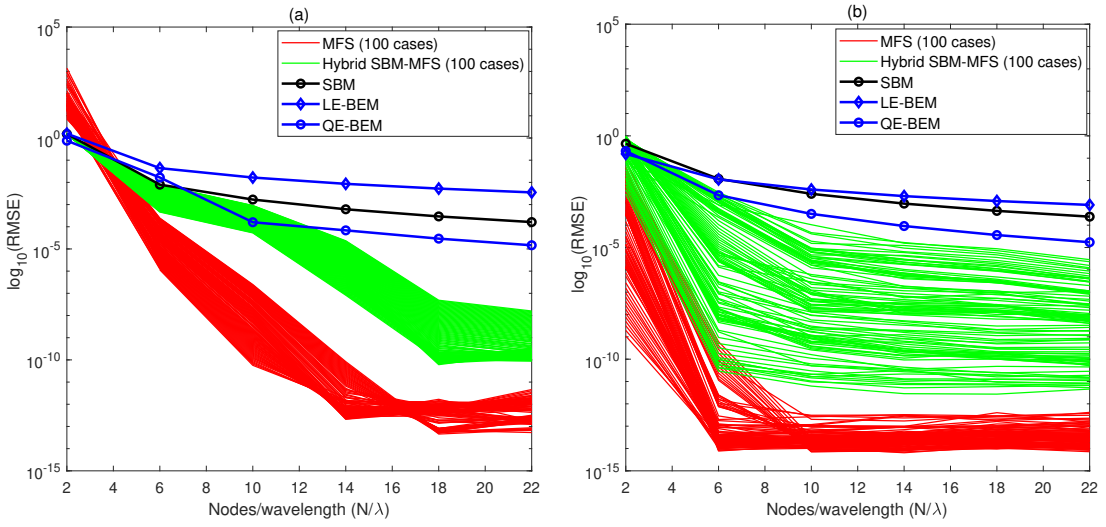

FIGURE 4.7: RMSE analysis of the different methods for the radiation problem of a square-shaped object subjected to a Dirichlet boundary condition at the frequencies of (a) 100 Hz and (b) 2000 Hz.

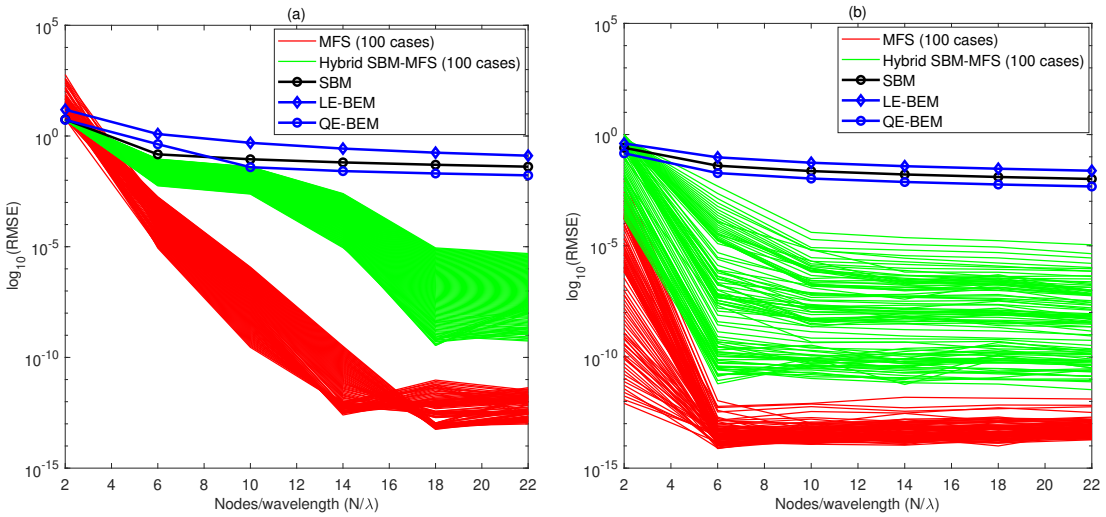

FIGURE 4.8: RMSE analysis of the different methods for the radiation problem of a square-shaped object subjected to a Neumann boundary condition at the frequencies of (a) 100 Hz and (b) 2000 Hz.

In the two previous examples, the proposed hybrid version of the SBM and MFS methods has been verified for the acoustic radiation problems involved with boundary geometry of the circular and square types. Nevertheless, among the strategies investigated, the MFS remains the most effective approach for addressing problems involving regular geometries with moderate geometrical singularities, such as the square geometry studied in this example. The next example is provided with the aim of demonstrating the capabilities of the proposed approach when dealing with more pronounced geometrical complexity. In this regard, the acoustic radiation problem of a L-shaped object is hereafter devised and analysed.

4.3.3 Example 4.3. Radiation problem of a L-shaped object

In this example, the problem of the sound field radiated by a L-shaped object is considered. The corresponding pressure and acoustic velocity on the boundary, as Dirichlet and Neumann boundary conditions, are supposed to be prescribed in a similar way as explained in Example 2. In order to compute the RMSE, a L-shaped geometry with a long side length of $a = 1$ m is considered, as shown in Figure 4.9a. Regarding the implementation of the MFS and hybrid SBM-MFS approaches, it is supposed that the virtual boundary also consists of a L-shaped

geometry scaled with respect to the physical one. Following the same conceptual ideas as in Example 2, a uniform sampling of 100 values of the scale factor of the fictitious boundary d varying in an interval from $0.2 \leq d \leq 0.8$ are considered in the current calculation. Once again, 20% less virtual sources than collocation points are considered and only the 30% of the ones employed in the hybrid SBM-MFS approach are of the SBM nature. Examples of the discretisation patterns of the MFS and hybrid SBM-MFS methods are shown in Figure 4.9b and c, respectively.

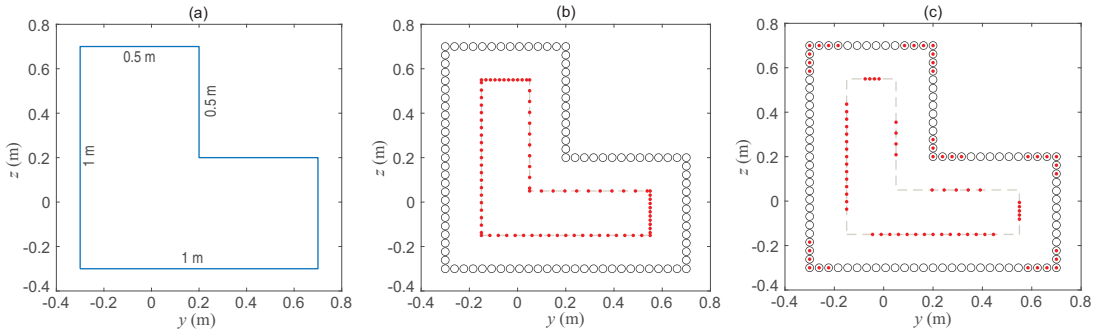

FIGURE 4.9: Sketch of Example 3 L-shaped problem: (a) adopted geometry and distributions of the collocation points (black circles) and virtual sources (red dots) adopted for (b) the MFS method and (c) the hybrid SBM-MFS method. Fictitious boundary case: $d = 0.5$.

Figures 4.10 and 4.11 illustrate a comparison in terms of the RMSE between the different numerical approaches adopted for Example 3 when the Dirichlet and Neumann boundary conditions are respectively considered. On the one hand, it can be seen that both the SBM and BEM approaches demonstrate low accuracy and slow convergence to the analytical solutions at the selected frequencies, especially in the case of the Neumann boundary condition problem. Compared with the results obtained in Example 1, i.e. the case of a circular boundary, it can be observed that the performance of these methods is significantly influenced by the presence of the geometric singularities that the corners of the boundary represent. On the other hand, the results obtained by the MFS method are also subjected to instabilities and errors for a majority of the fictitious boundaries adopted, particularly at the frequency of 100 Hz. Reversely, thanks to the significant capabilities of the hybrid method due to the combination of SBM- and MFS-type sources and the placement of the SBM ones at the corners of the boundary, the hybrid SBM-MFS methodology not only surprisingly remedies the errors delivered by the MFS, but

also significantly enhances the accuracy delivered by the SBM, for all fictitious boundaries adopted.

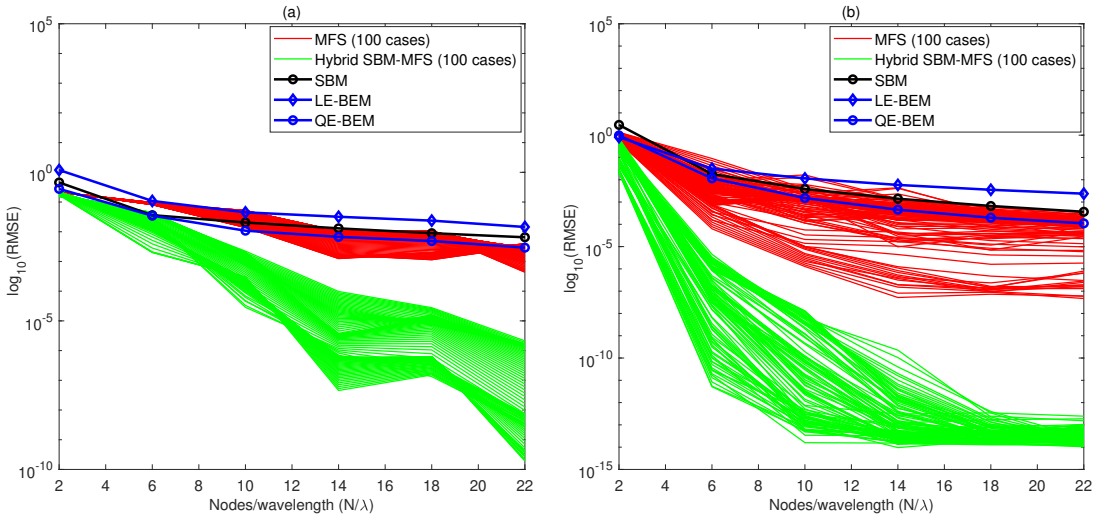

FIGURE 4.10: RMSE analysis of the different methods for the radiation problem of a L-shaped object subjected to a Dirichlet boundary condition obtained at the frequencies of (a) 100 Hz and (b) 2000 Hz.

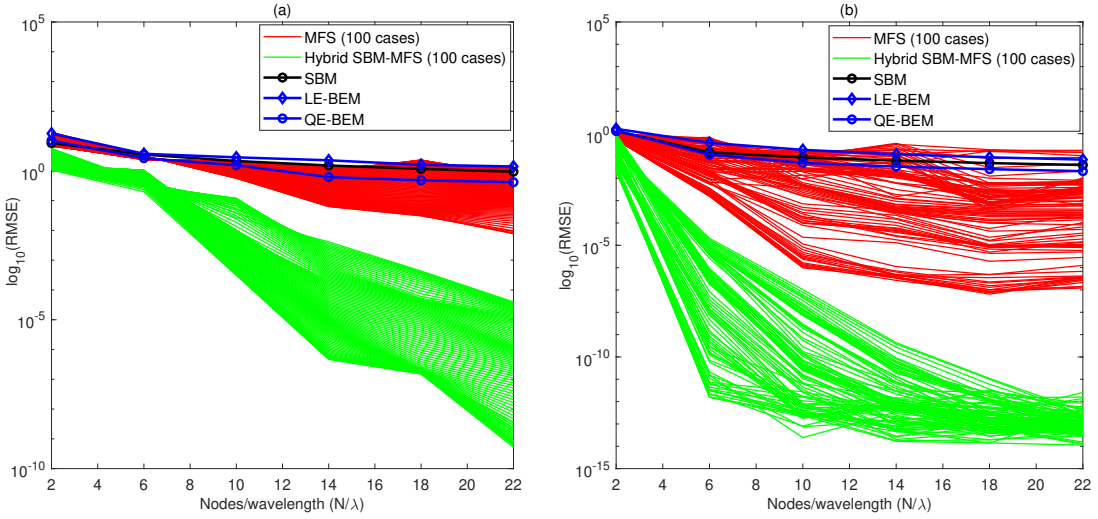

FIGURE 4.11: RMSE analysis of the different methods for the radiation problem of a L-shaped object subjected to a Neumann boundary condition obtained at the frequencies of (a) 100 Hz and (b) 2000 Hz.

4.4 Application of the hybrid SBM-MFS method

In this section, the applicability of the hybrid SBM-MFS methodology to real case scenarios is investigated. Thus, the proposed method is employed to analyze the 2D problem of line source diffraction in the presence of a T-shaped acoustic barrier. The schematic configuration of the problem under consideration is presented in Figure 4.12. In this analysis, a rigid T-shaped barrier of 2 m height with a cap width of 0.4 m located over a rigid ground is considered. The barrier is assumed to have a uniform thickness of 0.08 m. A line source is located at the position (-3, 0.5) m and the base of the T-shaped barrier is located at the origin of coordinates. The insertion loss (IL) is used to show the influence of the T-shaped barrier on the noise field generated at the right side of the barrier, opposite to where the source is located. It is defined as

$$\mathrm{IL} = -20\log_{10}\left(\frac{|\,p_{\mathrm{tot}}\,|}{|\,p_{\mathrm{inc}}\,|}\right), \tag{4.18}$$

where p_{tot} is the total pressure in an arbitrary point, defined as $p_{\mathrm{tot}} = p_{\mathrm{dif}} + p_{\mathrm{inc}}$, p_{dif} is the diffracted acoustic pressure field to be computed by the proposed hybrid SBM-MFS method employing half-space fundamental solutions presented in Eq. (4.5) and p_{inc} represents the incident acoustic pressure generated by the source considered in the problem without the presence of the barrier, which is given by

$$p_{\mathrm{inc}} = \frac{\mathrm{i}}{4}H_0\left(kr\right), \tag{4.19}$$

for the case of a unitary acoustic source strength, where r is the Euclidean distance between the source and the receiver and H_0 denotes the Hankel function of the first kind of order zero. In this simulation, the IL responses are calculated at one horizontal line of receivers placed at 1 m above the ground and reaching a maximum distance away from the barrier of 30 m, as shown in Figure 4.12.

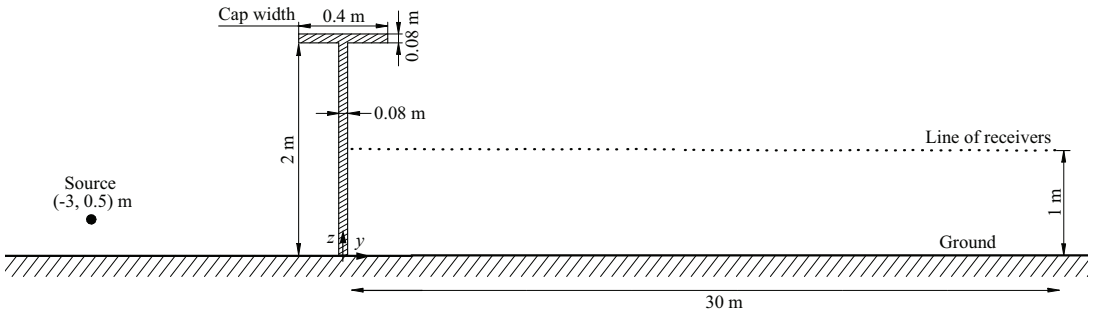

FIGURE 4.12: Schematic sketch of the T-shaped acoustic barrier, the acoustic line source considered and the evaluation points adopted.

In order to implement the hybrid SBM-MFS method, 245 collocation points having a uniform distribution along the boundary of the barrier are considered, as shown in Figure 4.13. The SBM-type sources are positioned at two parts of the barrier boundary. The first part is the cap, for which a total of 47 SBM-type sources including 2 placed at the neighbouring points where the cap is connected to the wall are considered. The second section, where the barrier is connected to the ground, consists of 4 SBM-type sources as depicted in Figure 4.13. The 140 MFS-type sources adopted are uniformly placed on two vertical lines inside the barrier geometry, as also shown in the discretisation sketch. Thus, a total number of 191 virtual sources are considered to implement the hybrid SBM-MFS method in this simulation. Moreover, the SBM approach is also adopted in this analysis for comparative studies between these two schemes. For this method, the same configuration of collocation points as presented for the hybrid SBM-MFS method is employed, together with a set of source points fully coincident with the collocation ones. Comparing the two methods, it can be seen that the hybrid method uses 54 source points less than the SBM. Furthermore, the QE-BEM is used as the reference model for comparison of the results computed by the proposed meshless methods. In this analysis, the QE-BEM was implemented with a high density of nodes per wavelength at the maximum frequency of interest, specifically $N/\lambda_{0.7\text{kHz}} = 100$. This choice was made to ensure a reference solution delivering highly accurate results.

Figure 4.14 illustrates the IL curves associated with the T-shaped barrier problem in hands computed by the proposed numerical methods at the frequencies of 100 Hz, 350 Hz, 500 Hz and 700 Hz. It can be observed, in a general point of view,

that the proposed hybrid SBM-MFS method exhibits a good agreement with the reference solution, the QE-BEM, across the four selected frequencies. Specifically, this method performs to effectively reduce the significant discrepancies near the peaks and valleys in the IL curves that are obtained through the SBM approach. It is worth emphasising that the hybrid SBM-MFS method achieves this performance while utilising 22% fewer virtual sources compared to the SBM strategy. Furthermore, it only requires the calculation of OIFs for the 51 SBM-type sources, which amounts to a significant 80% reduction compared to the SBM. This considerable decrease in virtual sources amount and OIFs calculation requirements demonstrates the significant advantages in terms of computational efficiency and reduced memory demands offered by the hybrid SBM-MFS approach compared to traditional SBM or BEM approaches. Noting that considering the inherent limitations of the conventional MFS and its tendency to yield unstable and inaccurate results for such complex geometries, this method was excluded from the studied methodologies for this analysis.

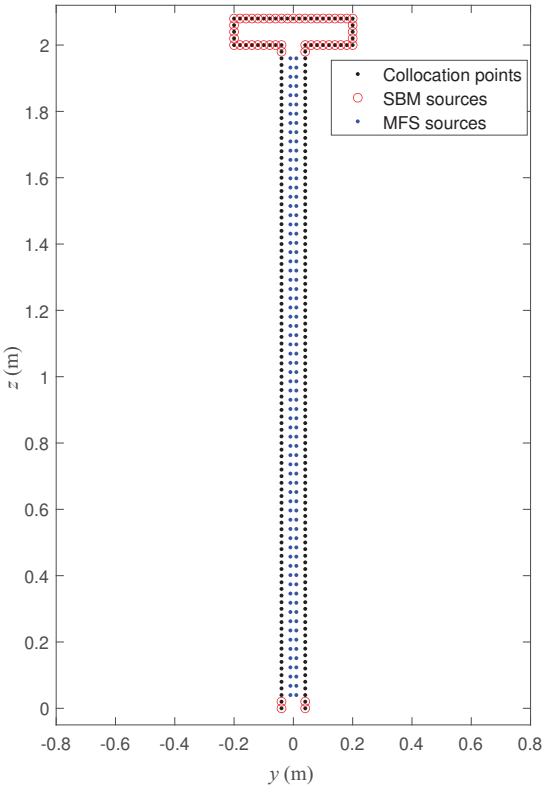

FIGURE 4.13: Configuration of the collocation points and sources used to adopt the hybrid SBM-MFS for the considered T-shaped barrier problem.

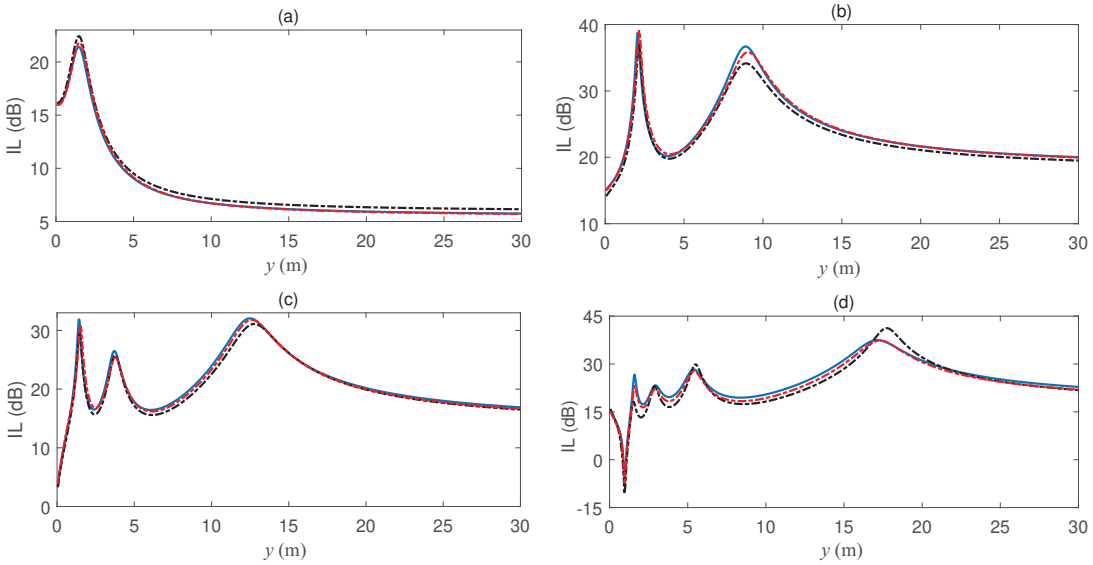

FIGURE 4.14: IL along the horizontal line of receivers, computed by the QE-BEM (solid blue line), the hybrid SBM-MFS (dashed red line) and the SBM (dashed black line) at the frequencies of (a) 100 Hz, (b) 350 Hz, (c) 500 Hz and (d) 700 Hz.

4.5 Conclusions

In this chapter, a novel numerical methodology to simulate 2D exterior acoustic wave propagation problems has been developed and studied. The methodology combines the SBM and MFS approaches to present a hybrid SBM-MFS formulation which is particularly devised to deal with problems including complex boundaries involved with geometric singularities of corner and sharp edge types. The proposed hybrid method uses a combination of SBM- and MFS-like sources to tackle problems involving complex geometries, placing the SBM-like sources at the intricate parts of the boundary. The validity and accuracy of the proposed hybrid method have been examined in comparison with the available analytical solutions in the context of three benchmark examples involving the acoustic radiation problems of circular-, square- and L-shaped objects in a full-space acoustic medium. Alternative numerical modelling techniques such as the MFS, the SBM and the BEM are also included in the comparisons to conduct a detail assessment of the proposed hybrid method in terms of numerical accuracy. Computational efficiency of the proposed method in comparison to the alternative approaches

presented has also been discussed. Furthermore, to investigate the applicability of the hybrid SBM-MFS methodology, the problem of acoustic pressure field produced by an acoustic line source in the presence of a T-shaped thin barrier has been studied. The most important findings extracted from the conducted numerical analysis can be summarised as follows:

- In the context of the three calculation examples studied in this chapter, it is found that the hybrid SBM-MFS methodology provides higher (or at least comparable) levels of accuracy and higher convergence rates than both BEM strategies considered, based on linear or quadratic boundary elements, and than the SBM in the majority of the situations. Notably, these results are found for both selected frequencies, being the smaller one (100 Hz) below the first fictitious eigenfrequency of the corresponding interior problem in all situations, demonstrating that this finding is not conditioned by the non-uniqueness solution problem. On the other side, the MFS has been demonstrated to be a strong competitor in the case of regular geometries such as circular- or square-shaped ones, while it shows poor performance as the geometry complexity increases. Further detailed conclusions derived from the comparisons between the hybrid SBM-MFS and pure MFS approaches are provided below.

- For the calculation example involving the acoustic radiation of a circular object, the hybrid SBM-MFS approach shows to be a highly accurate method and can compete with the levels of accuracy of the MFS. This is due to the fact that the MFS scheme performs particularly well in problems involving smooth circular boundaries [55, 71, 73, 74]. In any case, the pure MFS approach is still the best choice, among the studied methods, to deal with such a regular geometry in terms of accuracy, computational efficiency and method simplicity. However, in terms of the stability, the SBM demonstrates superior stability among all studied meshless methods. The combination of the SBM with the MFS method further enhances stability, making the hybrid SBM-MFS method more stable than the pure MFS approach.

- For the case of the square-shaped geometry, the feasibility of reducing source points against the collocation points in the implementation of both MFS and

hybrid SBM-MFS methods has been investigated by considering 20% fewer virtual sources than collocation points. For this specific configuration, the hybrid SBM-MFS method performs to effectively deal with the geometric singularities and it delivers highly accurate results compared with the SBM and BEM strategies. For this case, the MFS approach also performs even better than the hybrid one due to the symmetry of the boundary geometry of this problem.

- In the problem where the L-shaped geometry is studied, the MFS approach is found to be providing results with low levels of accuracy being highly sensitive to the placement of the fictitious boundary, demonstrating that this method is not an adequate approach for geometries involving geometric singularities. Conversely, the hybrid SBM-MFS method performs to be the most accurate strategy among all methods studied. Specifically, this methodology not only remedies the errors delivered by the MFS, but also surpasses the SBM in terms of accuracy.

- Due to the particular formulation of the hybrid SBM-MFS, which considers some virtual source of the MFS nature, i.e. located outside the domain of interest, the method naturally avoids the non-uniqueness problem arising at the vicinity of the fictitious eigenfrequencies of the corresponding interior problems.

- Finally, the investigation into the applicability of the proposed method in a real case scenario involving the line source diffraction problem in the presence of a T-shaped barrier has highlighted two important benefits of the proposed method. In comparison to the SBM, the hybrid SBM-MFS proves to be computationally efficient due to the strong reduction on the amount of OIFs to be computed. Additionally, the hybrid SBM-MFS demonstrates the potential to employ fewer virtual sources than collocation points without compromising numerical accuracy. Taking into account the already demonstrated computational benefits of the SBM with respect to the BEM [71], the proposed method offers a notably faster computational alternative to the latter. Finally, accounting for the discussed inability of conventional MFS to effectively tackle these complex geometric scenarios, the superiority of the

hybrid SBM-MFS with respect to the other studied numerical approaches in this context can be stated.

In conclusion, the hybrid SBM-MFS method presented in this work is found to be a potential alternative for the numerical simulation of acoustic problems involving complex boundaries, demonstrating a superiority in terms of numerical accuracy with respect traditional approaches such as the BEM, the SBM and the MFS when dealing with intricate domains. Furthermore, the method inherits the formulation simplicity of the MFS and SBM approaches as well as the superior computational efficiency with respect to the BEM.

Chapter 5

Modified 2.5D singular boundary methods to deal with spurious eigensolutions in exterior acoustic problems

This chapter studies the problem of spurious eigensolutions in the context of the SBM approach in the 2.5D domain and proposes two numerical schemes to overcome this numerical difficulty. Similar to other boundary-type discretisation schemes, the SBM also encounters the non-uniqueness problem at the vicinity of the eigensolutions of the corresponding interior problem. In the 2.5D domain framework, the so-called fictitious eigenfrequencies appearing in 3D problems arise in the form of spurious dispersion curves associated with propagation modes of the corresponding interior problem. The two enhanced 2.5D SBM approaches proposed in this chapter, based on the Burton–Miller method in one case and the dual surface method in the other, are designed to filter out the spurious eigenvalues from the simulation results and deliver accurate solutions along the wavenumber-frequency spectrum. Three benchmark examples including the radiation problems of an infinitely long cylinder under Dirichlet and Neumann boundary conditions and the radiation problem of a longitudinally infinite object with a constant star-like cross-section subjected to a Dirichlet boundary condition are considered to

study the proposed methods.

The following sections outline the organisation of the current chapter: Section 5.1 presents a brief overview of modification techniques used in the framework of the SBM and BEM approaches in order to overcome the fictitious eigenfrequency problem. Section 5.2 presents the formulations of the enhanced versions of the 2.5D SBM based on the Burton–Miller and dual surface techniques. In Section 5.3, an assessment of the feasibility and validity the proposed methods in the context of benchmark examples involving acoustic radiation problems of an infinitely long circular cylinder and an infinitely long star-like object is conducted. Finally, Section 5.4 concludes this chapter with some remarks.

5.1 Introduction

It is well known that one of the inherent drawbacks of the boundary integral equations (BIEs) and the BEM is the non-uniqueness of the solution of the resulting system of equations due to the spurious eigenvalue problem. In the field of acoustics, this problem arises in exterior acoustic problems, where interior problem eigenfrequencies are fictitiously arising. Consequently, the conventional BEM may fail to offer unique solutions at frequencies in the neighbourhood of the eigenfrequencies of the associated interior problem. These eigenfrequencies are usually called fictitious eigenfrequencies because they have no physical meaning, but just arise from the drawback of the boundary integral representation when solving exterior acoustic problems.

To solve this numerical issue, some techniques have been suggested by various authors. In this regard, the singular value decomposition (SVD) technique has been widely employed in contexts of the BIEs and BEM to overcome the non-uniqueness problem. Chen et al. [75] applied the dual multiple reciprocity method (MRM) in conjunction with the SVD technique to determine the critical wavenumbers of a cavity with or without a thin partition in where the SVD technique was proposed to filter out the spurious eigenvalues and to determine the multiplicity of the true eigenvalues for the case of square cavities. The SVD technique is also utilised in combination with the real-part dual BEM for solving acoustic problems of 2D cavities in [76, 77]. Kuo et al. [78] employed the generalised singular value decomposition (GSVD) method to eliminate spurious eigensolutions arisen in incomplete boundary element formulations used for solving the Helmholtz equation in circular domains.

Several studies proposed the combined Helmholtz integral equation formulation (CHIEF) method to deal with the non-uniqueness problem. For instance, Chen et al. [79] applied the CHIEF method to overcome the spurious eigensolutions of circular and rectangular cavities subjected to Dirichlet boundary conditions. In another study, Chen et al. [80] employed the CHIEF method in conjunction with the SVD technique to avoid the appearance of fictitious eigenfrequencies in exterior radiation and scattering problems. The application of the CHIEF method to deal with the spurious eigensolutions of the Helmholtz BIEs and the BEM for

2D acoustic cavity problems is investigated in [72].

The Burton–Miller formulation is another popular scheme in this regard and it has been extensively applied in the context of the BEM to obtain unique solutions. Chen et al. [81] employed the Burton–Miller method combined with the complex-valued BEM to solve Helmholtz eigenvalue problems with a multiply connected domain. More recently, the Burton–Miller method has been applied in the context of a modified version of the BEM based on the dual-level fast multipole (DL-FM) method for large-scale 3D sound field analysis [82]. On the one hand, the CHIEF method is based on adding additional constraints to the system by including the so-called CHIEF points, which are collocation points outside the domain that also satisfy the Helmholtz equation. Consequently, the resulting system of equations becomes overdetermined and inherently filters out the spurious solutions at low frequencies. On the other hand, the Burton–Miller method adds the imaginary double layer integral equation to the original one, resulting in a shift of the fictitious eigenfrequencies to the complex plane and allowing for computing the unique solutions, especially in the high frequency range. However, it should be noted that both methods involve more complex procedures and require higher computational times than conventional approaches.

Recently, the dual surface method has also been effectively utilised in a BEM context to remedy the non-uniqueness problem in exterior acoustic analysis [83]. The dual surface method creates a virtual surface, located outside the medium, to shift the fictitious eigenfrequencies to the complex plane and overcome the non-uniqueness instabilities in the BEM. Compared with the CHIEF method, the dual surface method employs 100% additional points but without building additional equations because the fundamental solution at these points is added to the conventional coefficients, multiplied by a combination factor, resulting in a linear combination like in Burton–Miller-based approaches.

Like the BEM, the non-uniqueness solution problem can also arise in boundary-type meshless methodologies, as their structural formulations rely on the boundary integral equation. In order to remedy this problem in the context of meshless methods, some modification approaches has been presented in different works during the last years. In this regard, Chen et al. [84] employed the MFS for solving the eigenfrequencies of multiply connected membranes and utilised the SVD technique

and the Burton–Miller method to filter out the spurious eigensolutions from the MFS solutions. Liu [85] proposed the regularised meshless method (RMM) for 3D exterior acoustic problems. In this study, two modification strategies are employed to circumvent the fictitious eigenfrequencies associated with the RMM solutions. These strategies involve combining the RMM with the Burton–Miller approach in one case and utilising the dual surface method in the other. The results obtained confirm that these modification methods effectively eliminate the fictitious eigenfrequencies in the RMM solutions, leading to satisfactory results.

The numerical issues related to the fictitious eigenfrequency difficulty appeared in the SBM has been discussed in several studies. For instance, Fu et al. [25] proposed to combine the SBM with the Burton and Miller's formulation to deal with fictitious eigenfrequencies arisen in the SBM solutions when dealing with exterior acoustic radiation and scattering problems. The numerical results demonstrated that the proposed scheme enhances the accuracy of the solution of exterior acoustic problems, particularly in the vicinity of the corresponding interior eigenfrequencies. Also, due to the OIFs, the present Burton–Miller SBM overcomes the troublesome numerical calculation of singular and hyper-singular integrals in the Burton–Miller BEM. Li et al. [86] applied the SBM along with the SVD technique and the Burton–Miller method to 2D and 3D acoustics eigenproblems in simply- and multiply-connected domains. The numerical results presented show that both SVD and Burton–Miller techniques are effective strategies to treat the spurious eigensolutions. However, the SVD updating terms may filter out the true eigenvalues by mistake in some Dirichlet cases. Thus, this work concludes that it is more reliable for engineering applications to use the SBM in conjunction with a particular SVD technique called SVD updating document or the Burton–Miller method. More recently, studies about the applicability of the SBM combined with the Burton–Miller method for 2D and 3D acoustic design sensitivity analysis have been reported in [87, 88]. The numerical examples presented, considering different design variable parameters, show that this scheme is robust and accurate when dealing with acoustic design sensitivity analysis, guaranteeing results devoid of fictitious frequencies. Wu et al. [89] introduced a modified formulation of the SBM by employing the CHIEF and the self-regularisation (SR) techniques, namely SR-CHIEF-SBM scheme, for 2D and 3D exterior acoustic problems. In contrast to the

CHIEF-SBM approach which adopts additional CHIEF points, as the collocation points outside the domain, in the SBM formulations, the SR-CHIEF-SBM scheme applies the CHIEF points as the extra source points to the SBM equations. Their numerical investigations demonstrate that, although the CHIEF-SBM can eliminate the non-uniqueness problem at the relatively small wavenumbers, it may still fail at large wavenumbers. In contrast, the proposed SR-CHIEF-SBM successfully resolves the non-uniqueness issue and consistently delivers accurate results across the entire wavenumber range in the conducted numerical experiments.

The objective of this chapter is to study the spurious eigensolution problem in the context of the previously developed 2.5D SBM and to propose modification strategies to effectively eliminate this problem from the 2.5D SBM solutions. In 3D acoustic problems, the terms fictitious frequencies or fictitious eigenfrequencies are normally used for exterior problems since its associated interior problem is bounded: the eigenvalues of the interior problem are representing natural frequencies of the cavity. In contrast, the terms spurious eigenvalues or spurious eigensolutions are typically employed when dealing with interior problems because the corresponding exterior problem is unbounded: the eigenvalues of this problem are not associated to eigenfrequencies, but to wave propagation modes. The term spurious refers to the fact that these waves vanish when they are propagating due to the unboundedness of the corresponding exterior medium. However, for problems simulated in a 2.5D context, the interior problem is also unbounded, due to the longitudinal invariancy condition of the 2.5D systems. Therefore, in the 2.5D domain, unlike 2D or 3D ones, the so-called fictitious eigenfrequencies become spurious dispersion curves associated to propagation modes of the corresponding interior problem. Dispersion curves are groups of eigenvalues related to the same wave pattern that typically occur at variable frequencies, being therefore not defined by a specific eigenfrequency but by pairs of frequencies and wavenumbers arising from the eigenvalues. The term spurious is employed since the eigenvalues of the corresponding interior problem are associated to wave propagation modes that may vanish along the cavity longitudinal direction. Thus, filtering spurious eigenvalues in the 2.5D SBM turns out to be more vital, since the accuracy of the method may be compromised at any frequency, while in 2D or 3D domains the problems arise just at the proximity of the fictitious eigenfrequencies.

In order to overcome the spurious eigensolutions problem in the 2.5D SBM and obtain unique solutions all along the wavenumber-frequency spectrum, this chapter proposes the Burton–Miller and dual surface methods to be used in conjunction with the 2.5D SBM. The feasibility, validity and accuracy of the proposed 2.5D modified approaches are studied in the framework of two benchmark examples: the acoustic radiation problem of an infinite cylinder with, separately, the Dirichlet and Neumann boundary conditions based on a simple geometry of the boundary. Furthermore, in order to assess the applicability of the proposed methods to deal with problems with arbitrary complex geometries, the acoustic radiation problem of a longitudinally infinite object with a constant star-like cross-section subjected to a Dirichlet boundary condition is devised and investigated. In addition, a detailed assessment in terms of the non-uniqueness problem of the 2.5D SBM developed in the basis of both single- and double-layer fundamental solutions is also presented in an error analysis framework. Furthermore, the MFS and BEM are classical approaches also included in the comparative study in order to better assess the performance of the proposed methods.

5.2 Mathematical formulation

The basic formulations of the proposed 2.5D SBM for solving exterior acoustic problems were presented in Section 2.2. These formulations were initially derived using the single-layer fundamental solutions. In order to enhance the methodology and incorporate the Burton–Miller technique, both single- and double-layer fundamental solutions are required. In this section, a unified framework is established by initially reviewing the formulations of the 2.5D SBM based on the single-layer fundamental solutions. Subsequently, the development of the 2.5D SBM in the basis of the double-layer fundamental solutions is introduced. Following this, the extended versions of the 2.5D SBM obtained from the combination with Burton–Miller and dual surface approaches are described in detail.

5.2.1 2.5D SBM in the basis of single-layer fundamental solutions

In this section, the required fundamental solutions and OIFs employed by the 2.5D SBM in the basis of single-layer potential, which referred to as the 2.5D SL-SBM from now on, are presented. In this context, the single-layer fundamental solutions of the 2.5D modified Helmholtz equation are presented as

$$\bar{G}^{\mathrm{SL}}(\mathbf{x},\mathbf{s},k_a) = \begin{cases} \dfrac{1}{2\pi}K_0(k_a r) \quad \text{for} \quad k_a \neq 0, \\ G_0^{\mathrm{SL}}(\mathbf{x},\mathbf{s}) \quad \text{for} \quad k_a = 0, \end{cases} \tag{5.1a}$$

$$\bar{H}^{\mathrm{SL}}(\mathbf{x},\mathbf{s},k_a,\mathbf{n}_x) = \begin{cases} -\dfrac{k_a}{2\pi}K_1(k_a r)\dfrac{\partial r}{\partial \mathbf{n}_x} \quad \text{for} \quad k_a \neq 0, \\ H_0^{\mathrm{SL}}(\mathbf{x},\mathbf{s},\mathbf{n}_x) \quad \text{for} \quad k_a = 0, \end{cases} \tag{5.1b}$$

where

$$G_0^{\mathrm{SL}}(\mathbf{x},\mathbf{s}) = -\frac{1}{2\pi}\ln(r), \tag{5.2a}$$

$$H_0^{\mathrm{SL}}(\mathbf{x},\mathbf{s},\mathbf{n}_x) = -\frac{1}{2\pi r}\frac{\partial r}{\partial \mathbf{n}_x}, \tag{5.2b}$$

are the single-layer fundamental solutions of potential and flux associated to the 2D Laplace equation, respectively.

By adopting a desingularisation process based on the subtracting and adding-back technique [25, 26, 33], the 2.5D OIFs, denoted by the terms $\bar{G}^{\mathrm{SL}}_{mm}$ and $\bar{H}^{\mathrm{SL}}_{mm}$ for the single-layer fundamental solutions, can be derived. Due to the fact that the order of the singularities arising for small source-receiver distances in both fundamental solutions of Laplace and Helmholtz equations is equal, $\bar{G}^{\mathrm{SL}}_{mm}$ and $\bar{H}^{\mathrm{SL}}_{mm}$ can be derived via the asymptotic form of the fundamental solutions of the 2D Laplace equation when the source-receiver distance is small, as [25, 42]

$$\bar{G}^{\mathrm{SL}}(\mathbf{s}_m,\mathbf{s}_j,k_a) = G_0^{\mathrm{SL}}(\mathbf{s}_m,\mathbf{s}_j) - \frac{1}{2\pi}\left(\ln\left(\frac{k_a}{2}\right)+\gamma\right) \quad \text{when} \quad r\to 0, \tag{5.3a}$$

$$\bar{H}^{\mathrm{SL}}(\mathbf{s}_m,\mathbf{s}_j,k_a,\mathbf{n}_x) = H_0^{\mathrm{SL}}(\mathbf{s}_m,\mathbf{s}_j,\mathbf{n}_x) \quad \text{when} \quad r\to 0. \tag{5.3b}$$

Accordingly, developing the 2.5D SBM in the basis of these single-layer fundamental solutions of the modified Helmholtz equation for exterior acoustic problems results in the following expression of the OIFs [71]

$$\bar{G}^{\mathrm{SL}}_{mm} = \begin{cases} {G_0^{\mathrm{SL}}}_{mm} - \dfrac{1}{2\pi}\left(\ln\left(\dfrac{k_a}{2}\right) + \gamma\right) & \text{for} \quad k_a \neq 0, \\ {G_0^{\mathrm{SL}}}_{mm} & \text{for} \quad k_a = 0, \end{cases} \tag{5.4a}$$

$$\bar{H}^{\mathrm{SL}}_{mm} = {H_0^{\mathrm{SL}}}_{mm}, \tag{5.4b}$$

where

$${G_0^{\mathrm{SL}}}_{mm} = \frac{1}{L_m}\int_{\Gamma_s} G_0^{\mathrm{SL}}(\mathbf{x}_m, \mathbf{s}_j)\,\mathrm{d}\Gamma_s(\mathbf{s}) = -\frac{1}{2\pi}\,\ln\left(\frac{L_m}{2\pi}\right), \tag{5.5a}$$

$${H_0^{\mathrm{SL}}}_{mm} = \frac{1}{L_m}\left(1 - \sum_{j=1, j\neq m}^{N} L_j H_0^{\mathrm{SL}}(\mathbf{x}_m, \mathbf{s}_j, \mathbf{n}_b)\right), \tag{5.5b}$$

are, respectively, the OIFs for the single-layer fundamental solutions of the 2D exterior Laplace equation.

5.2.2 2.5D SBM in the basis of double-layer fundamental solutions

Let consider that the fundamental solutions in which the 2.5D SBM is based are the double-layer ones. This approach will be referred to as the 2.5D DL-SBM from

now on. These fundamental solutions can be written as

$$\bar{G}^{\mathrm{DL}}(\mathbf{x},\mathbf{s},k_a,\mathbf{n}_x)=\begin{cases}-\dfrac{k_a}{2\pi}K_1(k_ar)\dfrac{\partial r}{\partial \mathbf{n}_x} & \text{for} \quad k_a\neq 0,\\ G_0^{\mathrm{DL}}(\mathbf{x},\mathbf{s},\mathbf{n}_x) & \text{for} \quad k_a=0,\end{cases} \tag{5.6a}$$

$$\bar{H}^{\mathrm{DL}}(\mathbf{x},\mathbf{s},k_a,\mathbf{n}_x)=\begin{cases}\dfrac{k_a}{2\pi r}\Bigg(\Big(2K_1(k_ar)+k_arK_0(k_ar)\Big)\dfrac{\partial r}{\partial \mathbf{n}_x}\dfrac{\partial r}{\partial \mathbf{n}_b}+ \\ K_1(k_ar)\langle \mathbf{n}_x,\mathbf{n}_b\rangle\Bigg) & \text{for} \quad k_a\neq 0,\\ H_0^{\mathrm{DL}}(\mathbf{x},\mathbf{s},\mathbf{n}_x) & \text{for} \quad k_a=0,\end{cases} \tag{5.6b}$$

where $\langle \mathbf{n}_x,\mathbf{n}_b\rangle$ denotes the inner product of the vectors $\mathbf{n}_x$ and $\mathbf{n}_b$. Moreover, for the special case when $k_a=0$, the fundamental solutions are the ones associated to the 2D Laplace equation which can be read as

$$G_0^{\mathrm{DL}}(\mathbf{x},\mathbf{s},\mathbf{n}_x)=-\frac{1}{2\pi r}\frac{\partial r}{\partial \mathbf{n}_x}, \tag{5.7a}$$

$$H_0^{\mathrm{DL}}(\mathbf{x},\mathbf{s},\mathbf{n}_x)=\frac{1}{2\pi r^2}\left(2\frac{\partial r}{\partial \mathbf{n}_x}\frac{\partial r}{\partial \mathbf{n}_b}+\langle \mathbf{n}_x,\mathbf{n}_b\rangle\right). \tag{5.7b}$$

The 2.5D OIFs for the double-layer fundamental solutions of the exterior modified Helmholtz equation are proposed to be derived based on the subtracting and adding-back technique [25]. Considering the asymptotic relationships between the double-layer fundamental solutions of the Laplace and Helmholtz equations for small source-receiver distances as

$$\bar{G}^{\mathrm{DL}}(\mathbf{s}_m,\mathbf{s}_j,k_a,\mathbf{n}_x)=G_0^{\mathrm{DL}}(\mathbf{s}_m,\mathbf{s}_j,\mathbf{n}_x) \quad \text{when} \quad r\to 0, \tag{5.8a}$$

$$\begin{aligned}\bar{H}^{\mathrm{DL}}(\mathbf{s}_m,\mathbf{s}_j,k_a,\mathbf{n}_x)=H_0^{\mathrm{DL}}(\mathbf{s}_m,\mathbf{s}_j,\mathbf{n}_x)+\frac{k_a^2}{2}(G_0^{\mathrm{SL}}(\mathbf{s}_m,\mathbf{s}_j)- \\ \frac{1}{2\pi}\left(\ln\left(\frac{k_a}{2}\right)+\gamma\right) \quad \text{when} \quad r\to 0,\end{aligned} \tag{5.8b}$$

the 2.5D OIFs for the double-layer fundamental solutions of the exterior modified Helmholtz equation can be now expressed as

$$\bar{G}^{\mathrm{DL}}_{mm} = {G_0^{\mathrm{DL}}}_{mm}, \tag{5.9a}$$

$$\bar{H}^{\mathrm{DL}}_{mm} = \begin{cases} {H_0^{\mathrm{DL}}}_{mm} + \dfrac{k_a^2}{2}\left({G_0^{\mathrm{SL}}}_{mm} - \dfrac{1}{2\pi}\left(\ln\left(\dfrac{k_a}{2}\right) + \gamma\right)\right) & \text{for} \quad k_a \neq 0, \\ {H_0^{\mathrm{DL}}}_{mm} + \dfrac{k_a^2}{2}{G_0^{\mathrm{SL}}}_{mm}, & \text{for} \quad k_a = 0. \end{cases} \tag{5.9b}$$

where

$${G_0^{\mathrm{DL}}}_{mm} = -\frac{1}{L_m}\sum_{j=1, j\neq m}^{N} L_j G_0^{\mathrm{DL}}(\mathbf{x}_m, \mathbf{s}_j, \mathbf{n}_b), \tag{5.10a}$$

$${H_0^{\mathrm{DL}}}_{mm} = -\frac{1}{L_m}\sum_{j=1, j\neq m}^{N} L_j H_0^{\mathrm{DL}}(\mathbf{x}_m, \mathbf{s}_j, \mathbf{n}_b), \tag{5.10b}$$

are, respectively, the OIFs for the double-layer fundamental solutions of 2D exterior Laplace equation.

5.2.3 2.5D Burton–Miller SBM

The Burton–Miller method is usually used to deal with fictitious eigenfrequencies in the BEM. It proposes a formulation solved by a linear combination of the singular integral equation and its normal derivative multiplied by a combination factor to yield unique solutions. Taking this concept into consideration, the 2.5D Burton–Miller method applied in the framework of a 2.5D SBM, referred to as the 2.5D BM-SBM, is proposed in the present study. This approach takes together both single-layer and double-layer fundamental solutions of the Helmholtz equation as its basis functions. Specifically, the 2.5D BM-SBM proposes to compute the acoustic responses in the domain using an extended version of Eqs. (2.7a) and

(2.7b) of the form

$$\bar{p}(\mathbf{x}) = \sum_{j=1}^{N} \alpha_j \left(\bar{G}^{\mathrm{SL}}(\mathbf{x}, \mathbf{s}_j, k_a) + \gamma^{\mathrm{BM}} \bar{G}^{\mathrm{DL}}(\mathbf{x}, \mathbf{s}_j, k_a, \mathbf{n}_x) \right) \quad \text{for} \quad \mathbf{x} \in \Omega, \tag{5.11a}$$

$$\mathrm{i}\rho\omega\bar{v}(\mathbf{x}) = \sum_{j=1}^{N} \alpha_j \left(\bar{H}^{\mathrm{SL}}(\mathbf{x}, \mathbf{s}_j, k_a, \mathbf{n}_x) + \gamma^{\mathrm{BM}} \bar{H}^{\mathrm{DL}}(\mathbf{x}, \mathbf{s}_j, k_a, \mathbf{n}_x) \right) \quad \text{for} \quad \mathbf{x} \in \Omega, \tag{5.11b}$$

where γ^{BM} is the coupling parameter, and it is typically defined as $-\mathrm{i}/k$ [86, 90]. The alternative form of the coupling factor presented in [25], $\gamma^{\mathrm{BM}} = -\mathrm{i}/(k+1)$, has also been tested in the framework of the present research, demonstrating a very similar behaviour. The associated OIFs required in the 2.5D BM-SBM can be now set as a linear combination of the OIFs of the single-layer and double-layer fundamental solutions given by

$$\bar{G}^{\mathrm{BM}}_{mm} = \bar{G}^{\mathrm{SL}}_{mm} + \gamma^{\mathrm{BM}} \bar{G}^{\mathrm{DL}}_{mm}, \tag{5.12a}$$

$$\bar{H}^{\mathrm{BM}}_{mm} = \bar{H}^{\mathrm{SL}}_{mm} + \gamma^{\mathrm{BM}} \bar{H}^{\mathrm{DL}}_{mm}. \tag{5.12b}$$

Thus, acoustic responses computed via the proposed 2.5D BM-SBM can be obtained following the same process as in the conventional SBM but using Eqs. (5.11a) and (5.11b) instead of Eqs. (2.7a) and (2.7b).

5.2.4 2.5D dual surface SBM

The dual surface method operates with the single-layer fundamental solutions as its kernel functions. Its particularity is to use a virtual surface (boundary) located outside the computational domain, apart from the physical one. This virtual surface is typically a reduced scale version of the physical boundary, as shown in Figure 5.1, being δ^{DS} the constant normal distance between the two surfaces. A new set of source points is arranged on this virtual surface based on the same (scaled) distribution defined for the physical boundary. The method's solution can be then obtained by considering the effect of two sets of virtual sources, the

original sources $\mathbf{s}$ on physical boundary and the additional sources $\mathbf{s}^{\mathrm{DS}}$ on the virtual one. The combination of this method with the 2.5D SBM leads to a 2.5D dual surface SBM approach, referred to as the 2.5D DS-SBM, which computes the acoustic responses in the domain based on Eqs. (2.7a) and (2.7b) as

$$\bar{p}(\mathbf{x}) = \sum_{j=1}^{N} \alpha_j \left(\bar{G}^{\mathrm{SL}}(\mathbf{x}, \mathbf{s}_j, k_a) + \gamma^{\mathrm{DS}} \bar{G}^{\mathrm{SL}}(\mathbf{x}, \mathbf{s}_j^{\mathrm{DS}}, k_a) \right) \quad \text{for} \quad \mathbf{x} \in \Omega, \tag{5.13a}$$

$$\mathrm{i}\rho\omega\bar{v}(\mathbf{x}) = \sum_{j=1}^{N} \alpha_j \left(\bar{H}^{\mathrm{SL}}(\mathbf{x}, \mathbf{s}_j, k_a, \mathbf{n}_x) + \gamma^{\mathrm{DS}} \bar{H}^{\mathrm{SL}}(\mathbf{x}, \mathbf{s}_j^{\mathrm{DS}}, k_a, \mathbf{n}_x) \right) \quad \text{for} \quad \mathbf{x} \in \Omega, \tag{5.13b}$$

where γ^{DS} is the coupling parameter and it is typically set to be the imaginary unit [83, 85]. The associated OIFs required in the 2.5D DS-SBM are the ones used for the 2.5D SL-SBM. Finally, the unique solutions via the proposed 2.5D DS-SBM are obtained through the same process in the conventional SBM but utilising Eqs. (5.13a) and (5.13b) instead of Eqs. (2.7a) and (2.7b). It is interesting to note that the proposed 2.5D DS-SBM approach can be seen as a particular linear combination between the 2.5D MFS and 2.5D SBM approaches, since the classical MFS typically uses an auxiliary boundary, outside of the computational domain, to place the sources, working in a similar manner than the virtual boundary in the dual surface method. It is worthwhile to note that compared with the Burton–Miller formulation, which involves both singular and hyper-singular kernels, one key advantage of the dual surface method is that no hyper-singularities arise. However, the additional set of source points used in the dual surface method leads to an increase in the computational cost.

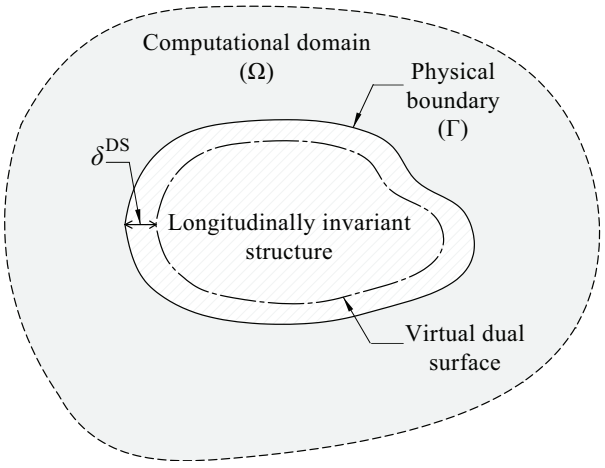

FIGURE 5.1: Schematic sketch of the dual surface model.

5.3 Numerical examples and discussions

In this section, the applicability, effectiveness and accuracy of the proposed 2.5D SBM-based schemes to deal with the spurious eigenvalue problem are verified and compared. In this study, three benchmark examples are considered: the first two examples involve the radiation problem of an infinitely long cylinder subjected, separately, to a Dirichlet boundary condition and a Neumann one, respectively, while the third example deals with the radiation problem of an infinitely long object with a constant star-like cross-section subjected to a Dirichlet boundary condition. The results are generally discussed in the basis of an error analysis framework and are separately presented in two sections for the cylinder and star-like object, respectively, as following. Furthermore, the 2.5D MFS and 2.5D BEM approaches are also utilised in the framework of these examples for comparative purposes, in order to present a detailed assessment between the proposed and the classical numerical methods to deal with non-uniqueness problem in a 2.5D context. Note that no technique for dealing with the arising spurious eigenvalues in the 2.5D MFS or 2.5D BEM is used in this work.

5.3.1 Example 5.1. Radiation problem of an infinite cylinder

The problem under consideration here is the radiation of an infinitely long cylinder of constant circular cross-section in the framework of two benchmark examples in which a Dirichlet boundary condition and a Neumann one are imposed, respectively. For the problem under Dirichlet boundary condition, the distribution of the prescribed pressure along the boundary is proposed to be

$$\bar{p}_b(\theta) = \cos(4\theta), \tag{5.14}$$

and, consequently, the analytical solution of the induced pressure field due to the proposed boundary condition in the wavenumber-frequency domain is given by [26]

$$\bar{p}(r,\theta) = -\frac{H_4^{(1)}(k_a r)}{H_4^{(1)}(k_a a)}\cos(4\theta) \quad \text{for} \quad r \geq a \quad \text{and} \quad 0 \leq \theta \leq 2\pi. \tag{5.15}$$

In the second example, the adopted acoustic velocity prescribed along the boundary is

$$\mathrm{i}\rho\omega\bar{v}_b(\theta) = k\cos(4\theta), \tag{5.16}$$

and the analytical solution of the radiation field in the wavenumber-frequency domain is [25]

$$\bar{p}(r,\theta) = -\frac{kaH_4^{(1)}(k_a r)}{k_a a H_3^{(1)}(k_a a) - 4H_4^{(1)}(k_a a)}\cos(4\theta) \quad \text{for} \quad r \geq a \quad \text{and} \quad 0 \leq \theta \leq 2\pi. \tag{5.17}$$

These analytical solutions of the considered problems are adopted as the reference methods in all comparative studies for the assessment of the proposed 2.5D numerical methods.

Furthermore, the available analytical solutions of the eigenvalues of the corresponding interior problems are employed to demonstrate the correspondence between

the numerical instabilities of the proposed numerical approaches and the eigenvalues of the corresponding interior problems. Depending whether the boundary condition is of Dirichlet or Neumann type, these eigenvalues can be computed by the following analytical equations

$$J_n\left(k_a a\right) = 0 \quad \text{for} \quad n = 0, 1, 2, ..., \tag{5.18a}$$

$$J'_n\left(k_a a\right) = 0 \quad \text{for} \quad n = 0, 1, 2, ..., \tag{5.18b}$$

respectively, where J_n and J'_n are the Bessel functions of the first kind of order n and its derivative, respectively. In all calculations, the radius of the cylinder is $a = 1$ m and the acoustic medium is assumed to be air with a density of $\rho = 1.225$ kg/m^3 and an associated wave speed of $c = 340$ m/s. Moreover, it is assumed that the virtual boundary of the 2.5D DS-SBM is adopted by a uniform angular distribution of the virtual sources, being equal to the number of collocation points, on a circle scaled with respect to the physical boundary such that the distance δ^{DS} is equal to 0.5 m.

5.3.1.1 Assessment of the methods in the wavenumber-frequency domain

In this section, the accuracy of the proposed 2.5D numerical schemes is assessed in the wavenumber-frequency domain in the basis of the RMSE analysis. The RMSE, initially described in Section 2.3, have been reformulated here to account for calculations in the wavenumber-frequency domain as as expressed by

$$\text{RMSE} = \frac{\sqrt{\dfrac{1}{N_t}\displaystyle\sum_{k=1}^{N_t} \left|\bar{p}_n(\mathbf{x}_k) - \bar{p}_a(\mathbf{x}_k)\right|^2}}{\sqrt{\dfrac{1}{N_t}\displaystyle\sum_{k=1}^{N_t} \left|\bar{p}_a(\mathbf{x}_k)\right|^2}}, \tag{5.19}$$

where $\bar{p}_n(\mathbf{x}_k)$ and $\bar{p}_a(\mathbf{x}_k)$ are the acoustic pressure responses computed by the numerical methods and the analytical solutions, respectively, at the kth test point. To obtain the RMSE in all benchmark examples, $N_t = 100$ test points uniformly distributed along a circumference of radius 1.1 m centred at the cylinder axis are

considered. The RMSE has been computed for frequencies varying from 1 Hz to 2000 Hz and wavenumbers ranging from 0 to 50 rad/m and the results are presented in the colour map plots shown in Figure 5.2 and Figure 5.3, which display the RMSE analysis of the different 2.5D numerical approaches for both benchmark examples. In addition, Figure 5.4 distinctly illustrates the described RMSE analysis for the 2.5D MFS method. All computations have been carried out using the same discretisation scheme, which adopts 10 collocation points (or nodes, depending on the method) per wavelength at the maximum frequency of interest (referred compactly as $N/\lambda_{2\text{kHz}} = 10$): a total of 370 uniformly distributed collocation points/nodes. Furthermore, the black dashed curves illustrate the dispersion curves of the eigenvalues of the corresponding interior problem analytically computed via Eqs. (5.18a) and (5.18b). In the following, the numerical behaviour demonstrated by each method is discussed and compared in detail.

Regarding the 2.5D SL-SBM approach, it is found that this method delivers low levels of accuracy at high frequencies for the case of the Dirichlet boundary condition problem, as shown in Figure 5.3. Specifically, due to the non-uniqueness problem, the 2.5D SL-SBM is severely in error at the vicinity of the dispersion curves of the spurious eigenvalues associated with propagation modes of the corresponding interior problem. These dispersion curves represent the zeros of Eq. (5.18a) considering a fourth order Bessel function in accordance to the angular distribution of the adopted boundary condition shown in Eq. (5.14). In contrast, in the case of the Neumann boundary condition problem, the 2.5D SL-SBM is delivering, in a general point of view, more accurate results across the whole wavenumber-frequency spectrum, as depicted in Figure 5.3. However, it can be observed that this method is also affected by spurious eigenvalues when the Neumann boundary condition is adopted. As seen, the corresponding dispersion curves of the spurious eigenvalues that are relevant in this situation are the same as before: the associated eigenvalues of the corresponding interior problem subjected to the Dirichlet boundary condition. Thus, it is shown that the nature of the corresponding spurious eigenvalues is not controlled by the boundary condition of the exterior problem under study, but governed by the type of virtual sources adopted. Particularly, since the single-layer potential assumes a discontinuity on the pressure field as the auxiliary source density, the relevant spurious eigenvalues

come from the interior problem under Dirichlet boundary condition.

On the other hand, the accuracy trends delivered by the 2.5D DL-SBM are quite reversed compared with the ones provided by the 2.5D SL-SBM with respect to the type of boundary condition adopted. Overall, the 2.5D DL-SBM demonstrates to be more accurate than the 2.5D SL-SBM for the problem under Dirichlet boundary condition. Reversely, the 2.5D DL-SBM suffers of accuracy problems in the Neumann case, while the 2.5D SL-SBM is found to be more accurate. Particularly, it can be seen from Figure 5.2 and Figure 5.3 that the spurious eigenvalues produced by the 2.5D SL-SBM in the Dirichlet example are inducing higher errors than the ones appearing in the 2.5D DL-SBM, while the reversed trend can be observed in the results obtained for the Neumann example. Furthermore, it is found that the 2.5D DL-SBM encounters non-uniqueness problems, for both Dirichlet or Neumann boundary conditions, at the vicinity of the dispersion curves associated to the corresponding interior problem under Neumann boundary condition, occurring at the zeros of Eq. (5.18b), following the same conceptual idea for the spurious eigenvalues appearance explained previously.

The results obtained reveal that, in a 2.5D domain context, the spurious eigenvalues appear in the form of dispersion curves that can potentially compromise the accuracy of the response at any frequency above the 2D eigenfrequency of the first propagation mode involved, which are 410.7 Hz and 287.8 Hz for this particular case study, for the 2.5D SL-SBM and 2.5D DL-SBM, respectively. This is in contrast to the numerical issues arising in the framework of 2D or 3D modelling, in which the problems appear just at the proximity of the fictitious eigenfrequencies.

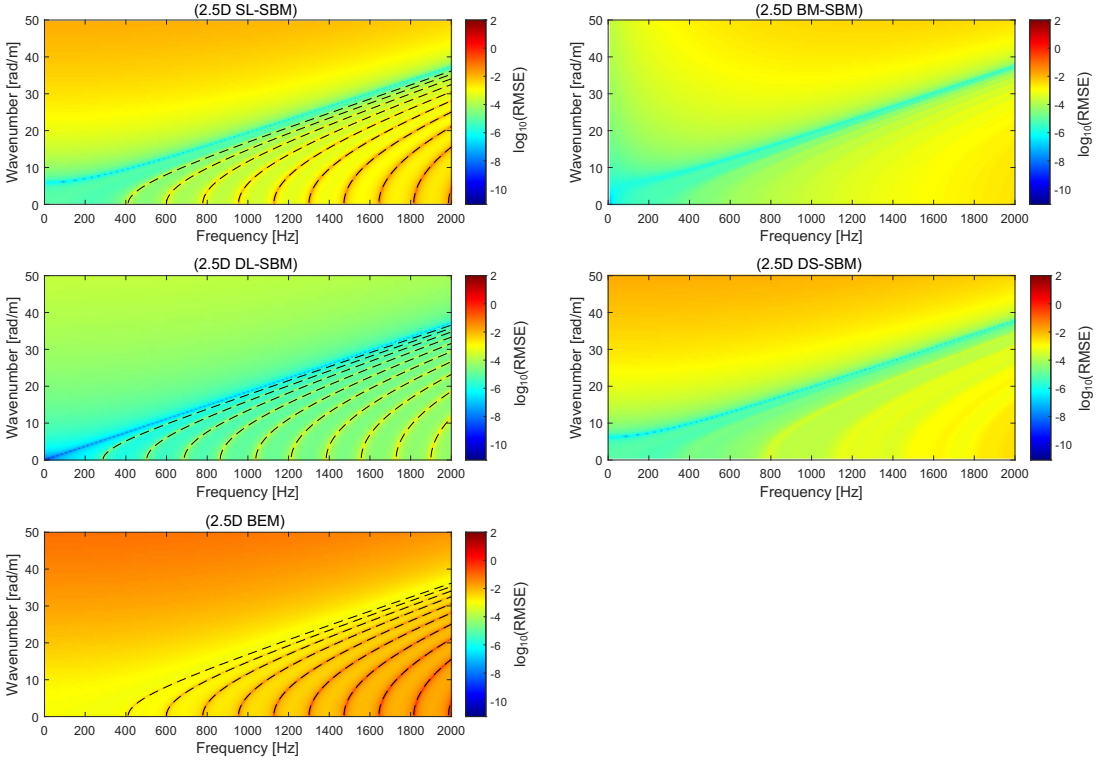

FIGURE 5.2: RMSE analysis of the proposed 2.5D numerical methods in the wavenumber-frequency domain for the radiation problem of the infinite cylinder under Dirichlet boundary condition considering $N/\lambda_{2\text{kHz}} = 10$. The black dashed lines illustrate the dispersion curves associated to the corresponding interior problem.

Regarding the 2.5D BM-SBM and 2.5D DS-SBM approaches, these modified versions of the 2.5D SBM approach are found to successfully avoid the spurious eigenvalue issues arisen in the 2.5D SL-SBM and 2.5D DL-SBM whatever the boundary condition is of Dirichlet or Neumann type. Using these methods, the accuracy of the solutions is particularly enhanced at the corresponding spurious eigenvalues. Consequently, the 2.5D BM-SBM and 2.5D DS-SBM are presenting a good agreement with the analytical solutions along all wavenumber-frequency spectrum, confirming the effectiveness of the Burton–Miller and dual surface modification techniques to solve the non-uniqueness problem in a 2.5D SBM context. Although the colour maps shown here provide an overview of the benefits associated to the 2.5D BM-SBM and 2.5D DS-SBM approaches, a more quantitative evaluation of the advantages of these methods is presented and discussed in the next section.

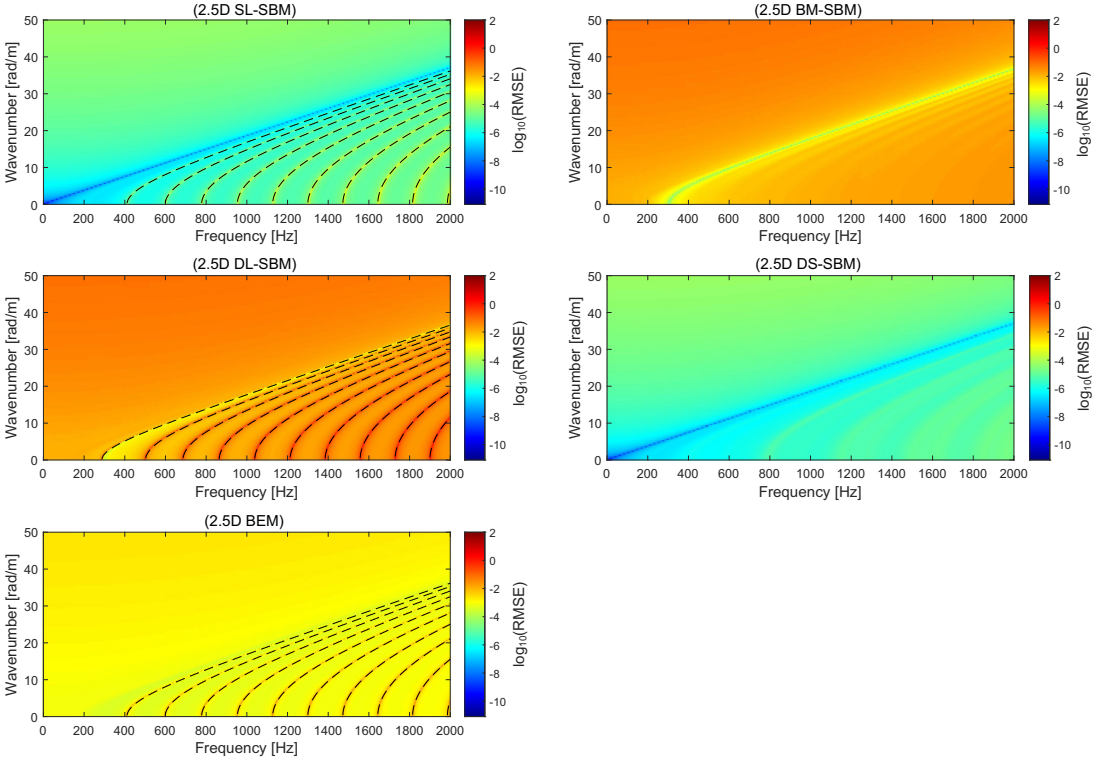

FIGURE 5.3: RMSE analysis of the proposed 2.5D numerical methods in the wavenumber-frequency domain for the radiation problem of the infinite cylinder under Neumann boundary condition considering $N/\lambda_{2\text{kHz}} = 10$. The black dashed lines illustrate the dispersion curves associated to the corresponding interior problem.

With respect to the 2.5D BEM approach, the method overally delivers the lowest levels of accuracy among all for the problem under Dirichlet boundary condition, as depicted in Figure 5.2. However, for the Neumann case presented in Figure 5.3, a different scenario is found: the 2.5D BEM shows to be more accurate than the 2.5D DL-SBM; instead, it is performing less accurately than the 2.5D SL-SBM and 2.5D DS-SBM. These behaviours are found to be in accordance to the previous studies in the topic [25, 26, 71]. Since the 2.5D BEM employs the single-layer potential, it is expected to be encountering similar non-uniqueness issues than the 2.5D SL-SBM. Results are demonstrating this hypothesis, since the dispersion curves of the spurious eigenvalues of the 2.5D BEM and 2.5D SL-SBM methods are matching.

The RMSE delivered by the 2.5D MFS method for both Dirichlet and Neumann examples is presented in Figure 5.4. In the current calculation, the 2.5D MFS is

implemented in the basis of the single-layer fundamental solution, considering the same number of virtual sources and collocation points and imposing a uniform distribution of the virtual sources on a circle of radius r_s, being $0 < r_s < a$. In the calculation, two trial values of r_s are adopted: $r_{s1} = 0.5$ m and $r_{s2} = 0.9$ m. According to Figure 5.4 and in a general point of view, it can be seen that the 2.5D MFS delivers the most accurate solutions among all discussed methods for both Dirichlet and Neumann examples, in accordance to previous studies in the topic [71, 74]. As expected, the 2.5D MFS solutions are sensitive to the placement of the virtual boundary, although the incurred error is generally highly small. However, it is observed that the 2.5D MFS solutions are also affected by spurious eigenvalues but, in this case, arising in different groups of spurious dispersion curves than the ones given by the SBM and BEM approaches shown in Figures 5.2 and 5.3. The results show that the spurious eigensolutions associated with the MFS depend on the location of the virtual boundary where the sources are distributed, as also concluded and proved in [84]. Therefore, for the 2.5D MFS implemented based on the single-layer fundamental solutions and whatever the boundary condition is of Dirichlet or Neumann type, the spurious dispersion curves appearing here occur at the vicinity of the zeros of $J_n(k_a r_{s1}) = 0$ and $J_n(k_a r_{s2}) = 0$, as illustrated with red dashed lines in sub-figures (i) and (ii), respectively, i.e. depending on the location of the virtual boundary adopted: $r_{s1} = 0.5$ m and $r_{s2} = 0.9$ m, respectively.

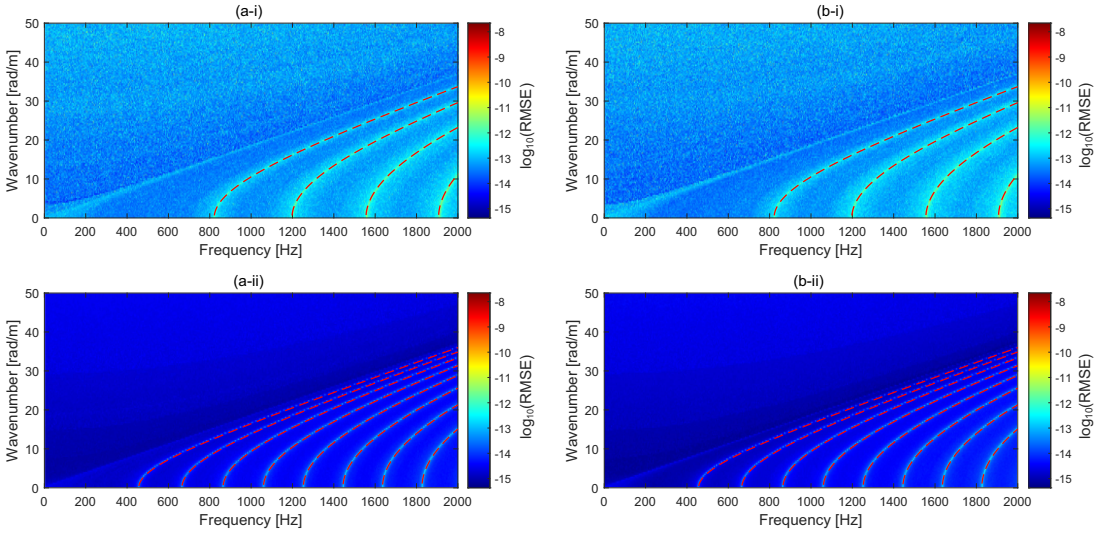

FIGURE 5.4: RMSE analysis of the 2.5D MFS approach in the wavenumber-frequency domain for the radiation problem of the infinite cylinder under (a) Dirichlet boundary condition and (b) Neumann boundary condition, adopting virtual boundaries placed at (i) $r_{s1} = 0.5$ m and (ii) $r_{s2} = 0.9$ m and considering $N/\lambda_{2\text{kHz}} = 10$. The red dashed lines illustrate the dispersion curves associated to the corresponding eigenvalues of the interior problem bounded by the virtual boundary adopted.

5.3.1.2 Assessment of the methods in the spatial-frequency domain

In order to investigate in detail the accuracy of the discussed methods, the acoustic responses in the spatial-frequency domain for the two benchmark examples defined are evaluated and compared. In this context, the acoustic pressure response at $x = 0$ induced by unitary boundary conditions with spatial-temporal distribution of the form $\delta(x)e^{\mathrm{i}\omega t}$ are used for comparison purposes. These responses, referred to as transfer functions from now on, are computed employing Eq. (2.4) for which the numerical integration is carried out by the trapezoidal rule along a wavenumber sampling with 2^8 points logarithmically distributed between 10^{-3} rad/m and 50 rad/m. In this analysis, the previously RMSE formula in terms of the transfer functions is used as denoted by Eq. (2.16).

The results of the proposed RMSE analysis are presented in Figure 5.5, where the methods studied are compared in the framework of the two benchmark examples with a cylindrical boundary. Focusing firstly on the 2.5D SBM-based approaches, severe numerical instabilities can be clearly observed for both 2.5D SL-SBM and

2.5D DL-SBM methods at frequencies above the first relevant eigenfrequencies of the corresponding 2D interior problem, in accordance to the results shown in Figures 5.2 and 5.3. In contrast, it can be observed that the enhanced 2.5D SBM approaches based on the Burton–Miller and dual surface methods are able to remove the numerical instabilities induced by the spurious eigenvalues, in accordance to the findings reported for the error analysis performed in the wavenumber-frequency domain. Due to that ability, these methods are producing smooth transfer function spectra. Going into detail on the results presented for these two methods, it is found that the 2.5D BM-SBM provides more accurate results than the 2.5D DS-SBM for frequencies lower than 1022 Hz in the case of the Dirichlet boundary condition problem. In contrast, the 2.5D DS-SBM is the one performing more accurately at higher frequencies. For the Neumann boundary condition example, the 2.5D DS-SBM shows a much more accurate performance than the 2.5D BM-SBM at all frequencies due to the fact that it only uses the single-layer fundamental solutions, which has been found to be quite effective in this problem, as the results of the 2.5D SL-SBM point out. The accuracy of the 2.5D BM-SBM is severely compromised due to the hyper-singularities arisen in this method, but its results are still acceptable with less than 2% for 10 collocation points per wavelength.

Regarding the 2.5D BEM approach, it can be seen that this method also experiences tremendous numerical instabilities rising up from frequencies greater than the first relevant eigenfrequency of the corresponding 2D interior problem, which is in similarity with the behaviour found in the 2.5D SL-SBM. This is expected, since BEM approach adopted here is based also on the single-layer fundamental solutions. Regarding the 2.5D MFS approach, this method operates with errors approximately ten orders of magnitude lower than the other approaches, although the incurred error also experience an unstable behaviour in a similar manner than the 2.5D SL-SBM and 2.5D BEM approaches, having in mind that the spurious eigenvalues come, in this case, from the interior problem bounded by the virtual boundary.

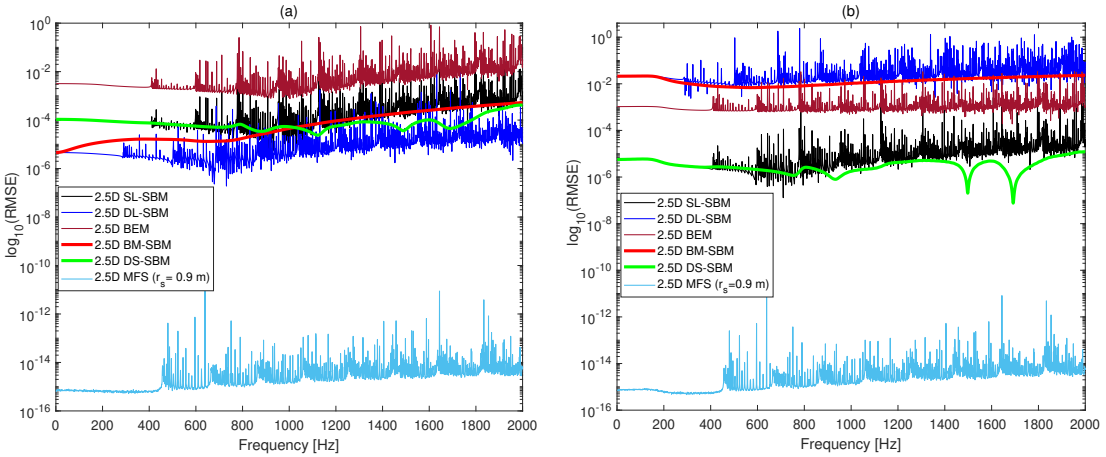

FIGURE 5.5: RMSE analysis for the transfer functions computed by the proposed 2.5D numerical methods for the radiation problems of an infinite cylinder under (a) Dirichlet boundary condition and (b) Neumann boundary condition.

Complementary to the previous analysis, simulations were performed to study the evolution of the RMSE for the transfer functions of the 2.5D BM-SBM and 2.5D DS-SBM with respect to the number of collocation points per wavelength (N/λ). This analysis has been done for collocation points per wavelength ranging between 2 and 20 at two selected frequencies of interest: 500 Hz and 2000 Hz. The corresponding results for the radiation problem of a cylinder under Dirichlet and Neumann boundary conditions are presented in Figure 5.6. Overall, it can be observed that the RMSE associated to both 2.5D BM-SBM and 2.5D DL-SBM methods smoothly approach the analytical solutions by increasing the number of collocation points, following different trends depending on the type of boundary condition adopted. On the one hand, the curves associated to both 2.5D BM-SBM and 2.5D DS-SBM methods have almost the same slopes in the Dirichlet example. Results show a slightly better performance of the 2.5D BM-SBM at 500 Hz while reversed behaviour can be observed at 2000 Hz. On the other hand, in the Neumann boundary condition example, the results of the 2.5D DS-SBM method approach the analytical solution significantly faster than the 2.5D BM-SBM, as expected from the previous results.

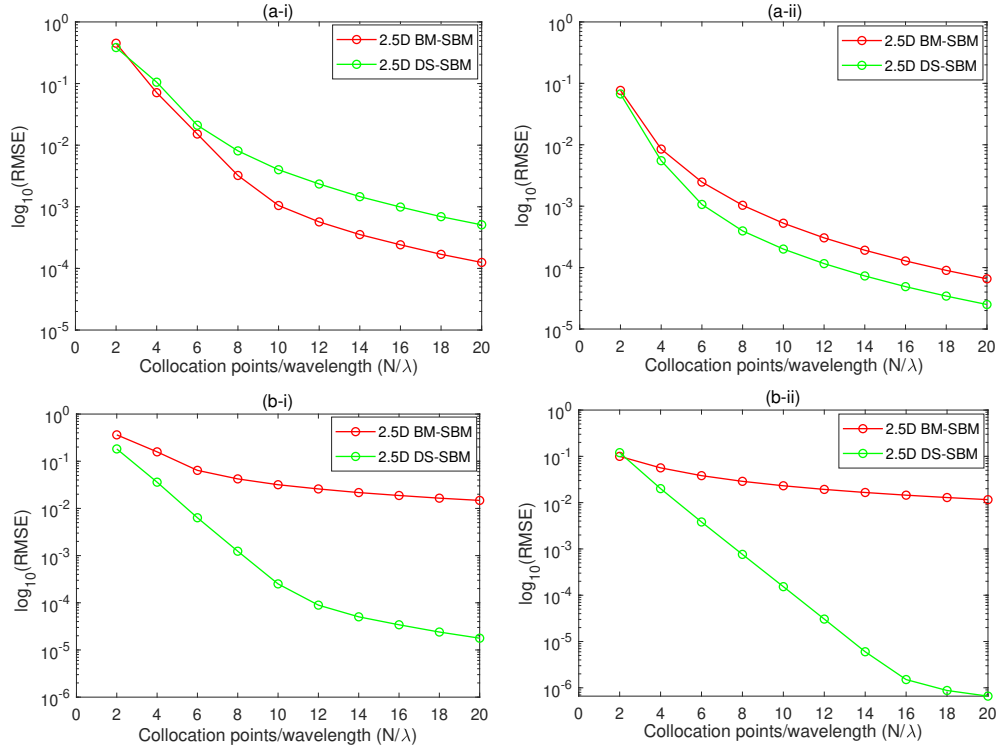

FIGURE 5.6: RMSE analysis for the acoustic pressure transfer functions with respect to the number of collocation points per wavelength computed associated to the 2.5D BM-SBM and 2.5D DS-SBM schemes for the radiation problems of an infinite cylinder under (a) Dirichlet boundary condition and (b) Neumann boundary condition obtained for the frequencies of (i) 500 Hz and (ii) 2000 Hz.

In the two previous examples, the proposed modified versions of the 2.5D SBM to deal with the spurious eigensolutions issue have been verified for the acoustic radiation problem of an infinitely long circular cylinder. The accuracy of the proposed methods is discussed in detail and compared with the traditional BEM, MFS and SBM approaches. However, the feasibility of using the proposed methods to deal with problems having arbitrary complex geometries can not be demonstrated only with these calculation examples. In order to study the capabilities of the proposed methods in the context of arbitrary complex boundaries, the acoustic radiation problem of a longitudinally infinite object having a constant star-like cross-section is hereafter devised and analysed.

5.3.2 Example 5.2. Radiation problem of an infinitely long object with a constant star-like cross-section

In this example, the problem of the sound field radiated by a longitudinally infinite object with an invariant star-like cross-section subjected to a Dirichlet boundary condition is considered. The star-like shape adopted in this example, as shown in Figure 5.7a, is parametrically given by

$$\begin{aligned} r_b(\theta) &= \frac{d}{2m^2}\left[m^2 + 2m + 2 - 2(m+1)\sin(m\theta)\right], \\ y(\theta) &= r_b(\theta)\cos\theta, \quad z(\theta) = r_b(\theta)\sin\theta, \end{aligned} \tag{5.20}$$

where $d = 1$ and $m = 5$.

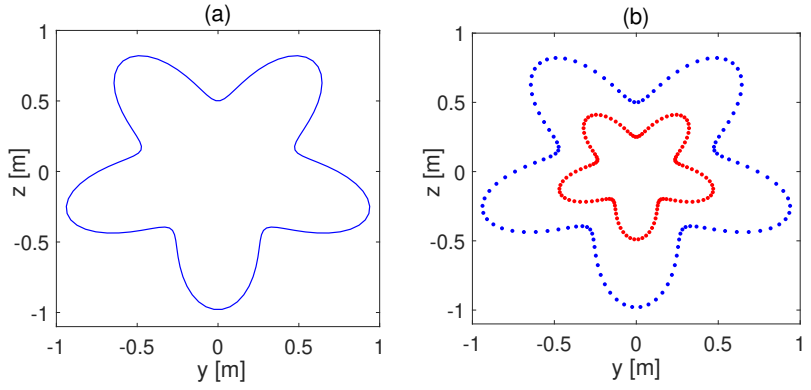

FIGURE 5.7: (a) Star-like shape captured by Eq. (5.20) with $d = 1$ and $m = 5$. (b) Discretised physical boundary (blue) and the virtual boundary adopted for the 2.5D DS-SBM with $d = 0.5$ (red).

For the problem described, if a distribution of the prescribed pressure along the boundary of the form

$$\bar{p}_b(r_b, \theta) = -\frac{H_4^{(1)}(k_a r_b)}{H_4^{(1)}(k_a a)}\cos(4\theta) \tag{5.21}$$

is imposed, the radiation pattern on the acoustic medium is exactly defined by the analytical solution of a circular cylinder of radius a, given by Eq. (5.15).

Regarding the implementation of the 2.5D DS-SBM in this example, it is supposed that the virtual boundary has also a star-like shape scaled with respect to the

physical one. Accordingly, the virtual boundary is parametrically defined by Eq. (5.20) where d, being $0 < d < 1$, refers to the scale factor of the virtual boundary. Thus, by considering the same number of the virtual sources than the collocation points, as before, it is assumed that the virtual sources also form a uniform angular distribution along the virtual boundary with the scale factor d, as captured in Figure 5.7b for the case of $d = 0.5$.

To study the proposed methods in the context of this example, the RMSE of the transfer functions in the spatial-frequency domain has been computed via Eq. (2.16), taking into account the same assumptions adopted for the previous examples. The computation is carried out using a discretisation scheme which adopts 10 collocation points per wavelength at the maximum frequency of interest, referred compactly as $N/\lambda_{2\text{kHz}} = 10$, resulting in a total of 408 uniformly distributed collocation points/nodes. The results obtained are illustrated in Figure 5.8. As shown, due to the non-uniqueness problem, both 2.5D SL-SBM and 2.5D DL-SBM approaches are experiencing strong numerical instabilities at frequencies above the first relevant eigenfrequencies of the corresponding 2D interior problem. Instead, the modified versions of the 2.5D SBM based on the Burton–Miller and dual surface methods are able to overcome the instabilities induced by the spurious eigenvalues and, consequently, they exhibit low RMSE along the whole spatial-frequency domain. Specifically, it is found that the 2.5D BM-SBM delivers stable responses with approximately 0.1 % error along all frequency range of interest for 10 collocation points per wavelength. In contrast, the 2.5D DS-SBM approach demonstrates a more accurate performance than the 2.5D BM-SBM at frequencies lower than 1383 Hz, while at high frequencies this method incurs to higher errors due to its stronger sensitivity to the spurious eigenvalues compared the 2.5D BM-SBM. Regarding the 2.5D BEM approach, it can be seen that this method overally operates similarly to the 2.5D SL-SBM when encounters the non-uniqueness problem, due to utilising the single-layer potential, but delivers solutions with errors severely higher than the 2.5D SL-SBM, specifically at frequencies above 334 Hz.

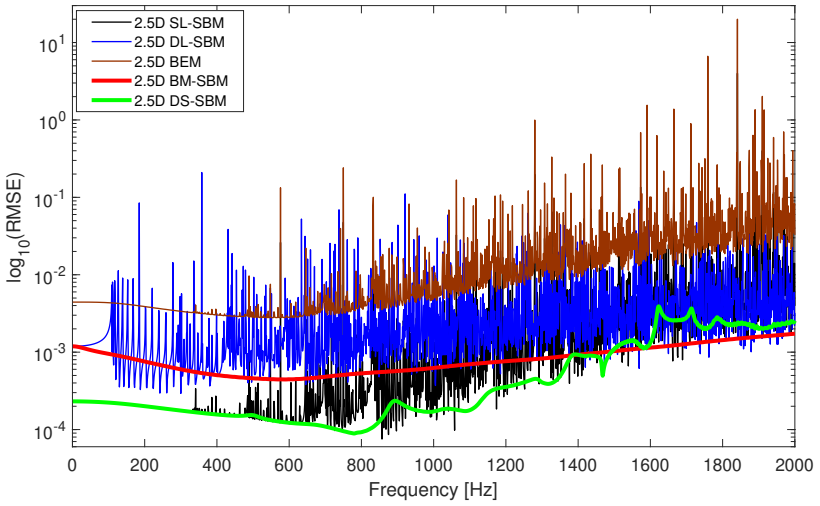

FIGURE 5.8: RMSE analysis for the transfer functions in spatial-frequency domain computed by the proposed 2.5D numerical methods for the radiation problem of an infinite star-like object under Dirichlet boundary condition.

5.4 Conclusions

In this chapter, the 2.5D SBM approach to deal with exterior acoustic wave propagation problems in which the geometry of the boundary has a constant cross-section along its longitudinal direction is studied, with focusing on the spurious eigenvalue problem. In a similar manner as the BEM when dealing with exterior acoustic problems, the SBM formulated in the spatial-frequency domain also suffers the spurious eigenvalue problem which yields to exhibit non-unique solutions at the vicinity of the corresponding interior problem eigenvalues. This numerical phenomenon arises differently in 2.5D domain problems: the spurious eigenvalues appear in the form of spurious dispersion curves associated to propagation modes of the corresponding interior problem. This study proposes two approaches to overcome this numerical difficulty and to produce unique solutions in 2.5D modelling based on the SBM: the 2.5D BM-SBM, which combines the traditional SBM with the Burton–Miller approach, and the 2.5D DS-SBM, which employs the dual surface method instead. The validity and accuracy of the proposed numerical schemes are examined in comparison with the available analytical solutions in the context of three benchmark examples: the acoustic radiation of an infinitely long cylinder under, separately, Dirichlet and Neumann boundary conditions, and

the problem of the sound field radiated by a longitudinally infinite object with a constant star-like cross-section subjected to a Dirichlet boundary condition.

The detailed comparison carried out in this chapter demonstrates the validity and accuracy of the proposed 2.5D BM-SBM and 2.5D DS-SBM schemes to remedy the severe numerical instabilities arisen in the 2.5D SBM using the single-layer or double-layer fundamental solutions. Both 2.5D BM-SBM and 2.5D DS-SBM successfully avoid the non-uniqueness problem and, as a consequence, significantly enhance the accuracy of the simulations at frequencies in the range where the dispersion curves of the corresponding interior problem are present. For the benchmark example considered for the circular cylinder where the Dirichlet boundary condition is adopted, these modified versions of the 2.5D SBM deliver similar accuracy rates. The 2.5D BM-SBM shows a slightly more accurate performance at frequencies lower than 1022 Hz, while the opposite trend is observed at higher frequencies. In contrast, it is found that the 2.5D DS-SBM is clearly the best alternative in the problem under Neumann boundary condition, since it operates with errors approximately three orders of magnitude lower than the ones associated with the 2.5D BM-SBM along all wavenumber-frequency spectrum and it approaches rapidly to the analytical solution by increasing the number of collocation points. The low levels of accuracy as well as slow convergence rates demonstrated by the 2.5D BM-SBM in this case are induced by the hyper-singularities associated to the double-layer fundamental solutions. In the case study of the star-like object, the 2.5D BM-SBM and 2.5D DS-SBM are also showing an effective performance when dealing with spurious eigenvalues, delivering accurate solutions along the whole wavenumber-frequency spectrum and demonstrating the feasibility of the proposed methods to solve problems with a complex boundary geometry.

Along this study, it is found that the spurious eigenvalues arising in the 2.5D SBM depend on the employed potentials instead of the type of boundary condition. Thus, all the examples show that the 2.5D SL-SBM approach involves spurious eigenvalues associated with the corresponding interior problem under Dirichlet boundary condition, since the method is based on single-layer potential. In contrast, the spurious eigenvalues affecting the 2.5D DL-SBM scheme are those of the corresponding interior problem under Neumann boundary condition, since the method is based on double-layer fundamental solutions.

Additionally, results from classic approaches such as the 2.5D BEM and 2.5D MFS are included in the comparisons to study the appearance and severity of the spurious eigenvalues in the 2.5D SL-SBM and 2.5D DL-SBM with respect to those traditional methods. The presented numerical studies confirm that the 2.5D SL-SBM suffers from the non-uniqueness issue in a similar manner than the 2.5D BEM, since both methods employ the single-layer fundamental solutions as their kernels, while it shows a higher accuracy than the 2.5D BEM. This work also shows that 2.5D MFS is affected by the spurious eigenvalues associated to the interior problem bounded by the virtual boundary, as proved for 2D cases in previous works [84]. Results for the 2.5D MFS approach are not presented for the benchmark example of the star-like object since the strong challenges associated with finding an optimal virtual boundary in the case of complex boundary geometries are out of scope of this study. However, it is worth mentioning that the non-uniqueness difficulty should be taken in serious consideration in those cases.

In conclusion, the enhanced versions of the 2.5D SBM scheme that involve the Burton–Miller and dual surface methods are found to be competitive alternatives for exterior acoustic analysis that not only significantly reduce the computational costs of mesh-based methods, but also robustly overcome the troublesome non-uniqueness problem of boundary-type discretisation methods.

Chapter 6

Conclusions and future work

In this chapter, an overview of the most important contributions of the present thesis is provided. Furthermore, a number of recommendations for advancing research on this topic is conveyed.

6.1 Thesis conclusions

The main objective of the PhD studies that resulted in the present dissertation present was to investigate and develop new numerical meshless methodologies to address various acoustic radiation and scattering problems. In pursuit of this objective, the present thesis has particularly centred on developing a novel generation of boundary-type numerical meshless methodologies, owing to their remarkable advantages in terms of computational efficiency and the simplicity of formulation compared with domain-type numerical approaches. In this regard, this thesis has specifically focused on studying and developing a novel method: the 2.5D SBM, that combines the computational benefits of the 2.5D formulation and the SBM itself. Additionally, a hybrid scheme combining the SBM and MFS methods has been pursued along the doctoral studies resulting in the proposition of a novel SBM-MFS methodology specially devised to tackle problems involving geometric singularities such as corners and sharp edges. Furthermore, modified versions of the 2.5D SBM based on the Burton–Miller and dual surface techniques, referred to as the 2.5D BM-SBM and the 2.5D DS-SBM, respectively, have been proposed specifically to mitigate the effect of the spurious eigensolutions arising in the proposed 2.5D SBM. Drawing upon the studies presented and the conducted numerical experiments employing the proposed SBM-based strategies, the following conclusions can be inferred from this thesis.

The detailed comparisons conducted across various calculation scenarios demonstrate the computational advantages of the proposed 2.5D SBM approach over former numerical methods. Due to its meshless nature and the discretisation strategy deployed the proposed 2.5D SBM scheme operates with higher efficiency compared to equivalent 2.5D BEM approaches. This remarkable superiority arises from its ability to avoid two procedures that are typically associated with BEM-based approaches: the construction of a boundary mesh and the numerical integration over the boundary. Furthermore, the proposed 2.5D SBM is found to offer an enhanced accuracy compared to the BEM approach constructed using constant and linear elements. The proposed 2.5D SBM also demonstrates greater robustness compared to the 2.5D MFS. Unlike the latter method, the 2.5D SBM

does not need to deal with the challenging task of the fictitious boundary placement, a process known to be complex and time-consuming, especially for complex boundary geometries. Moreover, it has been found that the proposed 2.5D SBM exhibits a higher stability and boarder applicability than the 2.5D MFS, as shown by several benchmark examples.

This thesis has also studied the proposed 2.5D SBM in the framework of the practical benchmark scenario of the point source diffraction in the presence of a noise thin barrier, where the advantages of this method over previous state-of-the-art modelling strategies become quite evident. The 2.5D SBM enables the transformation of the original 3D problem into a series of 2D problems, where the barrier boundary is represented by just a line. This, coupled with the computational advantages of the SBM, allows for an efficient assessment of the noise mitigation induced by barriers with constant cross-sections. The performance of the proposed 2.5D SBM has been assessed in scenarios involving a harmonic source at a fixed position and a scenario with a moving harmonic source at a constant speed. The obtained results are consistent with findings from previous numerical studies on the same subject.

The numerical experiments conducted with the proposed hybrid SBM-MFS methodology have demonstrated several significant advantages of the new method over the traditional MFS, SBM, and BEM approaches. Firstly, it has been observed that the hybrid SBM-MFS methodology consistently provides higher levels of accuracy and faster convergence rates when compared to the SBM and BEM approaches, and it matches or surpasses the accuracy of the MFS, especially in problems characterised by smooth circular boundary geometries. However, this scenario changes when dealing with geometries featuring corners and sharp edges, where the hybrid method effectively mitigates errors induced by MFS and SBM, resulting in highly accurate solutions. Lastly, due to the specific formulation of the hybrid SBM-MFS methodology, it naturally avoids the problem of the non-uniqueness solution arising near the fictitious eigenfrequencies of the corresponding interior problems, a characteristic that neither SBM nor BEM inherently possess.

The investigation into the issue of fictitious eigenfrequencies, which arises due to the non-uniqueness solution problem, reveals that this numerical phenomenon appears differently in 2.5D domain problems. In these scenarios, spurious eigenvalues

take the form of spurious dispersion curves, which are associated with the propagation modes of the corresponding interior problem. The proposed 2.5D BM-SBM and 2.5D DS-SBM methodologies, adopted in the basis of both single- and double-layer potentials, successfully mitigate this numerical issue in the 2.5D SBM. As a result, these approaches significantly improve the accuracy of simulations, particularly in the frequency range where the dispersion curves of the corresponding interior problem are present. Furthermore, results obtained from conventional methods like the 2.5D BEM confirm that the 2.5D SL-SBM experiences the non-uniqueness issue in a similar manner to the 2.5D BEM. This similarity arises because both methods employ single-layer fundamental solutions as their kernel functions. However, the spurious eigensolutions associated with the 2.5D MFS depend on the location of the virtual boundary where the sources are distributed.

6.2 Recommendations and future work

This thesis sets the stage for future investigations within this specific field and domain, offering valuable insights into various directions. While the methodologies presented here are promising, there are several ideas for their improvement. Looking ahead, the following section provides a concise overview of ideas for future work.

1. Throughout the research presented in this work, a uniform distribution of collocation points was consistently utilised in the framework of the proposed SBM approach. It would be of considerable interest to conduct a comprehensive study of the effects of collocation points distribution on the solutions, with the goal of determining the most effective and optimal distribution strategy for the employed SBM approach.

2. In the analyses carried out using the proposed hybrid SBM-MFS approach throughout this thesis, a common practice was to distribute MFS sources on the virtual boundary, typically constructed to be as a scaled version of the physical boundary. It is advisable to conduct a more thorough examination of the virtual source distribution in this method, with a concerted effort

to investigate any limitations on source placement to ensure more precise responses.

3. As a preliminary step, the hybrid SBM-MFS methodology has been introduced to address 2D acoustic wave propagation problems within the scope of this thesis. Thus, in future research, it would be valuable to explore the applicability of this approach for more complex scenarios in the context of 2.5D and 3D modelling.

4. Apart from the Burton–Miller and dual surface modification techniques used to address the non-uniqueness problem in this study, alternative modification strategies such as the SVD or CHIEF techniques have also been discussed in existing literature. An interesting direction for future research would involve examining how these approaches perform when combined with the 2.5D SBM, allowing for a detailed comparative analysis among these strategies to evaluate the most accurate and computationally efficient method for addressing the non-uniqueness solution problem in 2.5D SBM context.

5. Although this thesis demonstrates the potentialities of the proposed 2.5D SBM for effectively dealing with common practical acoustic problems, i.e. noise diffracted by thin barriers, it is expected to find even more complex engineering applications for this method. For instance:

    - Evaluating the performance of noise barriers with various shapes.
    - To study the suitability of the method to conduct acoustic sensitivity analyses to optimise the acoustic characteristics of structures, particularly in cases with a large number of design variables where conventional methods may be computationally inefficient.

Appendix A

Publications

Journals

Accepted manuscripts

- J. Fakhraei, R. Arcos, T. Pàmies, J. Romeu, 2.5D singular boundary method for exterior acoustic radiation and scattering problems, Engineering Analysis with Boundary Elements, 143 (1) (2022) 293–304.
- J. Fakhraei, R. Arcos, T. Pàmies, H. Liravi, J. Romeu, Modified 2.5D singular boundary methods to deal with spurious eigensolutions in exterior acoustic problems, Journal of Sound and Vibration, 550 (2023) 117597.

Appendix B

OIFs for the 2.5D fundamental solutions of the modified Helmholtz equation

In this appendix, the 2.5D OIFs associated with the modified Helmholtz equation are derived. To accomplish this, applying the subtracting and adding back technique to Eq. (2.7b) at collocation points on the boundary yields:

$$\begin{aligned}
\mathrm{i}\rho\omega\bar{v}(\mathbf{s}_m) &= \sum_{j=1}^{N}\alpha_j\bar{H}(\mathbf{s}_m,\mathbf{s}_j,k_a,\mathbf{n}_b) = \sum_{j=1}^{N}(\alpha_j-\alpha_m\Pi_{jm})\bar{H}(\mathbf{s}_m,\mathbf{s}_j,k_a,\mathbf{n}_b)\\
&+\alpha_m\sum_{j=1}^{N}\Pi_{jm}\Big(\bar{H}(\mathbf{s}_m,\mathbf{s}_j,k_a,\mathbf{n}_b)-H^{\mathrm{L}}(\mathbf{s}_m,\mathbf{s}_j,\mathbf{n}_b)\Big)\\
&+\alpha_m\sum_{j=1}^{N}\Pi_{jm}\Big(H^{\mathrm{L}}(\mathbf{s}_m,\mathbf{s}_j,\mathbf{n}_b)+H_{\mathrm{I}}^{\mathrm{L}}(\mathbf{s}_m,\mathbf{s}_j,\mathbf{n}_b)\Big)\\
&-\alpha_m\sum_{j=1}^{N}\Pi_{jm}H_{\mathrm{I}}^{\mathrm{L}}(\mathbf{s}_m,\mathbf{s}_j,\mathbf{n}_b),
\end{aligned} \tag{B-1}$$

where $H_{\mathrm{I}}^{\mathrm{L}}(\mathbf{s}_m,\mathbf{s}_j,\mathbf{n}_b)$ denotes the fundamental solutions of the flux for the Laplace equation in interior problems and where $\Pi_{jm} = L_j/L_m$, noting that $\Pi_{mm} = 1$. According to the dependency of the outward normal vectors on the fundamental solutions of interior and exterior problems for the Laplace equation, the following

identities can be stated:

$$\begin{aligned} H^{\mathrm{L}}(\mathbf{s}_m, \mathbf{s}_j, \mathbf{n}_b) &= -H_{\mathrm{I}}^{\mathrm{L}}(\mathbf{s}_m, \mathbf{s}_j, \mathbf{n}_b) \quad \text{for} \quad \mathbf{s}_m \neq \mathbf{s}_j \\ H^{\mathrm{L}}(\mathbf{s}_m, \mathbf{s}_j, \mathbf{n}_b) &= H_{\mathrm{I}}^{\mathrm{L}}(\mathbf{s}_m, \mathbf{s}_j, \mathbf{n}_b) \quad \text{for} \quad \mathbf{s}_m = \mathbf{s}_j \end{aligned} \tag{B-2}$$

and

$$\lim_{\mathbf{s}_j \to \mathbf{s}_m} \left(\frac{\partial G^{\mathrm{L}}(\mathbf{s}_m, \mathbf{s}_j)}{\partial \mathbf{n}_{b_m}} + \frac{\partial G^{\mathrm{L}}(\mathbf{s}_m, \mathbf{s}_j)}{\partial \mathbf{n}_{b_j}} \right) = 0. \tag{B-3}$$

If the boundary is a straight line, the above equation is explicitly equal to zero, since $\mathbf{n}_{b_m}(\mathbf{s}_m)$ is equal to $\mathbf{n}_{b_j}(\mathbf{s}_j)$ at all points. For problems with arbitrarily smooth geometries, fundamental solutions as well as normal vectors smoothly approach to their corresponding ones when source $\mathbf{s}_j$ and collocation $\mathbf{s}_m$ points get closer to each other along a line segment. In those situations, Eq. (B-3) is valid. Considering the relationship between the fundamental solutions of the Laplace and Helmholtz equations for small source-receiver distances as follows:

$$\bar{H}(\mathbf{s}_m, \mathbf{s}_j, k_a, \mathbf{n}_b) = H^{\mathrm{L}}(\mathbf{s}_m, \mathbf{s}_j, \mathbf{n}_b) \quad \text{when} \quad r \to 0, \tag{B-4}$$

and also using the help of Eqs. (B-2) and (B-3), Eq. (B-1) can be regularised as:

$$\begin{aligned} \mathrm{i}\rho\omega\bar{v}(\mathbf{s}_m) = & \sum_{j=1, j\neq m}^{N} (\alpha_j - \alpha_m \Pi_{jm}) \bar{H}(\mathbf{s}_m, \mathbf{s}_j, k_a, \mathbf{n}_b) \\ & + \alpha_m \sum_{j=1, j\neq m}^{N} \Pi_{jm} \Big(\bar{H}(\mathbf{s}_m, \mathbf{s}_j, k_a, \mathbf{n}_b) - H^{L}(\mathbf{s}_m, \mathbf{s}_j, \mathbf{n}_b) \Big) \\ & + \alpha_m \sum_{j=1, j\neq m}^{N} \Pi_{jm} \Big(H^{L}(\mathbf{s}_m, \mathbf{s}_j, \mathbf{n}_b) + H_I^{L}(\mathbf{s}_m, \mathbf{s}_j, \mathbf{n}_b) \Big) \\ & - \alpha_m \sum_{j=1}^{N} \Pi_{jm} H_I^{L}(\mathbf{s}_m, \mathbf{s}_j, \mathbf{n}_b). \end{aligned} \tag{B-5}$$

Now, the above equation is regularised except for its last term which still involves singularity. However, it has a finite value equal to $V_m = -1/L_m$, which can be

derived based on the following direct boundary integral equation:

$$u(\mathbf{x}_m) = \int_{\Gamma} \left(G_{\mathrm{I}}^{\mathrm{L}}(\mathbf{x}_m, \mathbf{s}) \frac{\partial u(\mathbf{s})}{\partial \mathbf{n}_b} - u(\mathbf{s}) H_{\mathrm{I}}^{\mathrm{L}}(\mathbf{x}_m, \mathbf{s}, \mathbf{n}_b) \right) \mathrm{d}\Gamma(\mathbf{s}) \quad \text{for} \quad \mathbf{x}_m \in \Omega_{\mathrm{I}}. \tag{B-6}$$

Substituting the simple test solution $u(\mathbf{s}) = 1$ and $\partial u(\mathbf{s})/\partial \mathbf{n}_b = 0$ into Eq. (B-6), we can obtain the following equation:

$$\int_{\Gamma} H_{\mathrm{I}}^{\mathrm{L}}(\mathbf{x}_m, \mathbf{s}, \mathbf{n}_b) \mathrm{d}\Gamma(\mathbf{s}) = -1 \quad \text{for} \quad \mathbf{x}_m \in \Omega_{\mathrm{I}}. \tag{B-7}$$

When the field point $\mathbf{x}_m$ approaches the boundary, we can discretize Eq. (B-7) as follows:

$$\begin{aligned} &\int_{\Gamma} H_{\mathrm{I}}^{\mathrm{L}}(\mathbf{x}_m, \mathbf{s}, \mathbf{n}_b) \mathrm{d}\Gamma(\mathbf{s}) = \sum_{j=1}^{N} \int_{\Gamma_j} H_{\mathrm{I}}^{\mathrm{L}}(\mathbf{x}_m, \mathbf{s}, \mathbf{n}_b) \mathrm{d}\Gamma_j(\mathbf{s}) \\ &\approx \sum_{j=1}^{N} H_{\mathrm{I}}^{\mathrm{L}}(\mathbf{x}_m, \mathbf{s}_j, \mathbf{n}_b) L_j = -1 \quad \text{for} \quad \mathbf{x}_m \in \Gamma. \end{aligned} \tag{B-8}$$

Dividing by non-zero value L_m, we have

$$\sum_{j=1}^{N} \Pi_{jm} H_{\mathrm{I}}^{\mathrm{L}}(\mathbf{x}_m, \mathbf{s}_j, \mathbf{n}_b) = V_m \quad \text{for} \quad \mathbf{x}_m \in \Gamma, \tag{B-9}$$

where $V_m = -1/L_m$. Then, the regular formulation of Eq. (B-1) is represented as:

$$\begin{aligned} \mathrm{i}\rho\omega\bar{v}(\mathbf{s}_m) &= \sum_{j=1, j\neq m}^{N} \alpha_j \bar{H}(\mathbf{s}_m, \mathbf{s}_j, k_a, \mathbf{n}_b) + \alpha_m \sum_{j=1, j\neq m}^{N} \Pi_{jm} H_{\mathrm{I}}^{\mathrm{L}}(\mathbf{s}_m, \mathbf{s}_j, \mathbf{n}_b) - \alpha_m V_m \\ &= \sum_{j=1, j\neq m}^{N} \alpha_j \bar{H}(\mathbf{s}_m, \mathbf{s}_j, k_a, \mathbf{n}_b) - \alpha_m \sum_{j=1, j\neq m}^{N} \Pi_{jm} H^{\mathrm{L}}(\mathbf{s}_m, \mathbf{s}_j, \mathbf{n}_b) - \alpha_m V_m. \end{aligned} \tag{B-10}$$

Compared with Eq. (2.10b) at $\mathbf{s}_m = \mathbf{s}_j$, it is obtained that:

$$\bar{H}_{mm} = H_{mm}^{\mathrm{L}} = -V_m - \sum_{j=1, j\neq m}^{N} \Pi_{jm} H^{\mathrm{L}}(\mathbf{s}_m, \mathbf{s}_j, \mathbf{n}_b), \tag{B-11}$$

which is the OIFs of the 2.5D fundamental solutions of Helmholtz equation for Neumann boundary conditions in Eq.(2.10b). Thanks to the following asymptotic expression between the Helmholtz and Laplace fundamental solutions:

$$\bar{G}(\mathbf{s}_m, \mathbf{s}_j, k_a) = G^{\mathrm{L}}(\mathbf{s}_m, \mathbf{s}_j) - \frac{1}{2\pi}\left(\ln\left(\frac{k_a}{2}\right) + \gamma\right) \quad \text{when} \quad r \to 0 \tag{B-12}$$

the OIFs $\bar{G}_{mm}$ of the 2.5D fundamental solutions of Helmholtz equation in (2.10a) can be determined indirectly by calculating the OIFs G^{L}_{mm} of the Laplace equation, namely,

$$\bar{G}_{mm} = G^{\mathrm{L}}_{mm} - \frac{1}{2\pi}\left(\ln\left(\frac{k_a}{2}\right) + \gamma\right), \tag{B-13}$$

where the OIFs G^{L}_{mm} can be derived as [30, 33]:

$$G^{\mathrm{L}}_{mm} = \frac{1}{L_m}\int_{\Gamma_s} G^{\mathrm{L}}(\mathbf{x}_m, \mathbf{s})\,\mathrm{d}\Gamma_s(\mathbf{s}) = -\frac{1}{2\pi}\ln\left(\frac{L_m}{2\pi}\right). \tag{B-14}$$

References

[1] I. Harari, A survey of finite element methods for time-harmonic acoustics, Comput Meth Appl Mech Eng 195 (2006) 1594–1607.

[2] Y. Liu, On the BEM for acoustic wave problems, Eng Anal Boundary Elem 107 (2019) 53–62.

[3] G. Fairweather, A. Karageorghis, P. A. Martin, The method of fundamental solutions for scattering and radiation problems, Engineering Analysis with Boundary Elements 27 (2003) 759–769.

[4] A. H.D. Cheng, Y. X. Hong, An overview of the method of fundamental solutions—Solvability, uniqueness, convergence, and stability, Engineering Analysis with Boundary Elements 120 (2020) 118–152.

[5] J. Li, Z. J. Fu, Y. Gu, Q. H. Qin, Recent Advances and Emerging Applications of the Singular Boundary Method for Large-Scale and High-Frequency Computational Acoustics, Advances in Applied Mathematics and Mechanics 14 (2022) 315–343.

[6] Z. J. Fu, Q. Xi, Y. Gu, J. Li, W. Qu, L. Sun, X. Wei, F. Wang, J. Lin, W. Li, W. Xu, C. Zhang, Singular boundary method: A review and computer implementation aspects, Engineering Analysis with Boundary Elements 147 (2023) 231–266.

[7] P. A. Costa, P. Amado-mendes, Prediction of Vibrations and Reradiated Noise Due to Railway Traffic : A Comprehensive Hybrid Model Based on a Finite Element Method and Method of Fundamental Solutions Approach, J Vib Acoustic 139 (2017) 1–10.

[8] D. Ghangale, A. Colaço, P. Alves Costa, R. Arcos, A methodology based on structural FEM-BEM and acoustic BEM models in 2.5D for the prediction of re-radiated noise in railway-induced ground-borne vibration problems, Journal of Vibration and Acoustics 141 (2019) 1–14.

[9] D. Ghangale, R. Arcos, A. Clot, J. Cayero, J. Romeu, A methodology based on 2.5D FEM-BEM for the evaluation of the vibration energy flow radiated by underground railway infrastructures, Tunnelling and Underground Space Technology 101 (2020) 103392.

[10] H. Li, D. Thompson, G. Squicciarini, X. Liu, M. Rissmann, F. D. Denia, J. Giner-Navarro, Using a 2.5D boundary element model to predict the sound distribution on train external surfaces due to rolling noise, J Sound Vib 486 (2020) 115599.

[11] T. Deng, X. Sheng, H. Jeong, D. J. Thompson, A two-and-half dimensional finite element/boundary element model for predicting the vibro-acoustic behaviour of panels with poro-elastic media, J Sound Vib 505 (2021) 116147.

[12] H. Liravi, R. Arcos, D. Ghangale, B. Noori, J. Romeu, A 2.5D coupled FEM-BEM-MFS methodology for longitudinally invariant soil-structure interaction problems, Computers and Geotechnics 132 (2021) 104009.

[13] H. Liravi, R. Arcos, A. Clot, K. F. Conto, J. Romeu, A 2.5D coupled FEM–SBM methodology for soil–structure dynamic interaction problems, Engineering Structures 250 (2022) 113371.

[14] D. J. Shippy, P. S. Kondapalli, G. Fairweather, Analysis of acoustic scattering in fluids and solids by the method of fundamental solutions, Mathematical and Computer Modelling 14 (1990) 74–79.

[15] P. S. Kondapalli, D. J. Shippy, G. Fairweather, Analysis of acoustic scattering in fluids and solids by the method of fundamental solutions, Journal of the Acoustical Society of America 91 (1992) 1844–1854.

[16] A. Karageorghis, The Method of Fundamental Solutions for the Calculation of the Eigenvalues of the Helmholtz Equation, Applied Mathematics Letters 14 (2001) 837–842.

[17] A. Karageorghis, D. Lesnic, L. Marin, The MFS for the identification of a sound-soft interior acoustic scatterer, Eng Anal Boundary Elem 83 (2017) 107–112.

[18] W. Qu, C. M. Fan, Y. Gu, Localized method of fundamental solutions for interior Helmholtz problems with high wave number, Eng Anal Boundary Elem 107 (2019) 25–32.

[19] J. T. Chen, M. H. Chang, K. H. Chen, S. R. Lin, The boundary collocation method with meshless concept for acoustic eigenanalysis of two-dimensional cavities using radial basis function, Journal of Sound and Vibration 257 (2002) 667–711.

[20] W. Chen, Y. C. Hon, Numerical investigation on convergence of boundary knot method in the analysis of homogeneous helmholtz, modified helmholtz, and convection-diffusion problems, Computer Methods in Applied Mechanics and Engineering 192 (2003) 1859–1875.

[21] F. Wang, Y. Gu, W. Qu, C. Zhang, Localized boundary knot method and its application to large-scale acoustic problems, Comput Meth Appl Mech Eng 361 (2020) 112729.

[22] X. Yue, F. Wang, C. Zhang, H. Zhang, Localized boundary knot method for 3D inhomogeneous acoustic problems with complicated geometry, App Math Modell 92 (2021) 410–421.

[23] D. L. Young, K. H. Chen, C. W. Lee, Singular meshless method using double layer potentials for exterior acoustics, The Journal of the Acoustical Society of America 119 (2006) 96–107.

[24] W. Chen, F. Z. Wang, A method of fundamental solutions without fictitious boundary, Engineering Analysis with Boundary Elements 34 (2010) 530–532.

[25] Z. J. Fu, W. Chen, Y. Gu, Burton-Miller-type singular boundary method for acoustic radiation and scattering, Journal of Sound and Vibration 333 (2014) 3776–3793.

[26] Z. J. Fu, W. Chen, J. Lin, A. H.-D. Cheng, Singular Boundary Method for Various Exterior Wave Applications, International Journal of Computational Methods 12 (2014) 1550011.

[27] W. Qu, W. Chen, Y. Gu, Fast multipole accelerated singular boundary method for the 3D Helmholtz equation in low frequency regime, Comput Math Appl 70 (2015) 679–690.

[28] W. Qu, W. Chen, C. Zheng, Diagonal form fast multipole singular boundary method applied to the solution of high-frequency acoustic radiation and scattering, International Journal for Numerical Methods in Engineering 111 (2017) 803–815.

[29] W. Li, A fast singular boundary method for 3D Helmholtz equation, Computers and Mathematics with Applications 77 (2019) 525–535.

[30] Z. Fu, W. Chen, P. Wen, C. Zhang, Singular boundary method for wave propagation analysis in periodic structures, Journal of Sound and Vibration 425 (2018) 170–188.

[31] F. Wang, Z. Chen, P. W. Li, C. M. Fan, Localized singular boundary method for solving Laplace and Helmholtz equations in arbitrary 2D domains, Engineering Analysis with Boundary Elements 129 (2021) 82–92.

[32] Y. Gu, W. Chen, Infinite domain potential problems by a new formulation of singular boundary method, Applied Mathematical Modelling 37 (2013) 1638–1651.

[33] Z. J. Fu, W. Chen, J. T. Chen, W. Z. Qu, Singular boundary method: Three regularization approaches and exterior wave applications, CMES - Computer Modeling in Engineering and Sciences 99 (2014) 417–443.

[34] J. Li, W. Chen, Z. Fu, L. Sun, Explicit empirical formula evaluating original intensity factors of singular boundary method for potential and Helmholtz problems, Engineering Analysis with Boundary Elements 73 (2016) 161–169.

[35] J. Li, Z. Fu, W. Chen, Q. H. Qin, A regularized approach evaluating origin intensity factor of singular boundary method for Helmholtz equation with

high wavenumbers, Engineering Analysis with Boundary Elements 101 (2019) 165–172.

[36] X. Wei, W. Chen, L. Sun, B. Chen, A simple accurate formula evaluating origin intensity factor in singular boundary method for two-dimensional potential problems with Dirichlet boundary, Engineering Analysis with Boundary Elements 58 (2015) 151–165.

[37] L. Sun, W. Chen, A. H. Cheng, Evaluating the Origin Intensity Factor in the Singular Boundary Method for Three-Dimensional Dirichlet Problems, Advances in Applied Mathematics and Mechanics 9 (2017) 1289–1311.

[38] F. Wang, W. Chen, Q. Hua, A simple empirical formula of origin intensity factor in singular boundary method for two-dimensional Hausdorff derivative Laplace equations with Dirichlet boundary, Computers and Mathematics with Applications 76 (2018) 1075–1084.

[39] X. Sheng, C. J. C. Jones, D. J. Thompson, Prediction of ground vibration from trains using the wavenumber finite and boundary element methods, J Sound Vib 293 (2006) 575–586.

[40] X. Sheng, T. Zhong, Y. Li, Vibration and sound radiation of slab high-speed railway tracks subject to a moving harmonic load, J Sound Vib 395 (2017) 160–186.

[41] X. Wei, W. Luo, 2.5D singular boundary method for acoustic wave propagation, Applied Mathematics Letters 112 (2021) 106760.

[42] W. Chen, J.-Y. Zhang, Z.-J. Fu, Singular boundary method for modified Helmholtz equations, Engineering AnalysiswithBoundaryElements 44 (2014) 112–119.

[43] V. C. Henríquez, P. M. Juhl, OpenBEM - An open source boundary element method software in acoustics, 39th International Congress on Noise Control Engineering 2010, INTER-NOISE 2010 7 (2010) 5796–5805.

[44] E. Perrey-Debain, J. Trevelyan, P. Bettess, Plane wave interpolation in direct collocation boundary element method for radiation and wave scattering: numerical aspects and applications, Journal of Sound and Vibration 261 (2003) 839–858.

[45] D. Duhamel, Efficient calculation of the three-dimensional sound pressure field around a noise barrier, Journal of Sound and Vibration 197 (1996) 547–571.

[46] T. Ishizuka, K. Fujiwara, Performance of noise barriers with various edge shapes and acoustical conditions, Applied Acoustics 65 (2004) 125–141.

[47] L. Godinho, J. António, T. A., 3D sound scattering by rigid barriers in the vicinity of tall buildings, Applied Acoustics 62 (2001) 1229–1248.

[48] L. Godinho, J. António, T. A., The scattering of 3D sound sources by rigid barriers in the vicinity of tall buildings, Engineering Analysis with Boundary Elements 26 (2002) 1229–1248.

[49] L. A. Lacerda, L. C. Wrobel, W. J. Mansur, A dual boundary element formulation for sound propagation around barriers over an impedance plane, Journal of Sound and Vibration 202 (1997) 235–247.

[50] R. Toledo, J. Aznárez, O. Maeso, D. Greiner, Optimization of thin noise barrier designs using Evolutionary Algorithms and a Dual BEM Formulation, Journal of Sound and Vibration 334 (2015) 219–238.

[51] L. Cheng, L. Chen, W. Zhao, H. Chen, Shape optimization of sound barrier using an isogeometric fast multipole boundary element method in two dimensions, Engineering Analysis with Boundary Elements 85 (2017) 142–157.

[52] F. Jiang, W. Zhao, L. Chen, C. Zheng, H. Chen, Combined shape and topology optimization for sound barrier by using the isogeometric boundary element method, Engineering Analysis with Boundary Elements 124 (2021) 124–136.

[53] E. G. A. Costa, L. M. Godinho, J. A. Santiago, W. J. Mansur, F. C. Peters, Application of the method of fundamental solutions to predict the acoustic

performance of T-shaped thin barriers, Engineering Analysis with Boundary Elements 99 (2019) 142–156.

[54] M. Veloso, M. Pereira, L. Godinho, P. Amado-Mendes, J. Redondo, Insertion loss prediction of sonic crystal noise barriers covered by porous concrete using the Method of Fundamental Solutions, Applied Acoustics 211 (2023) 109543.

[55] M. Martins, L. Godinho, L. Picado-Santos, Numerical Evaluation of Sound Attenuation Provided by Periodic Structures, ARCHIVES OF ACOUSTICS 38 (2013) 503–516.

[56] L. Godinho, D. Soares Jr, P. G. Santos, Efficient analysis of sound propagation in sonic crystals using an ACA–MFS approach, Engineering Analysis with Boundary Elements 69 (2016) 72–85.

[57] X. Wei, X. Cheng, D. Chen, S. Chen, H. Zheng, L. Sun, Acoustic sensitivity analysis for 3D structure with constant cross-section using 2.5D singular boundary method, Engineering Analysis with Boundary Elements 155 (2023) 948–955.

[58] H. Liu, F. Wang, A novel semi-analytical meshless method for the thickness optimization of porous material distributed on sound barriers, Applied Mathematics Letters 147 (2024) 108844.

[59] J. Li, W. Chen, A modified singular boundary method for three-dimensional high frequency acoustic wave problems, Applied Mathematical Modelling 54 (2018) 189–201.

[60] J. António, A. Tadeu, L. Godinho, A three-dimensional acoustics model using the method of fundamental solutions, Engineering Analysis with Boundary Elements 32 (2008) 525–531.

[61] Z. Y. Yan, Treatment of sharp edges & corners in the acoustic boundary element method under Neumann boundary condition, CMES - Computer Modeling in Engineering and Sciences 13 (2006) 81–90.

[62] J. T. Chen, M. T. Liang, I. L. Chen, S. W. Chyuan, K. H. Chen, Dual boundary element analysis of wave scattering from singularities, Wave Motion 30 (1999) 367–381.

[63] L. Marin, D. Lesnic, V. Mantič, Treatment of singularities in Helmholtz-type equations using the boundary element method, Journal of Sound and Vibration 278 (2004) 39–62.

[64] B. Gilvey, J. Trevelyan, G. Hattori, Singular enrichment functions for Helmholtz scattering at corner locations using the boundary element method, International Journal for Numerical Methods in Engineering 121 (2020) 519–533.

[65] L. Marin, Treatment of singularities in the method of fundamental solutions for two-dimensional Helmholtz-type equations, Applied Mathematical Modelling 34 (2010) 1615–1633.

[66] P. R. Antunes, S. S. Valtchev, A meshfree numerical method for acoustic wave propagation problems in planar domains with corners and cracks, Journal of Computational and Applied Mathematics 234 (2010) 2646–2662.

[67] N. K. Dezfouli, M. R. Hematiyan, M. Mohammadi, A modification of the method of fundamental solutions for solving 2D problems with concave and complicated domains, Engineering Analysis with Boundary Elements 123 (2021) 168–181.

[68] J. Lin, W. Chen, C. S. Chen, Numerical treatment of acoustic problems with boundary singularities by the singular boundary method, Journal of Sound and Vibration 333 (2014) 3177–3188.

[69] J. Ma, W. Chen, J. Lin, Crack analysis by using the enriched singular boundary method, Engineering Analysis with Boundary Elements 72 (2016) 55–64.

[70] J. Lin, L. Qiu, F. Wang, Localized singular boundary method for the simulation of large-scale problems of elliptic operators in complex geometries, Computers and Mathematics with Applications 105 (2022) 94–106.

[71] J. Fakhraei, R. Arcos, T. Pàmies, J. Romeu, 2.5D singular boundary method for exterior acoustic radiation and scattering problems, Engineering Analysis with Boundary Elements 143 (2022) 293–304.

[72] J. T. Chen, K. Chen, C. I. L., L. Liu, A new concept of modal participation factor for numerical instability in the dual BEM for exterior acoustics, Mechanics Research Communications 30 (2003) 161–174.

[73] J. Fakhraei, R. Arcos, T. Pàmies, H. Liravi, J. Romeu, Modified 2.5D singular boundary methods to deal with spurious eigensolutions in exterior acoustic problems, Journal of Sound and Vibration 550 (2023).

[74] Z. Razafizana, Z. J. Fu, Singular boundary method for water wave problems, Ocean Engineering 96 (2015) 330–337.

[75] J. T. Chen, C. X. Huang, F. C. Wong, Determination of spurious eigenvalues and multiplicities of true eigenvalues in the dual multiple reciprocity method using the singular-value decomposition technique, Journal of Sound and Vibration 230 (2000) 203–219.

[76] J. T. Chen, C. X. Huang, K. H. Chen, Determination of spurious eigenvalues and multiplicities of true eigenvalues using the real-part dual BEM, Computational Mechanics 24 (1999) 41–51.

[77] S. R. Kuo, J. T. Chen, C. X. Huang, Analytical study and numerical experiments for true and spurious eigensolutions of a circular cavity using the real-part dual BEM, International Journal for Numerical Methods in Engineering 48 (2000) 1401–1422.

[78] S. R. Kuo, W. Yeih, Y. C. Wu, Applications of the generalized singular-value decomposition method on the eigenproblem using the incomplete boundary element formulation, Journal of Sound and Vibration 235 (2000) 813–845.

[79] I. L. Chen, J. T. Chen, S. R. Kuo, M. T. Liang, A new method for true and spurious eigensolutions of arbitrary cavities using the combined Helmholtz exterior integral equation formulation method, The Journal of the Acoustical Society of America 109 (2001) 982–998.

[80] I. L. Chen, J. T. Chen, M. T. Liang, Analytical study and numerical experiments for radiation and sattering problems using the CHIEF method, Journal of Sound and Vibration 13 (2001) 809–828.

[81] J. T. Chen, J. H. Lin, S. R. Kuo, S. W. Chyuan, Boundary element analysis for the Helmholtz eigenvalue problems with a multiply connected domain, Proceedings of the Royal Society A 457 (2001) 2521–2546.

[82] J. Li, W. Chen, Q. Qin, A modified dual-level fast multipole boundary element method based on the Burton–Miller formulation for large-scale three-dimensional sound field analysis, Computer Methods in Applied Mechanics and Engineering 340 (2018) 121–146.

[83] A. Mohsen, R. Piscoya, M. Ochmann, The application of the dual surface method to treat the nonuniqueness in solving acoustic exterior problems, Acta Acustica united with Acustica 97 (2011) 699–707.

[84] J. T. Chen, I. L. Chen, Y. T. Lee, Eigensolutions of multiply connected membranes using the method of fundamental solutions, Engineering Analysis with Boundary Elements 29 (2005) 166–174.

[85] L. Liu, Single layer regularized meshless method for three dimensional exterior acoustic problem, Engineering Analysis with Boundary Elements 77 (2017) 138–144.

[86] W. Li, W. Chen, G. Pang, Singular boundary method for acoustic eigenanalysis, Computers and Mathematics with Applications 72 (2016) 663–674.

[87] S. Cheng, F. Wang, P.-W. Li, W. Qu, Singular boundary method for 2D and 3D acoustic design sensitivity analysis, Computers and Mathematics with Applications 119 (2022) 371–386.

[88] S. Cheng, F. Wang, G. Wu, C. Zhang, A semi-analytical and boundary-type meshless method with adjoint variable formulation for acoustic design sensitivity analysis, Applied Mathematics Letters 131 (2022).

[89] Y. Wu, Z. Zhuojia Fu, , J. Min, A Modified Formulation of Singular Boundary Method for Exterior Acoustics, CMES-Computer Modeling in Engineering and Sciences 135 (2023) 377–393.

[90] C. J. Zheng, H. B. Chen, H. F. Gao, L. Du, Is the Burton-Miller formulation really free of fictitious eigenfrequencies?, Engineering Analysis with Boundary Elements 59 (2015) 43–51.